UC San Diego

UC San Diego Electronic Theses and Dissertations

Title

Mobile OFDM communications

Permalink

https://escholarship.org/uc/item/6jw7v22q

Author

Wang, Tiejun

Publication Date

2006

Peer reviewed|Thesis/dissertation

eScholarship.org Powered by the California Digital Library
University of California

UNIVERSITY OF CALIFORNIA, SAN DIEGO

Mobile OFDM Communications

A dissertation submitted in partial satisfaction of the
requirements for the degree
Doctor of Philosophy
in
Electrical Engineering (Communication Theory and Systems)

by

Tiejun (Ronald) Wang

Committee in charge:

Professor John G. Proakis, Chair
Professor James R. Zeidler, Co-Chair
Professor Robert R. Bitmead
Professor William S. Hodgkiss
Professor Laurence B. Milstein

2006

©Copyright
Tiejun (Ronald) Wang, 2006
All rights reserved.

The dissertation of Tiejun (Ronald) Wang is approved, and it is acceptable in quality and form for publication on microfilm:

_____

_____

_____

_____
Co-Chair

_____
Chair

University of California, San Diego

2006

To my sister and wife, with all my love.

TABLE OF CONTENTS

Signature Page . . . iii

Table of Contents . . . v

List of Figures . . . vii

List of Tables . . . ix

Acknowledgements . . . x

Vita and Publications . . . xii

Abstract . . . xiii

1 Introduction . . . 1
1.1 Introduction . . . 2
1.2 Outline of the Dissertation . . . 5

2 Doppler Sensitivity for OFDM System . . . 7
2.1 Motivation . . . 8
2.2 System Setup . . . 10
2.2.1 OFDM System . . . 10
2.2.2 Channel Model . . . 11
2.3 Expression for the ICI and its Power . . . 15
2.4 The Distribution and Moments of the ICI . . . 20
2.5 Evaluation of OFDM System Performance . . . 28
2.6 Conclusion . . . 36

3 Suppression of Intercarrier Interference . . . 38
3.1 Motivation . . . 39
3.2 System Setup . . . 42
3.3 OFDM Channel Estimation . . . 46
3.3.1 A 2-D Polynomial Surface Channel Estimator . . . 46
3.3.2 A Modified Polynomial Channel Estimator . . . 48
3.4 OFDM Data Detection Techniques . . . 51
3.4.1 Conventional OFDM Signal Detection . . . 51
3.4.2 MMSE Based Detection . . . 52
3.5 Numerical Results . . . 54
3.5.1 Channel Estimation Results . . . 54
3.5.2 Performance Comparison under Perfectly Known Channel 55
3.5.3 Performance Comparison under Channel Estimation . . . 56
3.5.4 Performance Comparison under Different Channel Estimation Quality . . . 57

3.6 Conclusion 63

4 Filtered Multitone Modulation vs. OFDM 65
4.1 Motivation 66
4.2 FMT System Setup 70
4.3 Interference Analysis 73
4.3.1 FMT Transmitter and Receiver Structures 73
4.3.2 FMT Over Quasi-static Frequency-Flat Fading Channel . 75
4.3.3 FMT Over Frequency-Selective Channel 76
4.3.4 FMT Over Frequency-Selective Time-Varying Channel . 81
4.3.5 Performance Comparison with OFDM System 84
4.4 Per-Channel Equalized FMT Modulation 87
4.4.1 FMT Modulation with Per-Channel Equalizer 87
4.4.2 Interference Analysis of Per-Channel Equalized FMT System 88
4.4.3 Performance Comparisons with Un-equalized FMT System and OFDM System 90
4.5 Numerical and Simulation Results 92
4.6 Conclusion 101

Bibliography 104

LIST OF FIGURES

2.1 Base-band OFDM Transmisson Model with N subcarriers . . . 10
2.2 Multipath delay profile and frequency correlation function . . . 13
2.3 C/I ratio curves of an OFDM system $N = 256$ subcarriers, subcarrier distance $\Delta f = 7.81KHz$, and carrier frequency $f_c = 2GHz$ 18
2.4 C/I ratio curves of an OFDM system $N = 256$ subcarriers, subcarrier distance $\Delta f = 7.81KHz$, and carrier frequency $f_c = 2GHz$ 19
2.5 Performance for 16-QAM OFDM system with $f_c = 5$ GHz, $T = 1\mu$s ($W \approx 1MHz$), and speed of 50km/hr 31
2.6 Performance for 16-QAM OFDM system with $f_c = 5$ GHz, $T = 1\mu$s ($W \approx 1MHz$), and speed of 200km/hr 32
2.7 Performance comparison for BPSK OFDM and 16-QAM OFDM system with $f_c = 5$ GHz, $T = 1\mu$s ($W \approx 1MHz$), and speed of 100km/hr 33
2.8 Performance for 16-QAM system with 128 subcarriers, $fc = 5$ GHz, $T = 1\mu$s ($W \approx 1MHz$), and speed of 100km/hr 34
2.9 Performance for 16-QAM OFDM system with $f_c = 5$ GHz, $T = 1\mu$s ($W \approx 1MHz$), and speed of 100km/hr 35
2.10 Performance for 16-QAM OFDM system with 128 subcarriers, $fc = 5$ GHz, $T = 1\mu$s ($W \approx 1MHz$), speed of 100km/hr, and transmitting over different frequency-selective fading channels . 36

3.1 Baseband model of the OFDM system 42
3.2 Actual Channel 55
3.3 Estimated Channel 56
3.4 Actual Channel 57
3.5 Estimated Channel 58
3.6 Error rate performance for a known channel 59
3.7 Error rate performance using modified polynomial channel estimation 60
3.8 Symbol error rate comparison of OFDM system with 16 subcarriers under different channel estimation quality 61
3.9 Symbol error rate comparison of OFDM system with 256 subcarriers under different channel estimation quality 62

4.1 System model of the filtered multitone (FMT) modulation system 70
4.2 Frequency spectrum of an FMT system with M subcarriers under upsampling (or downsampling) factor of K 72
4.3 CIR graphs of an FMT system with $M = 64$ subcarriers under different upsampling factors $K = 71, 80, 91, 107$, and 128 93
4.4 Carrier over ICI interference ratio (C/I_{ici}) graphs of an FMT system with $M = 64$ subcarriers under different upsampling factors $K = 68, 71, 80, 91, 107$, and 128 94

4.5 CIR curves of an FMT system with ideal per-channel equalizer with $M = 64$ subcarriers under different upsampling factors $K = 80, 84, 91, 107$, and 128 95
4.6 Comparison of symbol error probability of an FMT system with $M = 64$ subcarriers under different spectral efficiency over low frequency selective and slowly time-varying fading channel . . . 97
4.7 Comparison of symbol error probability of an FMT system with $M = 64$ subcarriers under different spectral efficiency over highly frequency selective and fast fading channel 98
4.8 CIR graphs of an FMT system with $M = 64$ subcarriers under different upsampling factors 99
4.9 CIR graphs comparison between OFDM and FMT system with $M = 64$ subcarriers under different upsampling factors 100

LIST OF TABLES

2.1 Performance Degradation vs. Doppler Spread 31

ACKNOWLEDGEMENTS

I would like to acknowledge those who, throughout my life, have inspired me to imagine, learn and create.

First of all, I would like to thank my parents for bringing me into this world. Making them proud and happy has always been the greatest source of inspiration for me to challenge any impossible and endure any hardship in my life.

I am thankful to my sister, who teamed with me for every achievement I have made.

I am also thankful to my wife, for her every day support and help in the last two and half years, especially for the food she cooked for me with love being the ingredient.

Besides the love and support from my family, I have benefited immeasurably from the professors in Northeastern University, Tsinghua University, Columbia University, and University of California, San Diego. They taught me knowledge and shed lights on my exploration in both academics and in life.

I would like to express my profound gratitude to Prof. John Proakis, my PhD advisor and committee chair. It has been a great privilege working with him. I am grateful for the excellent topics he picked for my research. I am also grateful for his keen technical insight that guided every progress I made in my PhD research. I am especially grateful for his time and effort editing my papers. It is hard to forget so many times a paper turned into red all over after he corrected the grammar mistakes I had made.

I owe heartfelt thanks to Prof. James Zeidler, who has been a great mentor and academic advisor. He gave me fatherly support and help on every step I made in my PhD life.

I wish to thank Prof. Larry Milstein for his question marks and comments that impelled my first journal paper. I learned a lot from his class of digital communication.

I wish to thank Prof. Robert Bitmead for his valuable comments and suggestions on the OFDM channel estimation paper. And also I'd like to thank Prof. William Hodgkiss for his time and support from his busy work.

Last but not least, I would like to thank Prof. Richard Gitlin for his encouragement and suggestions that led me the PhD program at UCSD.

Thank you all very much! If I have achieved any progress in my life I can be proud of - that is because you raise me up to more than I can be.

The text in this thesis, in part, was originally published in the following papers, of which I was the primary researcher and author: T. Wang, J. Proakis, and J. Zeidler, "Performance analysis of high QAM OFDM system over frequency selective time-varying fading channel," *in Proc. on Personal, Indoor and Mobile Radio Communications*, 14th IEEE PIMRC, vol. 1, pp. 793-798, September 2003; T. Wang, J. Proakis, E. Masry, and J. Zeidler, "Performance degradation of OFDM system due to Doppler spreading," *IEEE Transactions on Wireless Communications*, vol. 5, NO. 6, June 2006; (Chapter 2) T. Wang, J. Proakis, and J. Zeidler, "Techniques for suppression of Intercarrier Interference in OFDM system," *in Proc. on IEEE Wireless Communications and Network Conference*, IEEE WCNC'05, Vol. 1, pp. 39-44, March 2005; (Chapter 3) T. Wang, J. Proakis, and J. Zeidler, "Interference analysis of filtered multitone modulation over time-varying fading channels," *in Proc. on IEEE Globecom*, Vol. 6, pp. 3586-3591, November 2005; T. Wang, J. Proakis, and J. Zeidler, "Interference analysis of filtered multitone modulation over time-varying fading channels," to appear in *IEEE Transactions on Communications*, 2006; T. Wang, J. Proakis, and J. Zeidler, "Analysis of per-channel equalized filtered multitone modulation over time-varying fading channels," accepted by *IEEE PIMRC*, 2006. (Chapter 4)

VITA

1996	BSc in Electrical Engineering Northeastern University, Shenyang, China
2002	MSc in Electrical Engineering Columbia University, New York City
2002–2005	Research Assistant Center for Wireless Communications University of California, San Diego
2006	Ph.D. University of California, San Diego

PUBLICATIONS

T. Wang, J. Proakis, and J. Zeidler, "Performance analysis of high QAM OFDM system over frequency selective time-varying fading channel," *in Proc. on Personal, Indoor and Mobile Radio Communications*, 14th IEEE PIMRC, vol. 1, pp. 793-798, September 2003.

T. Wang, J. Proakis, E. Masry, and J. Zeidler, "Performance degradation of OFDM system due to Doppler spreading," *IEEE Transactions on Wireless Communications*, vol. 5, NO. 6, June 2006.

T. Wang, J. Proakis, and J. Zeidler, "Techniques for suppression of Intercarrier Interference in OFDM system," *in Proc. on IEEE Wireless Communications and Network Conference*, IEEE WCNC'05, Vol. 1, pp. 39-44, March 2005.

T. Wang, J. Proakis, and J. Zeidler, "Interference analysis of filtered multitone modulation over time-varying fading channels," *in Proc. on IEEE Globecom*, Vol. 6, pp. 3586-3591, November 2005.

T. Wang, J. Proakis, and J. Zeidler, "Interference analysis of filtered multitone modulation over time-varying fading channels," to appear in *IEEE Transactions on Communications*, 2006.

T. Wang, J. Proakis, and J. Zeidler, "Analysis of per-channel equalized filtered multitone modulation over time-varying fading channels," accepted by *IEEE PIMRC*, 2006.

ABSTRACT OF THE DISSERTATION

Mobile OFDM Communications

by

Tiejun (Ronald) Wang
Doctor of Philosophy in Electrical Engineering
(Communication Theory and Systems)
University of California, San Diego, 2006
Professor John G. Proakis, Chair
Professor James R. Zeidler, Co-Chair

Orthogonal frequency division multiplexing (OFDM) has recently received increased attention due to its capability of supporting high-data-rate communications in frequency-selective fading environments with a comparatively simple receiver structure. However, the time variations (high mobility) of the channel during one OFDM symbol destroy the orthogonality of the different subcarriers and generate power leakage among the subcarriers, known as Inter-Carrier Interference (ICI), which will cause degradation in system performance. Therefore, our research emphasis on Doppler sensitivity is especially meaningful given the popularity that fixed wireless/low mobility OFDM systems have experienced (e.g. 802.11a).

In this dissertation, we first analyze the theoretical performance degradation of OFDM system due to Doppler spreading by developing a two-dimensional Gram-Charlier representation for the bivariate pdf of the ICI, after the bivariate probability density function (pdf) of the ICI is shown to be a weighted Gaussian mixture.

Secondly, in order to suppress ICI in OFDM systems, we describe a minimal mean square error (MMSE) based OFDM detection according to the estimated channel information through a simple and efficient polynomial surface channel estimation technique.

Thirdly, we consider filtered multitone (FMT) modulation over frequency-selective time-varying fading channels. Both ICI and ISI are quantified under several different fading channels conditions. An analysis of the C/I ratio of the FMT system is compared with the conventional OFDM system in order to demonstrate the underlying trade-offs between the spectral efficiency and system performance.

Finally, a per-channel tap-delay-line equalizer is proposed at the FMT receiver to mitigate the ISI. A closed-form expression of the upper bound for its C/I ratio is derived for the per-channel equalized FMT system and used to evaluate the system performance. Performance comparisons are made with an un-equalized FMT system as well as a standard OFDM system.

1

Introduction

1.1 Introduction

Orthogonal frequency division multiplexing (OFDM) has recently received increased attention due to its capability of supporting high-data-rate communications in frequency-selective fading environments with a comparatively simple receiver structure. However, the increased symbol duration makes an OFDM system more sensitive to the time variations of mobile radio channels. In particular, the effect of Doppler spreading destroys the orthogonality of the sub-carriers, resulting in inter-carrier interference (ICI) due to power leakage among subcarriers. Therefore, our research is focused on the performance analysis and system design of OFDM systems over time-varying fading channels.

In the first part of this dissertation, we consider the evaluation of the error probability of an OFDM system transmitting over channels that are both frequency selective and time selective. The time variations of the channel during one OFDM symbol interval destroy the orthogonality of the different subcarriers and generate power leakage among the subcarriers, known as Inter-Carrier Interference (ICI). For conventional modulation methods such as phase-shift keying (PSK) and quadrature-amplitude modulation (QAM), the bivariate probability density function (pdf) of the ICI is shown to be a weighted Gaussian mixture, and can not be well approximated by a Gaussian distribution even with a large number of OFDM sub-carriers. Instead of using the weighted Gaussian mixture pdf to evaluate the error probability, which requires a large computational complexity, we developed a simple and efficient two-dimensional Gram-Charlier representation for the bivariate pdf of the ICI. It is demonstrated that its truncated version of order 4 or 6 provides a very good approximation in the evaluation of the error probability for PSK and QAM in the presence of ICI. Based on Jakes' channel model of the Doppler effects, and an exponential multipath intensity profile, numerical results for the error probability are obtained by utilizing the proposed two-dimensional

Gram-Charlier approximations under different mobile speeds.

It is well known that for an OFDM system transmitting over wireless fading environment, system performance is affected not only by the ICI interference, but also the distortions from the channel estimation error. Hence, it is very important to design robust and efficient OFDM channel estimation algorithms, and OFDM data detection algorithms that can supress interferences (ICI and AWGN). Therefore, we focus our attention in the second part of this dissertation on designing practical channel estimation and signal detection algorithms for OFDM systems over time-varying fading channels. We first propose a new modified polynomial channel estimator for OFDM systems over frequency selective and time-varying fading channels. The proposed estimation algorithm has better performance and low complexity compared with the original polynomial estimator and does not need any channel statistical knowledge (provide robust performance). Based on the estimated channel information, we describe a minimal mean square error (MMSE) based OFDM detection technique that can suppress the degradation caused by ICI distortions. Performance comparisons between conventional OFDM and the proposed MMSE-based OFDM receiver structure under the same channel conditions are provided in this thesis. Simulation results of the system performance further confirm the effectiveness of the new technique over the conventional OFDM receiver in suppressing ICI in OFDM systems.

Like OFDM, filtered multitone modulation (FMT) is also a promising technique in the multi-carrier communication system family, which has recently received much attention. In contrast to an OFDM system that does not use any pulse shape filters for its baseband signals, an FMT system uses a well designed baseband filter to combat ICI and ISI interference. Therefore, it is interesting to study the similarities and differences between these two multi-carrier systems in order to provide useful insights for system designs. First, we did a comparative study of the FMT modulation and OFDM modulation

over frequency-selective time-varying fading channels. We have shown that the orthogonality among different FMT subcarriers as well as the perfect Nyquist sampling condition of each baseband matched filters are destroyed due to the phase and amplitude distortion introduced by the fading channel. The interference caused by the channel frequency-selectivity and time-variance is therefore quantified by analyzing the demodulated signals at the receiver under several different fading channels conditions. An analysis of the average carrier to interference (C/I) ratio of the filtered multitone system is provided in order to demonstrate the underlying trade-off between spectral efficiency and system performance. For comparisons with other multicarrier communication systems (or modulation techniques), the C/I ratio of the conventional OFDM system is also provided and compared with that of the FMT system under the same channel conditions and spectral efficiency. Secondly, in contrast to OFDM system that has sufficiently long cyclic prefix to remove ISI, both ICI and ISI exist in an FMT system and cause performance degradation. By using a per-channel equalizer at the FMT receiver with a sufficiently large number of equalizer taps, the ISI can be mitigated significantly, but the ICI still exists. A closed-form expression of the upper bound for its C/I ratio is derived and used to evaluate the system performance of a per-channel equalized FMT system. Moveover, comparisons among a regular FMT system, a per-channel equalized FMT system and OFDM systems under the same channel conditions and spectral efficiency are also provided.

1.2 Outline of the Dissertation

Chapter 2 discusses the performance analysis of an OFDM system over frequency-selective time-varying fading channels. It is first proved that the ICI distribution has a non-Gauassian distribution even with a sufficiently large number of sub-carriers. Instead of utilizing the conventional Gaussian approximation on the ICI interference, we develop a two-dimensional Gram-Charlier representation for the bivariate pdf of the ICI. Demonstrated by simulation results, the truncated version of the Gram-Charlier approximations of order 4 or 6 provides a very good approximation in the evaluation of the error probability for PSK and QAM in the presence of ICI. Numerical results of the error probability of OFDM systems over time-varying fading channels are provided and compared to the obtained approximation results, which further confirms our approximation approach.

In Chapter 3, we first propose a new modified polynomial channel estimator for the frequency selective and time-varying fading channel. The proposed channel estimation algorithm is simple and efficient and does not need any channel statistical information knowledge such as channel covariance function or average SNR. Based on the estimated channel information, an MMSE-based OFDM detection technique is proposed that reduces ICI distortion. Performance comparisons between conventional OFDM and the proposed MMSE-based OFDM receiver structures under the same channel conditions are also provided in this chapter.

In Chapter 4, a comparative study of the FMT modulation and OFDM modulation over frequency-selective time-varying fading channels is provided. An analysis of the average carrier to interference (C/I) ratio of the FMT system is determined to quantify and demonstrate the underlying trade-off between spectral efficiency and system performance followed by comparisons with the conventional OFDM system under the same channel conditions and spectral efficiency. Based on the previous results, the FMT system is extended to a per-

channel equalized FMT system for mitigating ISI. A closed-form expression of its upper bound for the C/I ratio is provided and used to evaluate the system performance. Moveover, comparisons among a regular FMT system, a per-channel equalized FMT system and OFDM systems under the same channel conditions and spectral efficiency are also provided.

2

Doppler Sensitivity for OFDM System

2.1 Motivation

In OFDM systems, a serial data stream is split into parallel streams that modulate a group of orthogonal sub-carriers. Compared to single carrier modulation, OFDM symbols have a relatively long time duration, but a narrow bandwidth. Consequently, OFDM is robust to channel multipath dispersion and results in a decrease in the complexity of equalizers for high delay spread channels or high data rates. However, the increased symbol duration makes an OFDM system more sensitive to the time variations of mobile radio channels. In particular, the effect of Doppler spreading destroys the orthogonality of the sub-carriers, resulting in inter-carrier interference (ICI) due to power leakage among subcarriers.

In several previous publications [12]-[15], the system performance for OFDM was analyzed based on the assumption that the ICI distribution is Gaussian by invoking the central limit theorem. In other related papers [71]-[20], efforts have been made to evaluate the effect of ICI by calculating its average power and comparing it with the power of the desired signal. In [71][17], the carrier to interference (C/I) ratio has been introduced to demonstrate the effect of the ICI under various maximum Doppler spreads and different Doppler spectra. Through numerical evaluations of the C/I ratios, it is reported in [18] that an OFDM system is robust to frequency selectivity but quite sensitive to time varying fading channels. Li and Cimini [19] provide universal bounds on the ICI in an OFDM system over Doppler fading channels, which are easier to evaluate and can provide useful insights compared with the exact ICI expression. Furthermore, the closed-form expression of ICI power is derived and evaluated in [20], where the normalized ICI power is represented as a function of the normalized Doppler spread. However, all these papers do not attempt to determine the underlying probability distribution function (pdf) of the ICI.

In this chapter we focus on providing a statistical analysis for the ICI in an OFDM system that employs conventional PSK and QAM signal mod-

ulation in a frequency selective, Rayleigh fading time-varying channel. The channel, which is assumed to be wide-sense stationary with uncorrelated scattering (WSSUS), is modeled by a two-dimensional correlation function in time and frequency, representing the time variations and frequency selectivity of the channel. Each subchannel is assumed to be frequency flat and, based on the power series model developed by Bello [21], a two-term Taylor series expansion is used to model the time variations in an OFDM symbol. Jakes' model [84] is used as the model for the Doppler power spectrum and an exponential multipath intensity profile is the model adopted for the multipath effects. A cyclic prefix is assumed to remove the effects of inter-symbol interference. Based on this channel model, the ICI is expressed as the summation of leakage terms into each of the subcarriers and its pdf is shown to be characterized statistically by a bivariate pdf that is a weighted sum of Gaussian pdfs.

In deriving the probability of error for the OFDM system in the presence of ICI, the use of the weighted Gaussian pdf proves to be computationally intensive. This difficulty serves as the motivation to develop a two-dimensional Gram-Charlier series to represent the pdf of the ICI. A truncated version of the Gram-Charlier is used in the evaluation of the error probability for PSK and QAM signal modulations in an OFDM system.

This chapter is organized as follows: In Section 2.2.1 we describe the model for the OFDM system. In Section 2.2.2 we describe the channel model and use a Taylor series expansion for the time variations within an OFDM symbol. In Section 2.3 an expression for the ICI and its power is presented. Section 2.4 provides a thorough analysis of the statistics of the ICI, its joint probability density, joint moments, and a two-dimensional Gram-Charlier representation. In Section 2.5, the error rate performance of BPSK and 16-QAM OFDM systems are presented and compared. Finally, concluding remarks are given in Section 2.6.

2.2 System Setup

2.2.1 OFDM System

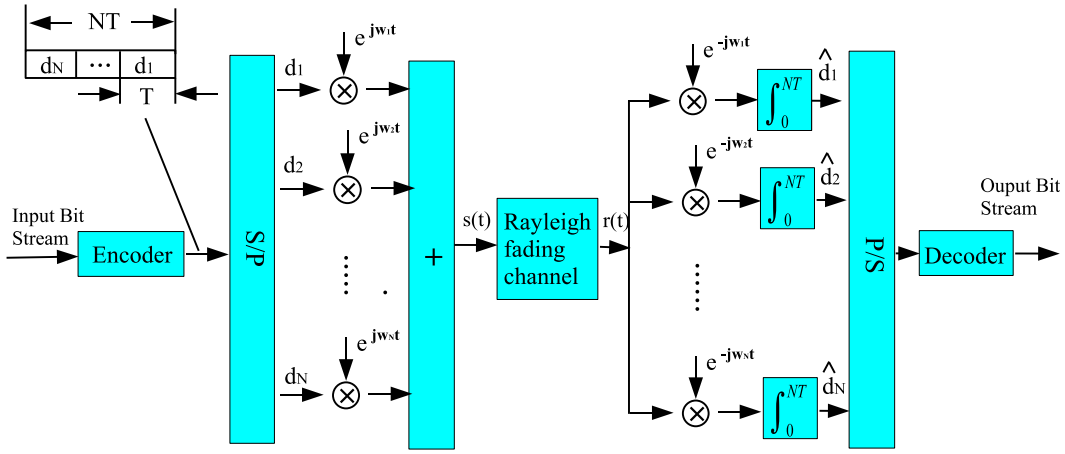


Figure 2.1: Base-band OFDM Transmisson Model with N subcarriers

An OFDM system with N subcarriers is represented in Figure 2.1. In an OFDM system that employs M-ary digital modulation, a block of $\log_2 M$ input bits is mapped into a symbol constellation point d_k by a data encoder, and then N symbols are transferred by the serial-to-parallel converter (S/P). If $1/T$ is the symbol rate of the input data to be transmitted, the symbol interval in the OFDM system is increased to NT, which makes the system more robust against the channel delay spread. Each sub-channel, however, transmits at a much lower bit rate of $\frac{\log_2 M}{NT}$ bits/s. The parallel symbols $(d_1, \cdots, d_N)$ modulate a group of orthogonal subcarriers, which satisfy

$$\frac{1}{NT}\int_0^{NT} \exp(j2\pi f_i t)\exp(j2\pi f_j t)dt = \begin{cases} 1 & i = j \\ 0 & i \neq j \end{cases} \tag{2.1}$$

where $f_i = \frac{i-1}{NT}, \quad (i = 1, 2, \cdots, N)$

Consider the system shown in Figure 2.1. The baseband transmitted

signal can be represented as

$$s(t) = \frac{1}{\sqrt{NT}} \sum_{k=1}^{N} s_k e^{j2\pi f_k t}, 0 \leq t \leq NT, \quad f_k = \frac{k-1}{NT}. \tag{2.2}$$

We denote by $2E_s$ the average energy for the complex baseband symbol s_k. Then s_k is given by

$$s_k = \sqrt{2E_s} d_k \tag{2.3}$$

where $d_k = d_{k,r} + j d_{k,i}$, is the signal constellation point (e.g. BPSK, QPSK, QAM, etc.) with normalized variance $E[|d_k|^2] = 1$. Square M-QAM signal constellations may be viewed as two independent $\sqrt{M}$-PAM signals on orthogonal carriers. In this case, the real and imaginary parts $d_{k,r}$ and $d_{k,i}$ are statistically independent, identically distributed and $E[d_{k,r}] = E[d_{k,i}] = 0$.

2.2.2 Channel Model

We consider a frequency selective randomly varying channel with impulse response $h(t, \tau)$. Within the narrower bandwidth of each sub-carrier, compared with the coherence bandwidth of the channel, the sub-channel is modeled as a frequency nonselective Rayleigh fading channel. Hence, the channel impulse response $h_k(t, \tau)$ for the k^{th} subchannel is denoted as

$$h_k(t, \tau) = \beta_k(t)\delta(\tau) \tag{2.4}$$

where the process $\{\beta_k(t), -\infty < t < \infty\}$ is a stationary, zero mean complex-valued process described as follows: It is assumed that the processes $\{\beta_k(t),\ k = 1, \ldots, N$, are complex-valued jointly stationary and jointly Gaussian with zero means and cross covariance function

$$R_{\beta_k,\beta_l}(\tau) := E[\beta_k(t+\tau)\beta_l^*(t)],\ k, l = 1, \ldots, N.$$

For each fixed k, the real and imaginary parts of the process $\{\beta_k(t), -\infty < t < \infty\}$ are assumed independent with identical covariance function. We further assume that the correlation function $R_{\beta_k,\beta_l}(\tau)$ has the following factorable form

$$R_{\beta_k,\beta_l}(\tau) = R_1(\tau)R_2(k-l) \tag{2.5}$$

which has been frequently used in the literature, e.g.,[15][26][27], and which is sufficient to represent the frequency selectivity and the time-varying effects of the channel. $R_1(\tau)$ gives the temporal correlation for the process $\{\beta_k(t), -\infty < t < \infty\}$ which is seen to be identical for all $k = 1, \ldots, N$. $R_2(k)$ represents the correlation in frequency across subcarriers. We assume in this chapter that the corresponding spectral density $\psi_1(f)$ to $R_1(\tau)$ is given by the Doppler power spectrum, modeled as in Jakes [84], i.e.,

$$\psi_1(f) = \begin{cases} \frac{1}{\pi F_d \cdot \sqrt{1-(\frac{f}{F_d})^2}} & |f| \leq F_d \\ 0 & otherwise \end{cases} \tag{2.6}$$

where F_d is the (maximum) Doppler bandwidth. Note that

$$R_1(\tau) = J_0(2\pi F_d \tau) \tag{2.7}$$

where $J_0(\tau)$ is the zero-order Bessel function of the first kind. In order to specify the correlation in frequency across subcarriers, we adopt an exponential multipath power intensity of the form $S(\tau) = \alpha e^{-\alpha\tau}, \quad \tau > 0, \alpha > 0$ where α is a parameter that controls the coherence bandwidth of the channel. The Fourier transform of $S(\tau)$ yields

$$\psi_2(f) = \frac{\alpha}{\alpha + j2\pi f} \tag{2.8}$$

which provides a measure of the correlation of the fading across the subcarriers as illustrated in Figure 2.2. Then $R_2(k) = \psi_2(\Delta f k)$ where $\Delta f = \frac{1}{NT}$ is the frequency separation between two adjacent subcarriers. The $3dB$ bandwidth of $\psi_2(f)$ is defined as the coherence bandwidth of the channel and easily shown to be $f_{coherent} = \frac{\sqrt{3}\alpha}{2\pi}$.

The channel model described above is suitable for modeling OFDM signal transmission in mobile radio systems, e.g., cellular systems and broadcasting systems. For example, in DVB-CS2 with 2000 subcarriers, the symbol duration NT is $500\mu s$. In contrast, the delay spread of many fading channels is much smaller, which make it reasonable to view each subcarrier as a flat

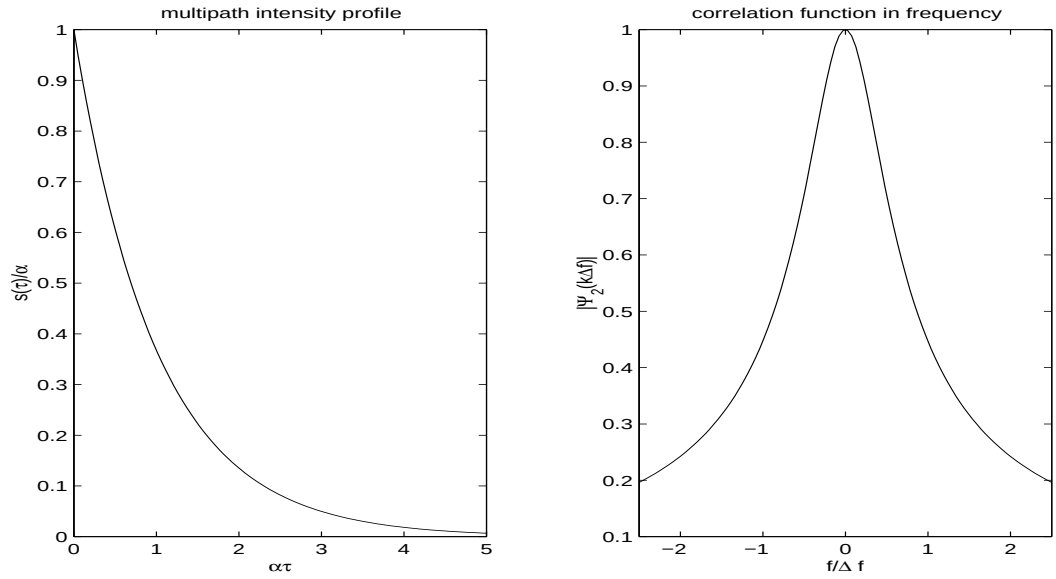


Figure 2.2: Multipath delay profile and frequency correlation function

fading channel. However, compared with the entire OFDM system bandwidth $W = 1/T$, the coherence bandwidth $f_{coherent}$ is usually smaller, $f_{coherent} < W$, especially in an outdoor wireless communication environment. Hence, the channel is frequency-selective over the entire OFDM bandwidth.

We now turn our attention to modeling the time variations of the channel within an OFDM symbol interval. For most practical mobile radio fading channels, the time-varying effects in the channel are sufficiently slow, i.e., the coherence time is always much larger than the interval of an OFDM symbol [28][83]. For such slow fading channels, we use the two terms Taylor series expansion, first introduced by Bello [21], to represent the time-varying fading response $\beta_k(t)$ as the following form:

$$\beta_k(t) = \beta_k(t_0) + \beta_k^{'}(t_0)(t - t_0), \quad t_0 = \frac{NT}{2}, 0 \leq t \leq NT. \tag{2.9}$$

Therefore, the impulse response of the k^{th} subchannel is expressed as

$$h_k(t, \tau) = \beta_k(t)\delta(\tau) = [\beta_k(t_0) + \beta_k^{'}(t_0)(t - t_0)]\delta(\tau). \tag{2.10}$$

Since $R_1(\tau)$ of (2.7) is infinitely differentiable, all mean-square derivatives exist

and thus the differentiation above is justified. We use this model for the time variations of the channel within an OFDM symbol.

2.3 Expression for the ICI and its Power

Let $s(t)$ be the baseband signal transmitted over the channel with impulse response $h(t,\tau)$ as modeled above. Then the baseband received signal with additive noise may be expressed as

$$r(t) = h(t,\tau) \star s(t) + n(t) = \frac{1}{\sqrt{NT}} \sum_{k=1}^{N} \beta_k(t) s_k e^{j2\pi f_k t} + n(t) \tag{2.11}$$

where $\star$ denotes convolution and $n(t)$ is the additive noise, which is modeled as a Gaussian process with zero mean and spectrally flat within the signal bandwidth, with one-sided spectral density N_0 watts/Hz. By using the Taylor series expansion for $\beta_k(t)$ as given in (2.10), we obtain

$$r(t) = \frac{1}{\sqrt{NT}} \sum_{k=1}^{N} \beta_k(t_0) s_k e^{j2\pi f_k t} + \frac{1}{\sqrt{NT}} \sum_{k=1}^{N} \beta_k^{'}(t_0)(t-t_0) s_k e^{j2\pi f_k t} + n(t). \tag{2.12}$$

The received signal in a symbol interval is passed through a parallel bank of correlators, where each correlator is tuned to one of the N subcarriers. The output of the i^{th} correlator is

$$\widehat{d_i} = \frac{1}{\sqrt{2E_s}} \frac{1}{\sqrt{NT}} \int_0^{NT} r(t) e^{-j2\pi f_i t} dt. \tag{2.13}$$

Substituting (2.12) into (2.13), we obtain

$$\begin{aligned} \widehat{d_i} \;=\; & \underbrace{\frac{1}{\sqrt{2E_s}} \frac{1}{\sqrt{NT}} \int_0^{NT} \frac{1}{\sqrt{NT}} \sum_{k=1}^{N} \beta_k(t_0) s_k e^{j2\pi (f_k - f_i) t} dt}_{(1)} \\ & + \underbrace{\frac{1}{\sqrt{2E_s}} \frac{1}{\sqrt{NT}} \int_0^{NT} \frac{1}{\sqrt{NT}} \sum_{k=1}^{N} \beta_k^{'}(t_0)(t-t_0) s_k e^{j2\pi (f_k - f_i) t} dt}_{(2)} \\ & + \underbrace{\frac{1}{\sqrt{2E_s}} \frac{1}{\sqrt{NT}} \int_0^{NT} n(t) e^{-j2\pi f_i t} dt}_{(3)} \end{aligned} \tag{2.14}$$

The first term yields

$$\sum_{k=1}^{N} \beta_k(t_0) d_k \left(\frac{1}{NT} \int_0^{NT} e^{j2\pi (f_k - f_i) t} dt \right) = \beta_i(t_0)\, d_i. \tag{2.15}$$

The second term yields

$$\begin{aligned}\sum_{k=1}^{N}\beta_k'(t_0)d_k\left(\frac{1}{NT}\int_0^{NT}(t-t_0)e^{j2\pi(f_k-f_i)t}dt\right)\\ =\sum_{\substack{k=1\\k\neq i}}^{N}\frac{\beta_k'(t_0)d_k}{j2\pi(f_k-f_i)}\\ =\frac{NT}{2\pi j}\sum_{\substack{k=1\\k\neq i}}^{N}\frac{\beta_k'(t_0)d_k}{k-i}.\end{aligned}\tag{2.16}$$

Finally, the additive noise term is

$$n_i=\frac{1}{\sqrt{2E_s}}\frac{1}{\sqrt{NT}}\int_0^{NT}n(t)e^{-j2\pi f_i t}dt\tag{2.17}$$

where n_i is a complex Gaussian noise with zero mean and variance N_0/E_s. Thus we have

$$\widehat{d}_i=\underbrace{\beta_i(t_0)d_i}_{desired_signal}+\underbrace{\frac{NT}{2\pi j}\sum_{\substack{k=1\\k\neq i}}^{N}\frac{\beta_k'(t_0)d_k}{k-i}}_{ICI}+n_i\,.\tag{2.18}$$

In Section 2.4 we establish the statistical properties of the ICI term. Here, we obtain the C/I ratio and we compare the result with those obtained in [71],[17],[19], and [20], which are based on different models for the time variations.

From Equation (2.18), the average power of the desired signal is

$$C=E[|\beta_i(t_0)d_i|^2]=E[|\beta_i(t_0)|^2]E[|d_i|^2]=1\,.\tag{2.19}$$

Since $R_{\beta_k,\beta_k}(\tau)=R_1(\tau)$ is infinitely differentiable, all (mean-square) derivatives of the process $\{\beta_k(t),-\infty<t<\infty\}$ exist. In particular, the first-order derivative process $\{\beta_k'(t),-\infty<t<\infty\}$ is a zero mean complex-valued Gaussian process with correlation function $E[\beta_k'(t+\tau)(\beta_k'(t))^*]=-R_1''(\tau)$ (identical for all k) with corresponding spectral density

$$\psi_3(f)=\begin{cases}\frac{(2\pi f)^2}{\pi F_d\cdot\sqrt{1-(\frac{f}{F_d})^2}} & |f|\leq F_d\\ 0 & otherwise\end{cases}\tag{2.20}$$

Then,

$$E[|\beta_k'(t)|^2]=\int_{-\infty}^{\infty}\psi_3(f)df=\int_{-F_d}^{F_d}\frac{(2\pi f)^2}{\pi F_d\sqrt{1-(\frac{f}{F_d})^2}}df=2\pi^2{F_d}^2\,.\tag{2.21}$$

Thus, the power of the interference (ICI) is

$$\begin{aligned} I &= E\left[\left|\frac{NT}{2\pi j}\sum_{\substack{k=1\\k\neq i}}^{N}\frac{\beta_k'(t_0)d_k}{k-i}\right|^2\right] \\ &= \left(\frac{NT}{2\pi}\right)^2\sum_{\substack{k=1\\k\neq i}}^{N}\sum_{\substack{l=1\\l\neq i}}^{N}\frac{1}{(k-i)(l-i)}E\left[(\beta_k'(t_0)d_k)(\beta_l'(t_0)d_l)^*\right] \\ &= \left(\frac{NT}{2\pi}\right)^2\sum_{\substack{k=1\\k\neq i}}^{N}\sum_{\substack{l=1\\l\neq i\\k\neq l}}^{N}\frac{1}{(k-i)(l-i)}E\left[(\beta_k'(t_0)d_k)(\beta_l'(t_0)d_l)^*\right] \\ &\quad +\left(\frac{NT}{2\pi}\right)^2\sum_{\substack{k=1\\k\neq i}}^{N}\frac{1}{(k-i)^2}E\left[|\beta_k'(t_0)d_k|^2\right] \\ &=: J_1+J_2. \end{aligned}$$

Note that $(\beta_k'(t_0), \beta_l'(t_0))$ is independent of (d_k, d_l). Also, the d_k's are i.i.d. with zero means. Thus $J_1 = 0$. It then follows that

$$I = \left(\frac{NT}{2\pi}\right)^2\sum_{\substack{k=1\\k\neq i}}^{N}\frac{E[|\beta_k'(t_0)|^2]E[|d_k|^2]}{(k-i)^2} = \frac{(NTF_d)^2}{2}\sum_{\substack{k=1\\k\neq i}}^{N}\frac{1}{(k-i)^2}. \tag{2.22}$$

Thus the signal to interference ratio (C/I) ratio can be expressed as

$$\frac{C}{I} = \frac{1}{\frac{(NTF_d)^2}{2}\sum\limits_{\substack{k=1\\k\neq i}}^{N}\frac{1}{(k-i)^2}} \tag{2.23}$$

The C/I curve of the middle subcarrier, i.e., subcarrier index $k = N/2$, is plotted versus the Doppler frequency F_d in Figure 2.3 (a). The OFDM system is assumed to have $N = 256$ sub-carriers, with subcarrier spacing $\Delta f = 1/NT = 7.81KHz$, and carrier frequency $f_c = 2GHz$. The C/I curve given in Figure 2.3 (a) matches very well with the results given in [71][17][20], which were obtained without the use of Taylor series approximation. Furthermore, using an expanded scale in Figure 2.3 (b), we compare our analytical result with the upper and lower bounds on C/I given by Li and Cimini [19].

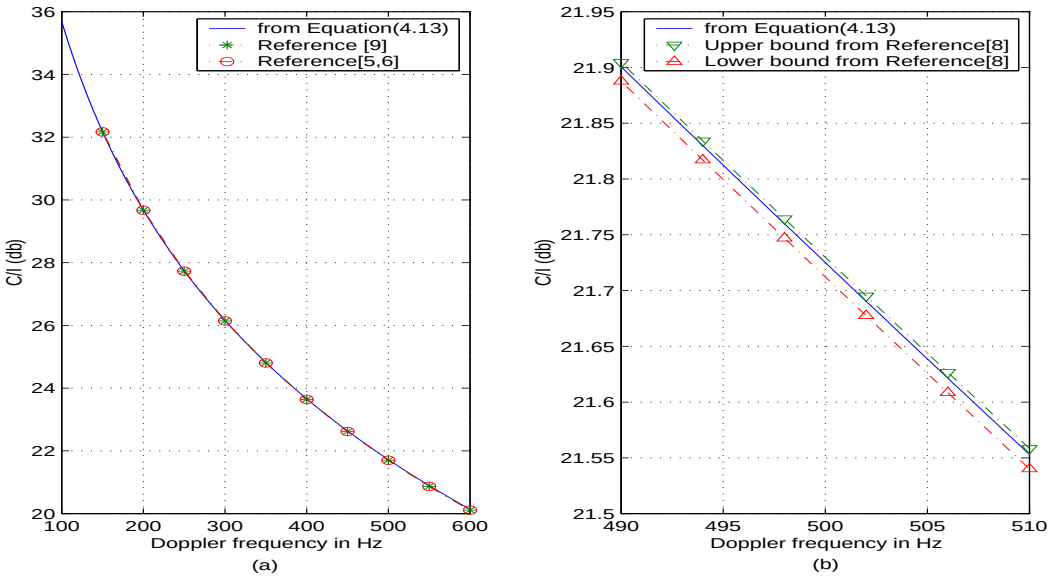


Figure 2.3 C/I ratio curves of an OFDM system $N = 256$ subcarriers, subcarrier distance $\Delta f = 7.81KHz$, and carrier frequency $f_c = 2GHz$

In order to evaluate the approximation effect embodied in the two-term Taylor series expansion, we also demonstrate in Figure 2.4 the comparison of the C/I ratio curves of the same OFDM system in very high Doppler frequency regimes. We can observe from Figure 2.4 that the two-term Taylor series expansion model well approximates the actual fading channel up to a relatively large Doppler frequency 10000Hz, i.e., the two-term Taylor series expansion model becomes inaccurate only when F_d is larger than 10000Hz, which is equivalent to a normalized Doppler frequency of 1.28. This is larger than any practical wireless fading channel for OFDM applications. For example, if we consider 802.11a with carrier frequency of $5GHz$, the terminal must be moving at a speed of 2160km/hr. Overall, the two term Taylor expansion channel model is a very good approximation of the time variations encountered in many physical channels.

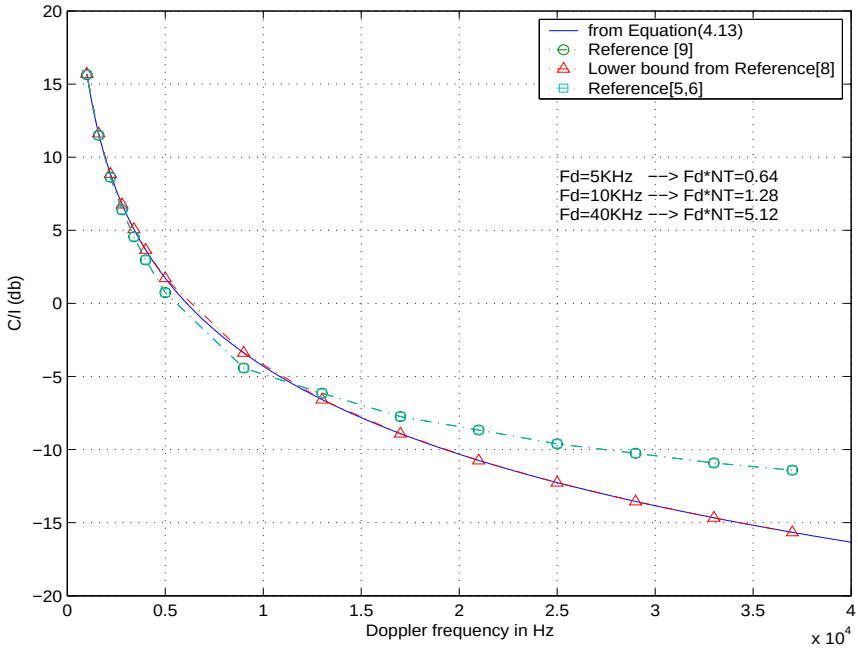


Figure 2.4 C/I ratio curves of an OFDM system $N = 256$ subcarriers, subcarrier distance $\Delta f = 7.81KHz$, and carrier frequency $f_c = 2GHz$

2.4 The Distribution and Moments of the ICI

In this section we derive expressions for the bivariate probability density and joint moments of the ICI complex random variable Z including a two-dimensional Gram-Charlier expansion. We carry out this analysis in a fairly general setting so that the results can be applied to situations where the channel model and the signal constellation are different from those assumed in the previous sections. Let

$$Z := \sum_{k=1}^{N} a_k X_k d_k \tag{2.24}$$

where the a_k's are real-valued constants and the sets of random variables $\{X_k\}_{k=1}^N$ and $\{d_k\}_{k=1}^N$ are independent. The random vector $\tilde{\boldsymbol{X}} := (X_1, \ldots, X_N)^T$ is complex-valued circular Gaussian with zero mean and $N \times N$ complex-valued covariance matrix $\widetilde{\Sigma} = E[\tilde{\boldsymbol{X}} \tilde{\boldsymbol{X}}^{*T}]$. We allow $\widetilde{\Sigma}$ to be an arbitrary covariance matrix. It is readily evident from (2.24) that, given the $\{d_k\}$, Z is conditionally complex Gaussian random variable. We seek an explicit expression for the the joint probability density of its real and imaginary parts. Decompose X_k into its real and imaginary parts, $X_k = X_{k,r} + jX_{k,i}, k = 1, \ldots, N$, and define the $2N \times 1$ real-valued Gaussian vector $\boldsymbol{X} := [X_{1,r} \cdots X_{N,r} X_{1,i} \cdots X_{N,i}]^T$. The $2N \times 2N$ real-valued covariance matrix $\Sigma = E[\boldsymbol{X}\boldsymbol{X}^T]$ is given by (see for example [30])

$$\Sigma = \frac{1}{2} \begin{bmatrix} \Re[\widetilde{\Sigma}] & -\Im[\widetilde{\Sigma}] \\ \Im[\widetilde{\Sigma}] & \Re[\widetilde{\Sigma}] \end{bmatrix} =: \begin{bmatrix} \Sigma_{11} & -\Sigma_{12} \\ \Sigma_{12} & \Sigma_{22} \end{bmatrix}. \tag{2.25}$$

Next the signal constellation points d_k's are assumed to be i.i.d. complex-valued random variables and we set $d_k = d_{k,r} + jd_{k,i}$ for its real and imaginary parts. Again, in the general setting here, we do <u>not</u> assume that $d_{k,r}$ and $d_{k,i}$ are independent taking values with equal probabilities. Instead we assume that

$$P[d_{k,r} = b_l, d_{k,i} = c_m] = p_{l,m}, \ l, m = 1, \ldots, L$$

where b_l and c_m are real-valued. This allows general signal constellations. Finally the constants $\{a_k\}$ appearing in (2.24) are arbitrary; in the special

case that will be considered later, we set $a_k = 1/(k-i)$, for $k \neq i$ and $a_k = 0$ for $k = i$. In this case, $ICI = \frac{NT}{2\pi j} Z$.

Decompose the complex-valued random variable Z of (2.24) into its real and imaginary parts,

$$Z := Z_r + jZ_i = \sum_{k=1}^{N} a_k[X_{k,r}d_{k,r} - X_{k,i}d_{k,i}] + j\sum_{k=1}^{N} a_k[X_{k,r}d_{k,i} + X_{k,i}d_{k,r}] \quad (2.26)$$

and let $f_{Z_r,Z_i}(u,v)$ be its joint probability density. We first seek an expression for this density and its joint moments.

It can be seen that $f_{Z_r,Z_i}(u,v)$ is a Gaussian mixture and one can write

$$f_{Z_r,Z_i}(u,v) = \sum_{l_1=1}^{L}\sum_{m_1=1}^{L} \cdots \sum_{l_N=1}^{L}\sum_{m_N=1}^{L} \left(\prod_{n=1}^{N} p_{l_n,m_n}\right) f_{Y_1,Y_2}(u,v)$$

where $f_{Y_1,Y_2}(u,v)$ is a bivariate Gaussian density with zero means and 2×2 dimensional covariance matrix whose entries depend on $(b_{l_1},\ldots,b_{l_N};c_{m_1},\ldots,c_{m_N})$ (i.e., on the values of the signal constellation points $\{d_k\}_{k=1}^{N}$). Moreover, one can verify that under our assumptions we have $\mathrm{cov}\{Y_1,Y_2\} = 0$ whereas the variance of Y_1 and Y_2 are identical and given by

$$\begin{aligned}\sigma_Y^2(b_{l_1},\ldots,b_{l_N};c_{m_1},\ldots,c_{m_N}) &= \sum_{i=1}^{N}\sum_{k=1}^{N} a_i a_k \sigma_{11}(i,k)[b_{l_i}b_{l_k} + c_{m_i}c_{m_k}] \\ &+ \sigma_{12}(i,k)[-c_{m_i}b_{l_k} + b_{l_i}c_{m_k}] \qquad (2.27)\end{aligned}$$

where $\sigma_{11}(i,k)$ is the (i,k)th entry of the matrix Σ_{11} and $\sigma_{12}(i,k)$ is the (i,k)th entry of the matrix Σ_{12} defined in (2.25). It follows that

$$f_{Z_r,Z_i}(u,v) = \sum_{l_1=1}^{L}\sum_{m_1=1}^{L} \cdots \sum_{l_N=1}^{L}\sum_{m_N=1}^{L} \left(\prod_{n=1}^{N} p_{l_n,m_n}\right) f_{Y_1}(u) f_{Y_2}(v) \qquad (2.28)$$

where $f_Y(u)$ is a one-dimensional Gaussian density with zero mean and variance given by (2.27). Equation (2.28) allows the computation of the joint moments of (Z_r, Z_i). We have

$$E[Z_r^{k_1} Z_i^{k_2}] = \sum_{l_1=1}^{L}\sum_{m_1=1}^{L} \cdots \sum_{l_N=1}^{L}\sum_{m_N=1}^{L} \left(\prod_{n=1}^{N} p_{l_n,m_n}\right) E[Y_1^{k_1}] E[Y_2^{k_2}]$$

and since

$$E[Y^k] = \begin{cases} 1 \times 3 \ldots \times (k-1)\sigma_Y^k, & k \text{ even} \\ 0, & k \text{ odd} \end{cases}$$

it follows that

$E[Z_r^{k_1} Z_i^{k_2}] =$

$$\begin{cases} \sum_{l_1=1}^{L} \sum_{m_1=1}^{L} \cdots \sum_{l_N=1}^{L} \sum_{m_N=1}^{L} \left(\prod_{n=1}^{N} p_{l_n,m_n} \right) [1 \cdot 3 \cdots (k_1-1)][1 \cdot 3 \cdots (k_2-1)] \sigma_Y^{k_1+k_2}, \\ \qquad\qquad\qquad\qquad\qquad\qquad\qquad\qquad\qquad\qquad k_1 \& \; k_2 \; even \\ 0, \qquad\qquad\qquad\qquad\qquad\qquad\qquad\qquad\qquad\qquad \text{otherwise} \end{cases} \tag{2.29}$$

Note that when the real and imaginary parts of the signal constellation points are independent and equally probable, there is a significant simplification in (2.28) and (2.29) since then $p_{l,m}$ is a constant. Computationally, finding $f_{Z_r,Z_i}(u,v)$ from (2.28) is very intensive for large N and L since the dependence on the values of the signal constellation points appear in the exponent of the Gaussian density $f_Y(u)$ via its variance σ_Y^2. On the other hand, computing the joint moments $E[Z_r^{k_1} Z_i^{k_2}]$ is considerably simpler as the dependence on the values of the constellation points appear directly in σ_Y and only in term of sums of products of <u>two</u> values as seen from (2.27). We therefore plan to use the joint moments $E[Z_r^{k_1} Z_i^{k_2}]$ to obtain an approximation of the joint probability density $f_{Z_r,Z_i}(u,v)$. This is carried out below using a two-dimensional Gram-Charlier expansion.

The one-dimensional Gram-Charlier expansion and its rate of convergence are as follows [31] [32]: Let $\phi(x)$ be the standard Gaussian probability density with zero mean and unit variance. The nth Hermite polynomial $H_n(x)$ is defined by $H_n(x) := (-1)^n e^{x^2/2} D^n[e^{-x^2/2}]$ where D stands for derivative. $H_n(x)$ is given explicitly as

$$H_n(x) = n! \sum_{k=0}^{[n/2]} \frac{(-1)^k x^{n-2k}}{k!\, 2^k\, (n-2k)!}\,. \tag{2.30}$$

The first few Hermite polynomials are given by

$$\begin{aligned} H_0(x) &= 1, \\ H_1(x) &= x, \\ H_2(x) &= x^2 - 1, \\ H_3(x) &= x^3 - 3x, \\ H_4(x) &= x^4 - 6x^2 + 3. \end{aligned} \tag{2.31}$$

The Hermite polynomials satisfy the orthogonality relationship

$$\int_{-\infty}^{\infty} H_n(x) H_k(x) \phi(x) dx = n!\, \delta_{n,k} \tag{2.32}$$

where $\delta_{n,k}$ is the Kronecker delta. Let $g(x)$ be a probability density function of a real-valued random variable X. It can be expanded in a Gram-Charlier series

$$g(x) = \sum_{n=0}^{\infty} \theta_n H_n(x) \phi(x) \tag{2.33}$$

where the coefficient θ_n is given by

$$\theta_n = \frac{1}{n!} \int_{-\infty}^{\infty} g(x) H_n(x) dx = \frac{1}{n!} E[H_n(X)] \tag{2.34}$$

and by (2.30), can be expressed in terms of the moments of X up to order n:

$$\theta_n = \sum_{k=0}^{[n/2]} \frac{(-1)^k E[X^{n-2k}]}{k!\, 2^k\, (n-2k)!}. \tag{2.35}$$

The convergence properties of the Gram-Charlier series are presented in [32]: Set

$$g_K(x) := \sum_{n=0}^{K} \theta_n H_n(x) \phi(x) \tag{2.36}$$

then if $g(x)$ has s continuous derivatives satisfying certain integrability conditions ([32], Theorem II and Corollary I), we have

$$|g(x) - g_K(x)| \leq \frac{constant}{K^{s/2}} \tag{2.37}$$

uniformly in x. Thus, the smoother $g(x)$ is, the better the approximation of $g(x)$ by $g_K(x)$. In two-dimensions, the Gram-Charlier series takes the following form (see for example [33]): Let (X, Y) be jointly distributed random variables with probability density function $g(x, y)$. We can then represent $g(x, y)$ in a two-dimensional Gram-Charlier series

$$g(x,y) = \sum_{n=0}^{\infty}\sum_{m=0}^{\infty} \theta_{n,m} H_n(x) H_m(y) \phi(x)\phi(y) \tag{2.38}$$

where the coefficient $\theta_{n,m}$ is given by

$$\theta_{n,m} = \frac{1}{n!\,m!}\int_{-\infty}^{\infty}\int_{-\infty}^{\infty} H_n(x)H_m(y)g(x,y)dxdy = \frac{1}{n!\,m!}E[H_n(X)H_m(Y)]. \tag{2.39}$$

In view of (2.30), it is seen that $\theta_{n,m}$ can be expressed in terms of the joint moments of (X, Y):

$$\theta_{n,m} = \sum_{k=0}^{[n/2]}\sum_{l=0}^{[m/2]} \frac{(-1)^{k+l} E[X^{n-2k}Y^{m-2l}]}{k!\,l!\,2^{k+l}\,(n-2k)!\,(m-2l)!}. \tag{2.40}$$

Applying the representation (2.38) to the bivariate density $f_{Z_r,Z_i}(u, v)$ we have

$$f_{Z_r,Z_i}(u,v) = \sum_{n=0}^{\infty}\sum_{m=0}^{\infty} \theta_{n,m} H_n(u) H_m(v) \phi(u)\phi(v) \tag{2.41}$$

where the coefficient $\theta_{n,m}$ is now given by

$$\theta_{n,m} = \sum_{k=0}^{[n/2]}\sum_{l=0}^{[m/2]} \frac{(-1)^{k+l} E[Z_r^{n-2k}Z_i^{m-2l}]}{k!\,l!\,2^{k+l}\,(n-2k)!\,(m-2l)!}. \tag{2.42}$$

Note that by (2.29) $\theta_{n,m}$ is nonzero only if both n and m are even. In practice the two-dimensional Gram-Charlier series (2.41) is truncated at a total order K, i.e.,

$$f^{(K)}_{Z_r,Z_i}(u,v) = \sum_{\substack{n=0\\ n+m\le K}}^{\infty}\sum_{m=0}^{\infty} \theta_{n,m} H_n(u) H_m(v) \phi(u)\phi(v). \tag{2.43}$$

Thus if, say, $K = 4$, we only need to compute the marginal moments $E[Z_r^4]$ and the joint moment $E[Z_r^2 Z_i^2]$ in (2.29); in turn this only requires the computation of σ_Y^2 of (2.27).

It should be noted that the standard Gram-Charlier expansion is generated by a normalized Gaussian density $\phi(x)$ with zero mean and unit variance. Clearly, if the variables Z_r and Z_i in (2.43) have variances substantially different from one, we are likely to need large truncation level K for an acceptable approximation. This problem could be easily remedied as follows: Let s_1^2 and s_2^2 be the variances of the random variables Z_r and Z_i respectively. We can generate a two-dimensional Gram-Charlier expansion starting from Gaussian density functions with zero means and variances s_1^2 and s_2^2. It is easy to see that instead of (2.41) we now have

$$f_{Z_r,Z_i}(u,v) = \frac{1}{s_1 s_2} \sum_{n=0}^{\infty} \sum_{m=0}^{\infty} \bar{\theta}_{n,m} H_n(u/s_1) H_m(v/s_2) \phi(u/s_1) \phi(v/s_2) \tag{2.44}$$

with coefficients

$$\bar{\theta}_{n,m} = \sum_{k=0}^{[n/2]} \sum_{l=0}^{[m/2]} \frac{(-1)^{k+l} E[Z_r^{n-2k} Z_i^{m-2l}]}{k!\, l!\, 2^{k+l}\, s_1^{n-2k}\, s_2^{m-2l} (n-2k)!\, (m-2l)!} \tag{2.45}$$

and the representation is truncated at $n + m \leq K$.

We now specialize the above general results to the case introduced in the previous sections. For the covariance matrix of the vector $\boldsymbol{X}$, set

$$X_{k,r} := \Re[\beta_k'(t_0)], \quad X_{k,i} := \Im[\beta_k'(t_0)]. \tag{2.46}$$

It then follows from (2.5) that the (i,k)th component of the covariance matrix Σ_{11} is given by

$$\sigma_{11}(i,k) := E[X_{i,r} X_{k,r}] = -\frac{1}{2} R_1''(0) \Re[R_2(i-k)], i,k = 1,\ldots,N. \tag{2.47}$$

Similarly, it is seen that the (i,k)th component of the covariance matrix Σ_{12} is given by

$$\sigma_{1,2}(l,k) := E[X_{l,r} X_{k,i}] = \frac{1}{2} R_1''(0) \Im[R_2(l-k)]. \tag{2.48}$$

Note that this vanishes for $l = k$. Next we specify the values and corresponding probabilities of the signal constellation points. Unlike the general formulation

earlier, we now assume that $d_{k,r}$ and $d_{k,i}$ are independent taking values from a square M-point QAM signal constellation with equal probabilities

$$P[d_{k,r} = ld] = P[d_{k,i} = ld] = \frac{1}{\sqrt{M}},\ l = \pm 1, \pm 3, \ldots, \pm(\sqrt{M} - 1). \tag{2.49}$$

This corresponds to setting $p_{l,m} = \frac{1}{\sqrt{M}}$ with $L = \sqrt{M}$ in our general formulation. Finally, we set $a_k = 1/(k-i),$ for $k \neq i$ and $a_k = 0$ for $k = i$. Thus for the special case, the expression for σ_Y^2 of (2.27) remains applicable with a_k as specified above and $b_k = kd,\ c_m = md$ and the values of $\sigma_{11}(i,k)$ and $\sigma_{12}(i,k)$ are specified in (2.47) and (2.48) respectively. The expression for $f_{Z_r,Z_i}(u,v)$ of (2.28) simplifies to

$$f_{Z_r,Z_i}(u,v) = \frac{1}{M^{N-1}} \sum_{l_1} \sum_{m_1} \cdots \sum_{l_N} \sum_{m_N} f_{Y_1}(u) f_{Y_2}(v) \tag{2.50}$$

where we use the compact notation

$$\sum_{l} := \sum_{\substack{l=-(\sqrt{M}-1) \\ l\ odd}}^{\sqrt{M}-1}. \tag{2.51}$$

The joint moments $E[Z_r^{k_1} Z_i^{k_2}]$ simplify to $E[Z_r^{k_1} Z_i^{k_2}] = \frac{1}{M^{N-1}}$

$$\times \begin{cases} \sum_{l_1} \sum_{m_1} \cdots \sum_{l_N} \sum_{m_N} [1 \times 3 \ldots \times (k_1 - 1)][1 \times 3 \ldots \times (k_2 - 1)] \sigma_Y^{k_1+k_2}, \\ \qquad\qquad\qquad\qquad\qquad\qquad\qquad\qquad k_1 \text{ and } k_2 \text{ even} \\ 0, \qquad\qquad\qquad\qquad\qquad\qquad\qquad\qquad \text{otherwise} \end{cases} \tag{2.52}$$

The truncated two-dimensional Gram-Charlier representation is again given by (2.43) with coefficients $\theta_{n,m}$ given by (2.42) involving the joint moments $E[Z_r^{k_1} Z_i^{k_2}]$ now given by (2.52). Thus, we only need to obtain an expression for σ_Y^2. Straightforward calculations using (2.27) (2.47) and (2.48) show that

$$\sigma_Y^2 = \left(\frac{NTF_d}{2}\right)^2 d^2 \sum_{\substack{r=1 \\ r\neq i}}^{N} \sum_{\substack{s=1 \\ s\neq i}}^{N} \frac{\Re[\psi_2(\Delta f(r-s))](l_r l_s + m_r m_s) + \Im[\psi_2(\Delta f(r-s))](-m_r l_s + l_r m_s)}{(r-i)(s-i)}. \tag{2.53}$$

Similar computations hold for the scaled Gram-Charlier expansion (2.44).

The above Gram-Charlier approximation method can be easily applied to Rician fading statistics. The only difference in applying the above proposed approximation approach is to adjust the corresponding ICI joint moments. In this chapter, our results are limited to Rayleigh fading statistics.

2.5 Evaluation of OFDM System Performance

We now evaluate the error probability for an M-QAM system with coherent detection. In view of (2.18) and (2.24) we can write

$$\widehat{d_i} = \beta_i(t_0)d_i + \frac{NT}{2\pi j}Z + n_i \tag{2.54}$$

where Z represents the ICI contribution whose statistics were thoroughly studied in Section 2.4. We assume that we have perfect knowledge of $\beta_i(t_0)$ in each sub-channel and we form the decision variable

$$\widehat{D}_i = \frac{\widehat{d}_i\,\beta_i{}^*(t_0)}{|\beta_i(t_0)|^2} = d_i + \frac{NT}{2\pi j}\,\frac{Z\,\beta_i^*(t_0)}{|\beta_i(t_0)|^2} + \frac{n_i\,\beta_i^*(t_0)}{|\beta_i(t_0)|^2}. \tag{2.55}$$

Set $a := NT/(2\pi)$, $Z = Z_r + jZ_i$, $\beta_i(t_0) = W_1 + jW_2$, and $n_i = n_{i,1} + jn_{i,2}$ for their real and imaginary parts. Then

$$\Re[\widehat{D}_i] = \Re[d_i] + \frac{a(Z_iW_1 - Z_rW_2)}{W_1^2 + W_2^2} + \frac{n_{i,1}W_1 + n_{i,2}W_2}{W_1^2 + W_2^2} \tag{2.56}$$

$$\Im[\widehat{D}_i] = \Im[d_i] - \frac{a(Z_rW_1 + Z_iW_2)}{W_1^2 + W_2^2} + \frac{n_{i,2}W_1 - n_{i,2}W_2}{W_1^2 + W_2^2}. \tag{2.57}$$

A final decision is made by comparing the location of random variable $\widehat{D}_i$ with the M-QAM constellation points and selecting the signal point that is nearest to d_i. The decision of the detector is based on (2.55): Assuming a symmetric rectangular QAM signal constellation, the detector performs independent decisions on the real and imaginary parts conditioned on a particular channel realization $\beta_i(t_0)$ and ICI realization Z. A symbol error occurs if either the real or imaginary components are in error. Let A_i be the event of making an error in the real (or imaginary) part in the i^{th} sub-channel. Then, conditioned on a particular channel realization $\beta_i(t_0)$ and ICI realization Z, we have the following equations for the probability of error in the x (real) and y (imaginary) parts:

$$P_s^x[A_i|Z = u + jv, \beta_i(t_0) = w_1 + jw_2] = \frac{L-1}{L}$$
$$\left[Q\left(\frac{d(w_1^2 + w_2^2) + a(vw_1 - uw_2)}{[(N_0/2E_s)(w_1^2 + w_2^2)]^{1/2}}\right) + Q\left(\frac{d(w_1^2 + w_2^2) - a(vw_1 - uw_2)}{[(N_0/2E_s)(w_1^2 + w_2^2)]^{1/2}}\right)\right] \tag{2.58}$$

$$P_s^y[A_i|Z=u+jv,\beta_i(t_0)=w_1+jw_2]=\frac{L-1}{L}$$
$$\left[Q\left(\frac{d(w_1^2+w_2^2)+a(uw_1+vw_2)}{[(N_0/2E_s)(w_1^2+w_2^2)]^{1/2}}\right)+Q\left(\frac{d(w_1^2+w_2^2)-a(uw_1+vw_2)}{[(N_0/2E_s)(w_1^2+w_2^2)]^{1/2}}\right)\right] \tag{2.59}$$

where $d=\sqrt{\frac{3}{2(M-1)}}$ with $L^2=M$. The conditional symbol error probability is then given by

$$\begin{aligned}P_s[A_i|Z=u+jv,\beta_i(t_0)=w_1+jw_2]=&\\ 1-\Big((1-P_s^x[A_i|Z=u+jv,\beta_i(t_0)=w_1+jw_2])&\\ \times(1-P_s^y[A_i|Z=u+jv,\beta_i(t_0)=w_1+jw_2])\Big)&\end{aligned} \tag{2.60}$$

In order to obtain unconditional probability of error, we average over the distributions of the ICI variable Z and over the distribution of $\beta_i(t_0)$. We first note that the bivariate probability density $f_{Z_r,Z_i}(u,v)$ of the ICI disturbance Z is given in (2.50) and its Gram-Charlier approximation by (2.43). We further note that the ICI complex random variable Z and the channel random variable $\beta_i(t_0)$ are independent. This follows from the following argument: The process $\{\beta_l(t),-\infty<t<\infty\}$ is complex Gaussian with covariance function $R_{\beta_l,\beta_l}(\tau)=R_1(\tau)$ given by (2.7). The derivative process $\{\beta_k'(t),-\infty<t<\infty\}$ is complex Gaussian with covariance function $R_{\beta_k',\beta_k'}(\tau)=-R_1''(\tau)$. The cross covariance function $R_{\beta_k',\beta_l}(\tau)=R_1'(\tau)R_2(k-l)$ which vanishes at $\tau=0$. Since the processes are jointly Gaussian, the random variable $\beta_i(t_0)$ is independent of the random variables $\{\beta_k'(t_0)\}_{k=1}^N$ and thus independent of Z in view of the ICI term in (2.18). We finally note that the the real and imaginary parts of $\beta_i(t_0)$ are independent zero mean Gaussian random variables with identical variance equals 1/2. Thus

$$\begin{aligned}P_s[A_i]=&\int_{-\infty}^{\infty}\int_{-\infty}^{\infty}\int_{-\infty}^{\infty}\int_{-\infty}^{\infty}P_s[A_i|Z=u+jv,\beta_i(t_0)=w_1+jw_2]\\ &\times f_{Z_r,Z_i}(u,v)f_W(w_1)f_W(w_2)dudvdw_1dw_2\end{aligned} \tag{2.61}$$

where $f_W(w)=\frac{1}{\sqrt{\pi}}e^{-w^2}$. The above multidimensional integration can be evaluated by numerical integrations. The system performance is obtained by aver-

aging over all sub-channels,

$$P_s = \frac{1}{N}\sum_{i=1}^{N} P_s[A_i]. \tag{2.62}$$

Since the probability density $f_{Z_r,Z_i}(u,v)$ of the ICI variable is quite involved (see (2.50)), we use the Gram-Charlier approximation developed in Section 2.4. We have

$$f^{(K)}_{Z_r,Z_i}(u,v) = \frac{1}{s^2}\sum_{\substack{n=0\\ n+m\le K}}^{\infty}\sum_{m=0}^{\infty} \bar{\theta}_{n,m} H_n(u/s)H_m(v/s)\phi(u/s)\phi(v/s). \tag{2.63}$$

with coefficients $\bar{\theta}_{n,m}$ given by (2.45) and with joint moments given by (2.52). Here $s^2 = \mathrm{var}[Z_r] = \mathrm{var}[Z_i]$. This leads to an approximate probability of error,

$$P_s^{(K)} = \frac{1}{N}\sum_{i=1}^{N} P_s^{(K)}[A_i]. \tag{2.64}$$

Figures 2.5 through 2.6 illustrate the symbol error probability of uncoded 16-QAM OFDM system with bandwidth $W = 1/T = 1MHz$ over a frequency-selective channel with an exponential multipath power intensity and channel coherence bandwidth ($3dB$ bandwidth) of $W/4$ under different Doppler spreads, F_d, of 231.5 and $926.0Hz$, corresponding to mobile speeds of 50 and $200km/hr$. The carrier frequency is $f_c = 5GHz$. At the higher speeds, we observe that the ICI causes a large deterioration in performance as the number N of subcarriers increases. When the average SNR (E_b/N_0) is large, the ICI is ultimately the limiting factor in performance at any speed and for any N.

Figure 2.7 provides a comparison in error rate performance between BPSK (bit error probability) and 16-QAM (symbol error probability) when the mobile speed is $100km/hr$. In this case, we observe that the ICI causes a significantly higher degradation in performance for 16-QAM compared with that for BPSK.

Next we compare the performance for two practical OFDM systems. One is an IEEE 802.11a system, the other is a Digital Video Broadcasting

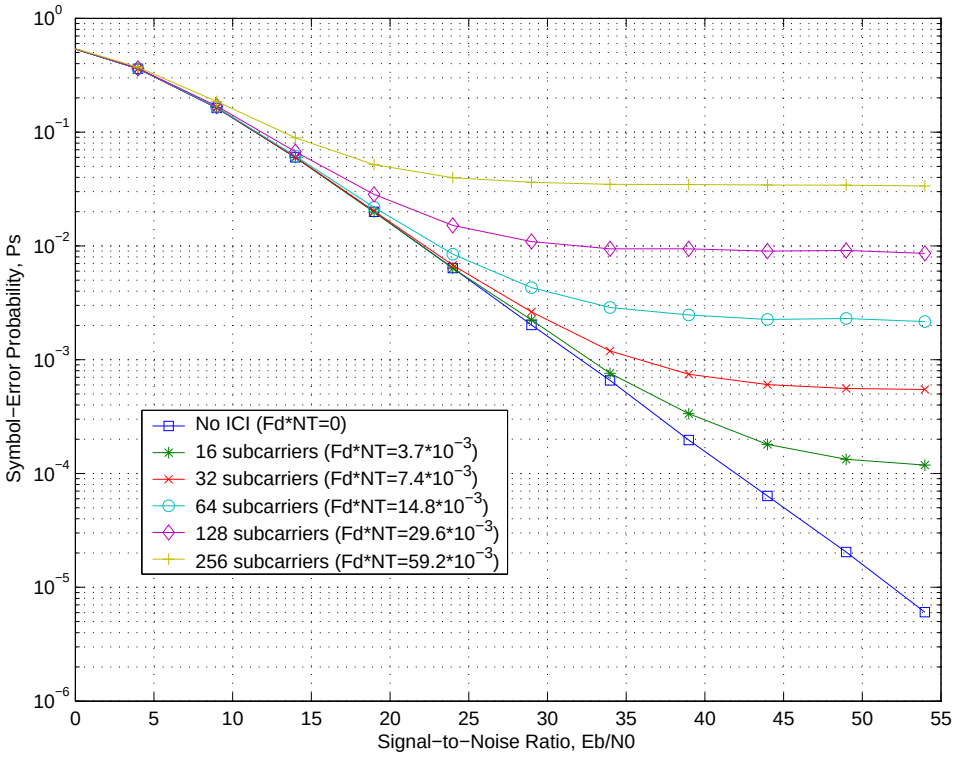


Figure 2.5 Performance for 16-QAM OFDM system with $f_c = 5$ GHz, $T = 1\mu$s ($W \approx 1MHz$), and speed of 50km/hr

(DVB) system operating in the CS2 mode. Both systems are operating at a signal to noise ratio (SNR) of $40dB$ in a vehicle traveling at a speed of $200km/hr$ and both employ uncoded 16-QAM modulation. The SER degradation for the two systems is different for the same mobile Rayleigh fading channel. As can be seen in the Table 2.1, the average error rates of 802.11a and DVB-CS2 increase by 1.94 times and 155 times respectively, compared to the case of no Doppler spread.

Table 2.1: Performance Degradation vs. Doppler Spread

	OFDM symbol (NT)	Carrier Frequency	Doppler Spread F_d at $v = 200km/hr$	SER $\times 10^{-4}$	SER No Doppler $\times 10^{-4}$
802.11a	$4\mu s$	$5GHz$	$1KHz$	3.5	1.8
DVBCS2	$500\mu s$	$480MHz$	$0.1KHz$	278	1.8

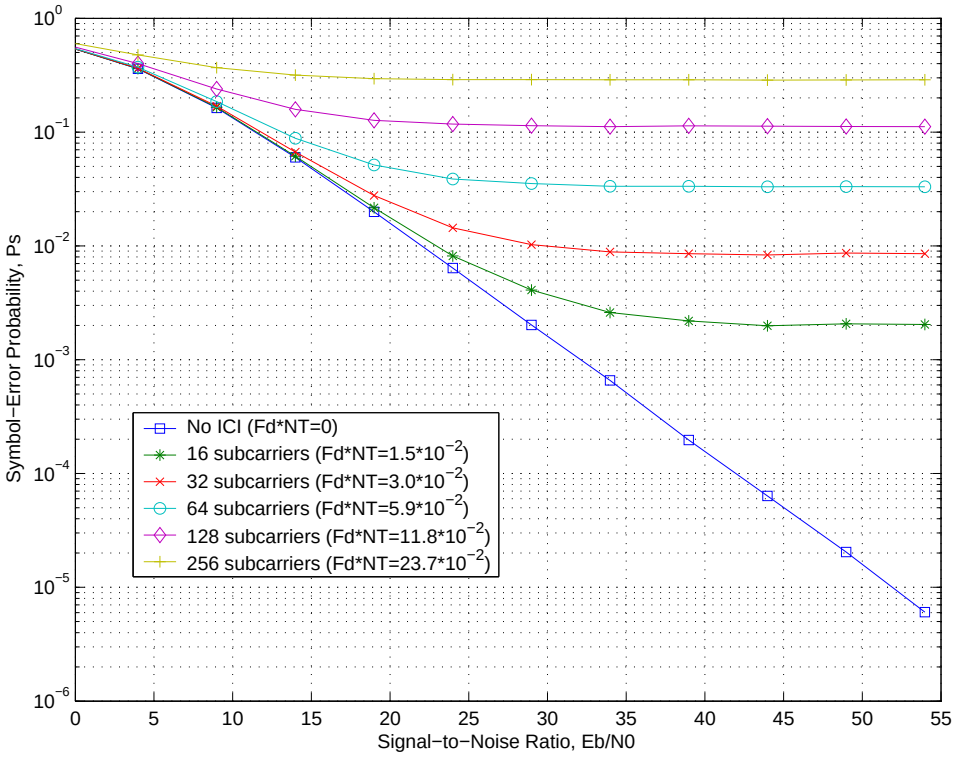


Figure 2.6 Performance for 16-QAM OFDM system with $f_c = 5$ GHz, $T = 1\mu$s ($W \approx 1MHz$), and speed of 200km/hr

The error probability shown in Figure 2.5 through 2.7 were evaluated by using equations (2.61), (2.63), and (2.64) with $K = 4$ in the Gram-Charlier expansion. We found that $K = 4$ provides a very close agreement with the error rate performance obtained from Monte Carlo simulation. For example, Figure 2.8 illustrates the probability of a symbol error for 16-QAM and a mobile speed of 100 km/hr for three different orders of the Gram-Charlier series, $K = 2, 4, 6$, and the result obtained from simulation. We observe that $K = 4$ provides a very close approximation to the simulation results. We point out that Gram-Charlier approximations of orders $K = 0$ and $K = 2$ both result in a bivariate Gaussian pdf with uncorrelated (Z_r, Z_i) components. Consequently, the approximation for $K = 0$ and $K = 2$ corresponds to the case in which the ICI is modeled as bivariate Gaussian with uncorrelated real and imaginary components. Figure

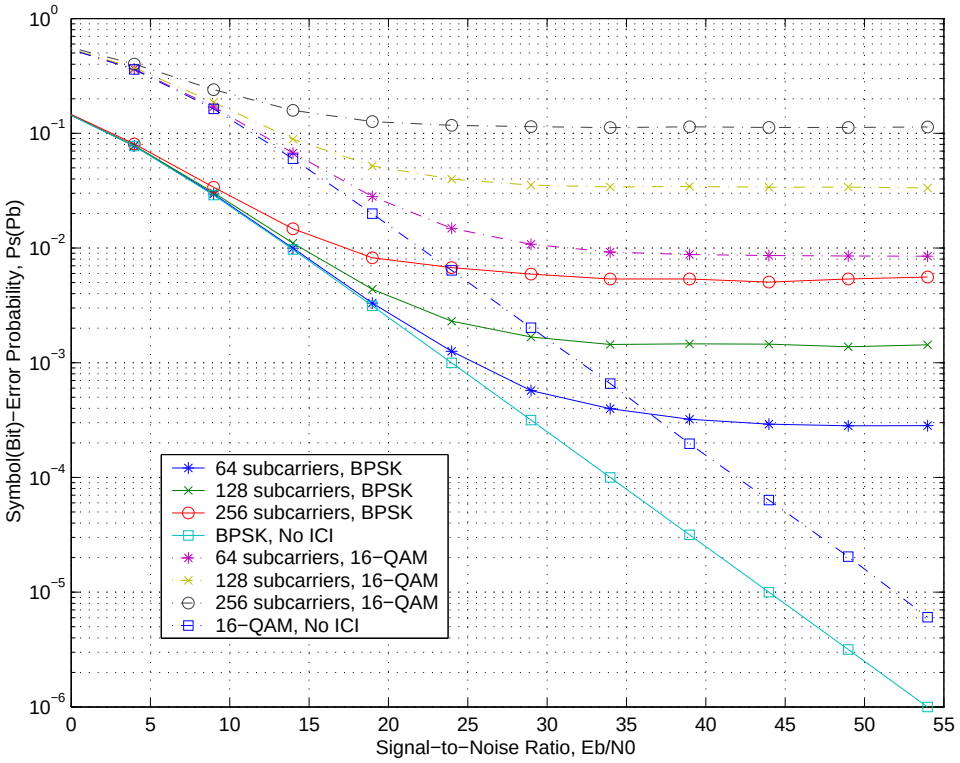


Figure 2.7 Performance comparison for BPSK OFDM and 16-QAM OFDM system with $f_c = 5$ GHz, $T = 1\mu$s ($W \approx 1MHz$), and speed of 100km/hr

2.9 illustrates the comparison of the performance obtained with the Gaussian approximation (Gram-Charlier expansion of order 2) for the ICI and the non-Gaussian approximation (Gram-Charlier expansion of order 4). We note that the Gaussian model ($K = 2$) give results that differ from the simulation results illustrated in Figure 2.8 and the non-Gaussian approximation (G.C. order 4) in Figure 2.9 by one or more dB depending on the SNR. The mismatch between the Gaussian approximation and the actual system performance is due to the fact that the ICI interference is not Gaussian distributed, as is illustrated in Section 2.4. The most important feature of the Gram-Charlier approximation lies in the property that it makes use of the higher order statistics (moments) of the ICI, by employing a higher order Gram-Charlier approximation. Thus, the Gram-Charlier expansion provides a better match to the pdf of the ICI

than the Gaussian approximation (which is based on second order statistics).

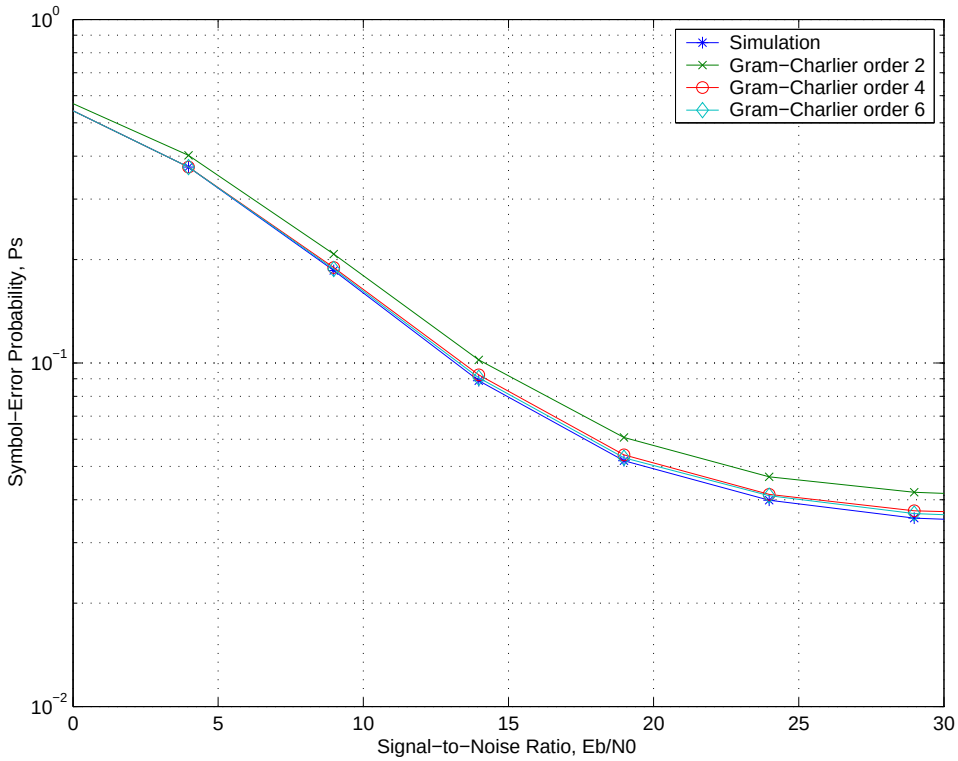


Figure 2.8 Performance for 16-QAM system with 128 subcarriers, $fc = 5$ GHz, $T = 1\mu$s ($W \approx 1MHz$), and speed of 100km/hr

There is also a major difference between Gram-Charlier approximation of higher order $K \geq 4$ and a Gaussian approximation for the ICI. In a Gaussian approximation, the system performance only depends on the number of OFDM subcarriers and the normalized Doppler spread, due to the fact the second order moment of the ICI only depends on these two parameters. Therefore, the performance approximation obtained with the Gaussian model for the ICI can not represent the effect of channel frequency selectivity of the overall OFDM system. On the other hand, by using Gram-Charlier approximation, the ICI joint moments of order $K \geq 4$ do not only depend on the normalized Doppler frequency and the number of subcarriers, but also depend on the correlation structure among the subcarriers (hence the power delay pro-

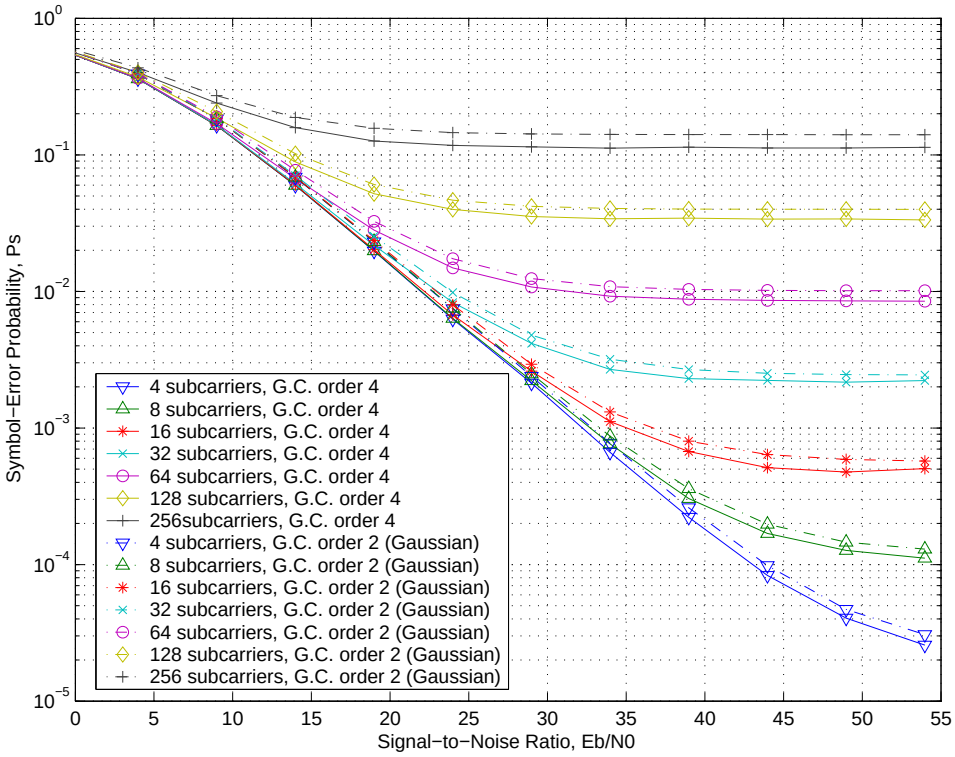


Figure 2.9 Performance for 16-QAM OFDM system with $f_c = 5$ GHz, $T = 1\mu$s ($W \approx 1MHz$), and speed of 100km/hr

file of the frequency selective fading channel), and the baseband modulation constellations. Therefore, the Gram-Charlier approximation provides us with a much more accurate approach in evaluating the performance of an OFDM system under different frequency selective fading channel conditions. As an example, we demonstrate in Figure 2.10 the system performance curves as well as their Gram-Charlier approximations (of order 4) of the same OFDM system transmitting over different frequency-selective fading channels with coherence bandwidth $W/4$ and $W/32$. We observe from the plot that the proposed Gram-Charlier approximation (with order $K = 4$) accounts for the effects of frequency-selectivity on ICI interference whereas the simple Gaussian approximation does not.

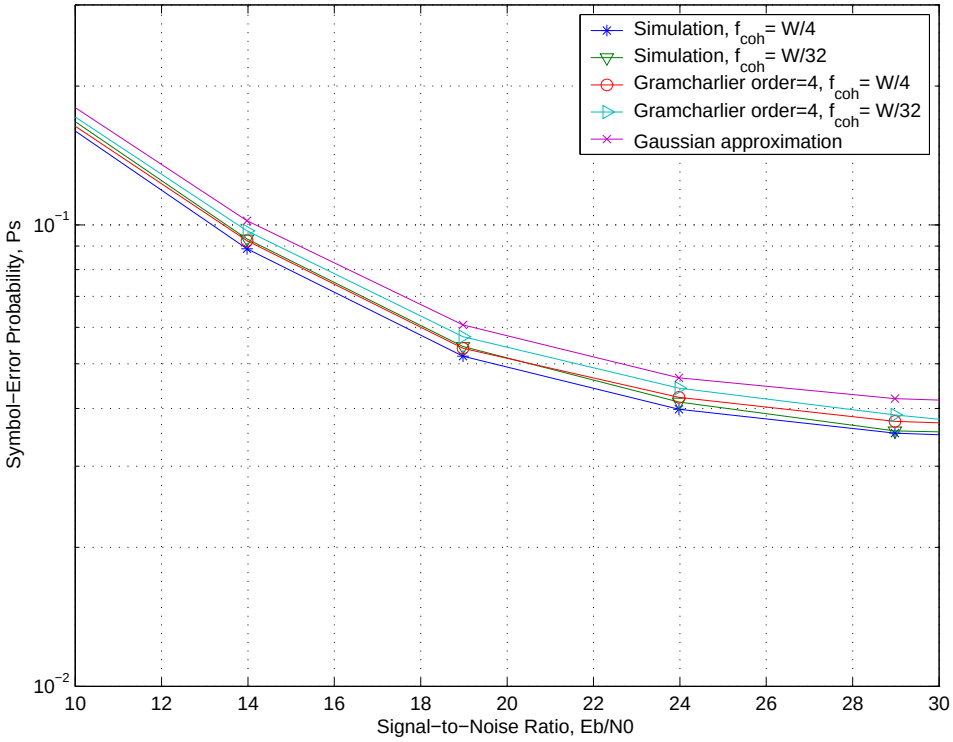


Figure 2.10 Performance for 16-QAM OFDM system with 128 subcarriers, $fc = 5$ GHz, $T = 1\mu$s ($W \approx 1MHz$), speed of 100km/hr, and transmitting over different frequency-selective fading channels

2.6 Conclusion

In this chapter, the performance of an OFDM system was analyzed with respect to its sensitivity to Doppler related inter-carrier interference. We obtained explicit formulas for the bivariate probability density of the ICI, its joint moments, as well as two-dimensional Gram-Charlier representation and approximation. The performance of the OFDM system was obtained based on a truncated Gram-Charlier expansion of the ICI bivariate density. The effect of the Doppler spread in a time variant mobile radio channel on the performance of QAM and BPSK OFDM systems was evaluated. The performance of OFDM systems for M-ary PSK can be evaluated in a similar manner using the methods described in this chapter.

Acknowledgement

The text in this chapter, in part, was originally published in the following papers, of which I was the primary researcher and author: T. Wang, J. Proakis, and J. Zeidler, "Performance analysis of high QAM OFDM system over frequency selective time-varying fading channel," *in Proc. on Personal, Indoor and Mobile Radio Communications*, 14th IEEE PIMRC, vol. 1, pp. 793-798, September 2003; T. Wang, J. Proakis, E. Masry, and J. Zeidler, "Performance degradation of OFDM system due to Doppler spreading," *IEEE Transactions on Wireless Communications*, vol. 5, NO. 6, June 2006.

3

Suppression of Intercarrier Interference

3.1 Motivation

Channel estimation is an important element of an OFDM receiver that employs coherent demodulation [79][44][45][46][47]. Approaches based on least-squares (LS), minimum mean-square (MMSE) estimation are studied in [79] by exploiting the training sequences that are transmitted along with the data. In [44], a low-rank approximation based on the discrete DFT is proposed by using the frequency correlation of the fading channel. A MMSE channel estimation based on the time and frequency correlation was proposed in [45]. However, in practice, the channel statistics, e.g, channel correlation function and average SNR per bit, are usually not available and the channel statistics may vary in time due to the mobility of the receiver(Doppler spread). In [48][49], a time-frequency polynomial model for channel estimation in OFDM systems is proposed, which does not require the knowledge of the channel statistics. A large polynomial order is required in order to represent the 2-D frequency channel response with sufficient accuracy for a frequency selective fading channel. ICI suppression techniques have been developed with pioneering works, e.g., the method of mapping symbols to a group of subcarriers; self-cancellation schemes, (but at the price of sacrificing spectral efficiency) [50][51][52]; linear approximation of the channel variation during one OFDM symbol [53][54]; frequency-domain equalization [55][56]; and time-domain windowing [57][58]. References [59][60][61], in order to reduce the number of 2D parameters to be estimated, assume each subchannel is a linear combination of the total number of OFDM subchannels when the variation between the subchannels is not significant. Another assumption widely used, e.g., [22][62][63], is that the channel can be assumed to vary linearly or is approximately constant within an OFDM symbol when the OFDM symbol duration is much less than the channel coherence time. Other related papers [64][65] focus on the method of pilot tone placement for optimizing the effect of estimation for rapidly time-varying environments. In [66], a training-based method is proposed to estimate

the frequency offset and then remove the ICI caused by multiplicative frequency offset.

In this chapter, we first propose a new modified polynomial channel estimator for the frequency selective and time-varying fading channel. In contrast to the estimator which estimates the channel response in the frequency domain, the modified estimation algorithm directly estimates the time domain response (has relatively slower variation and requires lower order to polynomial function representations), and hence achieves better estimation quality. Another point is that in [48][49], the fading channel is modelled as constant within one OFDM symbol, but changes from symbol to symbol, which is inaccurate for most cases, especially when ICI is to be shown and analyzed. The modified polynomial channel estimator in our paper not only estimates the variations symbol by symbol, but also within one OFDM symbol. We also propose in this chapter a minimum mean square error (MMSE) criterion-based OFDM receiver structure that takes into account both additive noise and the ICI disturbance. By applying the proposed modified polynomial channel estimation algorithm, a detailed comparison of the performance of a conventional OFDM receiver and a new MMSE-based OFDM receiver is provided. The numerical simulation results of the system performance that are provided under various channel conditions further confirm the superior performance of the MMSE-OFDM receiver over the conventional OFDM receiver.

The rest of the chapter is organized as follows: In Section 3.2, we describe the OFDM system model as well as the frequency-selective time-varying fading channel model considered in this chapter. In Section 3.3, the polynomial model is described for the channel and an estimation algorithm is provided and applied to perform the OFDM channel estimation. In Section 3.4, two different OFDM receiver structures, the conventional OFDM receiver and the MMSE-based receiver are described. In Section 3.5, the numerical system performance of these different detection techniques are presented and compared. Finally,

our conclusions are contained in Section 3.6.

3.2 System Setup

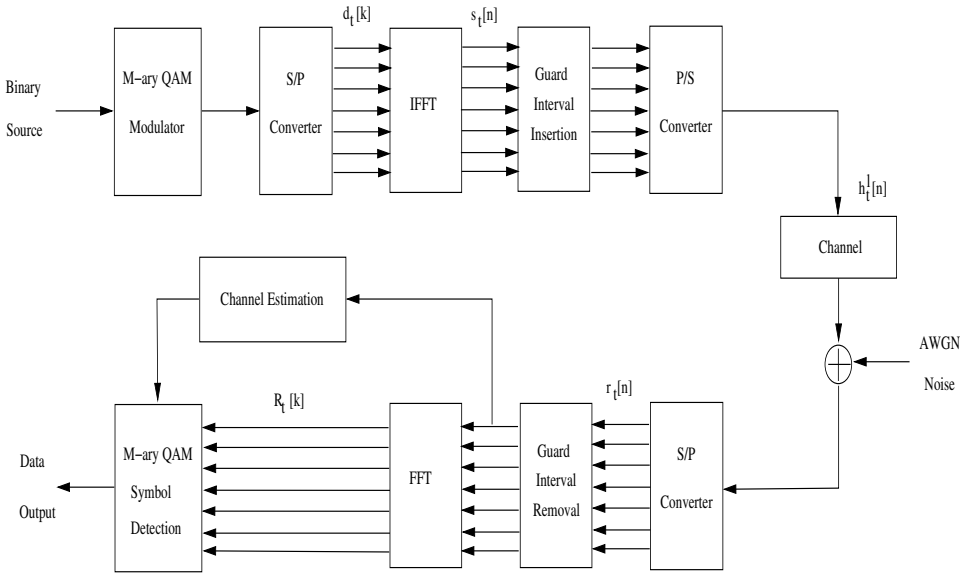


Figure 3.1: Baseband model of the OFDM system

An OFDM system with N subcarriers is considered in this chapter. A block of $N \cdot \log_2 M$ bits of data is first mapped into a sequence $\{d[k]\}$ of M-ary complex symbols of length N, each modulating an orthonormal exponential function $\exp(j\frac{2\pi kn}{N}), k = 0, \cdots, N-1$. Each data symbol $d[k]$ is normalized to have unit average signal power $E[|d[k]|^2] = 1$. As demonstrated in Fig. 3.1, information bearing sequences $\{d[k]\}$ are first serial to parallel converted and processed by an IFFT operation, given by

$$s_t[n] = \frac{1}{\sqrt{N}} \sum_{k=0}^{N-1} d_t[k] \cdot \exp(j\frac{2\pi kn}{N}), \qquad 0 \le n, k \le N-1 \ , \qquad (3.1)$$

where the subscript t represents the t^{th} OFDM symbol. A cyclic prefix is inserted into the transmitted signal to prevent possible intersymbol interference between successive OFDM symbols. After parallel to serial conversion, the signals are transmitted through a frequency-selective time-varying fading channel. At the receiver end, after removing the cyclic guard interval, the sam-

pled received signal is characterized in the following format, by applying the tapped-delay-line model [83]

$$r_t[n] = \sum_{l=0}^{L-1} h_t^l[n] \cdot s_t\big[|n-l|_N\big] + n_t'[n], \qquad n = 0, 1, \cdots, N-1 \ , \tag{3.2}$$

where $h_t^l[n]$ represents the channel response of the l^{th} path during the t^{th} OFDM symbol, L represents the total number of paths of the frequency-selective fading channel given by τ_{max}/T, τ_{max} is the maximum multipath delay, and $T = 1/W$, where W is the channel (OFDM signal) bandwidth, $n_t'[n]$ represents the additive Gaussian noise with zero mean and variance $E[|n_t'[n]|^2] = \sigma^2 = N_0/E_s$, and $|\cdot|_N$ represents the modular N operation.

The fading channel coefficients $h_t^l[n]$ are modelled as zero mean complex Gaussian random variables. Based on the Wide Sense Station Uncorrelated Scattering (WSSUS) assumption, the fading channel coefficients in different delay taps are statistically independent. We also assume that they have an exponential power delay profile, which is given by

$$E\big[\big|h_t^l[n]\big|^2\big] = \alpha \cdot \exp(-\beta \cdot l), \qquad \alpha = \frac{1-\exp(-\beta)}{1-\exp(-L\cdot\beta)} \ . \tag{3.3}$$

In the time domain, the fading coefficients $h_t^l[n]$ are correlated and have a Doppler power spectrum density modelled as in Jakes[84], given by

$$D(f) = \begin{cases} \frac{1}{\pi F_d \cdot \sqrt{1-\left(\frac{f}{F_d}\right)^2}} & |f| \le F_d \\ 0 & otherwise \end{cases} \ , \tag{3.4}$$

where F_d is the Doppler bandwidth. Hence $h_t^l[n]$ has an autocorrelation function given by

$$E[h_t^l[n] \cdot h_t^l[m]^\star] = \alpha \cdot \exp(-\beta \cdot l) \cdot J_0\Big(2\pi(n-m)F_d T_s\Big) \ . \tag{3.5}$$

where $J_0(\cdot)$ is the first kind Bessel function of zero order.

Written in a concise matrix form, we can represent (3.2) as,

$$\mathbf{r_t} = \mathbf{H_t} \cdot \mathbf{s_t} + \mathbf{n_t'} \ , \tag{3.6}$$

where $\mathbf{r_t}$ and $\mathbf{n'_t}$ are vectors of size $N \times 1$, and the channel matrix $\mathbf{H_t}$ is given by

$$\mathbf{H_t} = \begin{bmatrix} h_t^0[0] & 0 & \cdots & 0 & h_t^{L-1}[0] & \cdots & h_t^1[0] \\ h_t^1[1] & h_t^0[1] & 0 & \cdots & 0 & \ddots & \vdots \\ \vdots & \ddots & \ddots & \ddots & \ddots & \ddots & h_t^{L-1}[L-2] \\ h_t^{L-1}[L-1] & \ddots & \ddots & h_t^0[L-1] & 0 & \ddots & 0 \\ 0 & h_t^{L-1}[L] & \ddots & \ddots & h_t^0[L] & \ddots & \vdots \\ \vdots & \ddots & \ddots & \cdots & \ddots & \ddots & 0 \\ 0 & \cdots & 0 & h_t^{L-1}[N-1] & \cdots & h_t^1[N-1] & h_t^0[N-1] \end{bmatrix} . \tag{3.7}$$

Hence the received signal $\mathbf{r_t}$ is related to the data vector $\mathbf{d_t}$ as,

$$\mathbf{r_t} = \mathbf{H_t}\mathbf{W}\cdot\mathbf{d_t} + \mathbf{n'_t}, \qquad \mathbf{W} = \left[w_{n,m}\right]_{N\times N}, \quad w_{n,m} = \exp(j\frac{2\pi nm}{N})/\sqrt{N} \ , \tag{3.8}$$

where $\mathbf{W}$ is the inverse Fourier transformation matrix.

From another point of view, the received signal can be expressed in terms of the equivalent frequency domain channel model as

$$r_t[n] = \frac{1}{\sqrt{N}} \sum_{k=0}^{N-1} d_t[k] \cdot \tilde{h}_t^k[n] \exp\left(j\frac{2\pi kn}{N}\right) + n'_t[n], \quad n = 0, 1, \cdots, N-1 \ , \tag{3.9}$$

where $\tilde{h}_t^k[n]$ is the frequency domain channel response for the k^{th} subcarrier during the t^{th} OFDM symbol. We incorporate the result given by (3.2) into (3.9), then we have the frequency domain channel response $\tilde{h}_t^k[n]$ as

$$\tilde{h}_t^k[n] = \sum_{l=0}^{L-1} h_t^l[n] \exp\left(-j\frac{2\pi lk}{N}\right), \quad n = 0, 1, \cdots, N-1 \ . \tag{3.10}$$

At the receiver side, the FFT operation is performed on each block of N received signal samples $r_t[n]$. Thus, we obtain

$$R_t[k] = \frac{1}{\sqrt{N}} \sum_{n=0}^{N-1} r_t[n] \cdot \exp\left(-j\frac{2\pi kn}{N}\right) \ , \tag{3.11}$$

where $R_t[k]$ represents the received symbol at the k^{th} subcarrier of the t^{th} OFDM symbol.

It also can be written in a concise matrix form as

$$\mathbf{R}_t = \mathbf{W}^H \cdot \mathbf{r_t} = \mathbf{W}^H \mathbf{H_t} \mathbf{W} \cdot \mathbf{d_t} + \mathbf{W}^H \cdot \mathbf{n'_t} = \mathbf{G_t} \cdot \mathbf{d_t} + \mathbf{n_t} \ , \tag{3.12}$$

where $\mathbf{R}_t$, $\mathbf{d_t}$ and $\mathbf{n_t}$ are column vectors of size $N \times 1$, vector $\mathbf{n_t}$ is i.i.d complex white Gaussian noise due to the orthonormal transformation ${\mathbf{W_t}}^H$ of the original noise $\mathbf{n'_t}$, and the matrix $\mathbf{G_t}$ is related to the channel frequency response as follow:

$$\mathbf{G_t} = \mathbf{W}^H \mathbf{H_t} \mathbf{W} = \left[g_t^{i,j} \right]_{N \times N}, \qquad g_t^{i,j} = \frac{1}{N} \sum_{n=0}^{N-1} \tilde{h}_t^j[n] \cdot \exp\left(j \frac{2\pi(j-i)n}{N} \right) \ . \tag{3.13}$$

The decision symbol $R_t[k]$ at the receiver end is unfortunately distorted not only by additive Gaussian noise, but also by ICI as well. We expand (3.12), and represent $R_t[k]$ in the following form:

$$R_t[k] = \left(\frac{1}{N} \sum_{n=0}^{N-1} \tilde{h}_t^k[n] \right) \cdot d_t[k] + \sum_{\substack{i=0 \\ i \neq k}}^{N-1} \left(\frac{1}{N} \sum_{n=0}^{N-1} \tilde{h}_t^i[n] \cdot \exp\left(j \frac{2\pi(i-k)n}{N} \right) \right) \cdot d_t[i] + n_t[k] \ , \tag{3.14}$$

The first term in (3.14) is the desired signal, the second term represents the ICI from the other subcarriers, and finally the third term is the additive noise. Our objective is to reduce the effect of the ICI term by using knowledge of the channel state information.

3.3 OFDM Channel Estimation

In this chapter, we assume that perfect channel state information is not available at the receiver. The channel frequency response $\tilde{h}_t^k[n]$ and time domain impulse response $h_t^l[n]$ are estimated at the receiver end by inserting pilots at some of the subcarriers.

3.3.1 A 2-D Polynomial Surface Channel Estimator

We assume that the frequency-selective time-varying channel response is a mathematically smooth function with respect to time and frequency. Hence, we may model the continuous channel frequency response $\tilde{h}_t^k[n]$ as a 2-D polynomial surface function within a certain time-frequency region as in [48][49]. That is,

$$\tilde{h}_t^k[n] = \sum_{i+j \leq p} a_{i,j} \cdot k^i \cdot \big(t(N+I)+n\big)^j \quad , \tag{3.15}$$

where $\{a_{i,j}\}$ are the polynomial coefficients up to order p, k and $\big(t(N+I)+n\big)$ are the frequency and time indexes of the channel frequency response, and I is the length of the guard interval inserted into each OFDM symbol to avoid inter-symbol interference between consecutive symbols. The objective is to estimate the polynomial coefficients $\{a_{i,j}\}$.

Estimation may be performed every T OFDM symbols, which means that the assumed model region is a $N \times T(N+I)$ $(frequency \times time)$ 2-D plane. Pilots are inserted every p_f subcarriers, and every p_t OFDM symbols. Thus, the overhead ratio attributed to the pilots is $\frac{1}{p_f p_t}$.

In order to estimate the coefficients $\{a_{i,j}\}$ of the channel frequency

response, let us first rewrite (3.15) in the matrix form as

$$\tilde{h}_t^k[n] = \left[a_{p,0}, a_{p-1,1}, \cdots, a_{i,j} \cdots, a_{0,0}\right] \cdot \begin{bmatrix} k^p \\ k^{p-1}\big(t(N+I)+n\big) \\ \vdots \\ k^i \cdot \big(t(N+I)+n\big)^j \\ \vdots \\ 1 \end{bmatrix} = \mathbf{a}^H \cdot \mathbf{q_t^{k,n}} \ , \tag{3.16}$$

where $\mathbf{a}$ is the polynomial channel coefficients to be estimated, and $\mathbf{q_t^{k,n}}$ is a vector given by $\mathbf{q_t^{k,n}} = \left[k^p, k^{p-1}\big(t(N+I)+n\big), \cdots, k^i \cdot \big(t(N+I)+n\big)^j, \cdots, 1\right]^H$.

Since the additive noise in equation (3.12) is spherically symmetric and zero mean Gaussian, the ML estimate of the coefficients vector $\mathbf{a}$ is chosen such that

$$\sum_{(t,k)\in\mathcal{P}} \left| R_t[k] - \sum_{i\in\mathcal{P}_f} \widehat{g_t^{k,i}} \cdot d_t[i] \right|^2 \ , \tag{3.17}$$

is minimized, where the noisy estimated channel response $\widehat{g_t^{k,i}}$ is provided in the following form by applying the polynomial channel model in (3.15)

$$\widehat{g_t^{k,i}} = \frac{1}{N} \sum_{n=0}^{N-1} \widehat{\tilde{h}_t^i}[n] \cdot \exp\big(j\frac{2\pi(i-k)n}{N}\big) = \mathbf{a}^H \cdot \left(\frac{1}{N} \sum_{n=0}^{N-1} \mathbf{q_t^{i,n}} \cdot \exp\big(j\frac{2\pi(i-k)n}{N}\big) \right) \ . \tag{3.18}$$

and the set $\mathcal{P}$ in (3.17) contains all the pilot locations in the detection region, while $\mathcal{P}_f$ contains the frequency locations of the pilots,

$$\begin{aligned} \mathcal{P} &= \Big\{ (m,n) \Big| m = 0, p_f, 2p_f, \cdots, (N/p_f - 1)p_f; n = 0, p_t, 2p_t, \cdots, (T/p_t - 1)p_t \Big\} \ , \\ \mathcal{P}_f &= \Big\{ m \Big| m = 0, p_f, 2p_f, \cdots, (N/p_f - 1)p_f \Big\}. \end{aligned} \tag{3.19}$$

Hence, we can restate the problem of channel estimation, which is equivalent to finding the ML solution of (3.17), as solving

$$\min_{\mathbf{a}} \sum_{(t,k)\in\mathcal{P}} \left| R_t[k] - \mathbf{a}^H \cdot \mathbf{u_t^k} \right|^2 \ , \tag{3.20}$$

where $\mathbf{u_t^k}$ is given by

$$\mathbf{u_t^k} = \frac{1}{N} \sum_{i \in \mathcal{P}_f} \sum_{n=0}^{N-1} d_t[i] \exp\left(j \frac{2\pi(i-k)n}{N}\right) \cdot \mathbf{q_t^{i,n}} \ . \tag{3.21}$$

By taking the complex derivative of (3.20) with respect to $\mathbf{a}^H$ and, after straightforward manipulations, we obtain

$$\begin{aligned} \mathbf{a} &= \mathbf{U}^{-1} \cdot \mathbf{b} \ , \\ \mathbf{U} &= \sum_{(t,k) \in \mathcal{P}} \mathbf{u_t^k} \cdot \mathbf{u_t^k}^H \ , \\ \mathbf{b} &= \sum_{(t,k) \in \mathcal{P}} R_t^H[k] \cdot \mathbf{u_t^k} \ . \end{aligned} \tag{3.22}$$

Once the coefficients vector $\mathbf{a}^H$ is obtained, the estimated channel response within the considered region can be obtained by the following equation,

$$\widehat{\tilde{h}_t^i}[n] = \mathbf{a}^H \cdot \mathbf{q_t^{i,n}} \ , \tag{3.23}$$

where $\mathbf{a}$ and $\mathbf{q_t^{i,n}}$ are given by (3.22) and (3.16).

3.3.2 A Modified Polynomial Channel Estimator

In the estimator described above, a large polynomial order p may be required in order to represent the 2-D frequency channel response $\tilde{h}_t^k[n]$ with sufficient accuracy. If so, it is quite possible that some numerical problems may result from the large condition numbers of the matrix $\mathbf{U}$ in (3.22).

However, if we carefully study equation (3.10), we will observe that the variation of $\tilde{h}_t^k[n]$ with respect to the frequency index k is actually caused by the Fourier transformation of the time-varying fading channel response $h_t^l[n]$ with respect to the multipath index l. Therefore, it is much easier to estimate $h_t^l[n]$ directly using the same polynomial channel model. Thus, the time domain channel response $h_t^l[n]$ requires a small order polynomial function to describe when the channel fading is slow.

Hence we consider the modified polynomial channel estimator based on the model

$$h_t^l[n] = \sum_{i \le p} {a'}_i^l \cdot \big(t(N+I)+n\big)^i, \qquad 0 \le l \le L-1 \ , \tag{3.24}$$

where $h_t^l[n]$ represent the time-varying fading channel response for the l^{th} path, and $\{{a'}_i^l\}$ is the corresponding polynomial coefficient up to order p. Written in a matrix form, we have the following:

$$h_t^l[n] = {\mathbf{a'}^l}^H \cdot \mathbf{q_t^n} \ , \tag{3.25}$$

where $\mathbf{a'}^l$ and $\mathbf{q_t^n}$ are column vectors of length $(p+1)$ given by,

$$\mathbf{a'}^l = \big[{a'}_p^{\ l}, {a'}_{p-1}^{\ l}, \cdots, {a'}_0^{\ l}\big]^H \ , \tag{3.26}$$

$$\mathbf{q_t^n} = \big[\big(t(N+I)+n\big)^p, \big(t(N+I)+n\big)^{p-1}, \cdots, 1\big]^H \ . \tag{3.27}$$

By stacking the coefficients $\mathbf{a'}^l$ as a column vector,

$$\mathbf{a'} = \big[{\mathbf{a'}^0}^H, {\mathbf{a'}^1}^H, \cdots, {\mathbf{a'}^{L-1}}^H\big]^H \ , \tag{3.28}$$

and applying the same criterion as in the 2-D channel estimator, the optimal polynomial channel coefficient vector $\mathbf{a'}$ is chosen such that equation (3.17) is minimized, where now the estimated channel response $\widehat{g_t^{k,i}}$ is given by the following form according to (3.10) and (3.13),

$$\begin{aligned} \widehat{g_t^{k,i}} &= \frac{1}{N} \sum_{l=0}^{L-1} \sum_{n=0}^{N-1} \widehat{h_t^l}[n] \cdot \exp\big(j\frac{2\pi(i-k)n}{N}\big) \cdot \exp\big(j\frac{-2\pi il}{N}\big) \\ &= \sum_{l=0}^{L-1} {\mathbf{a'}^l}^H \cdot \exp\big(j\frac{-2\pi il}{N}\big) \cdot \Big(\frac{1}{N} \sum_{n=0}^{N-1} \exp\big(j\frac{2\pi(i-k)n}{N}\big) \cdot \mathbf{q_t^n}\Big) \end{aligned} \tag{3.29}$$

Hence the problem of channel estimation is reduced to finding the optimal $\mathbf{a'}$ which minimizes the following:

$$\min_{\mathbf{a'}} \sum_{(t,k) \in \mathcal{P}} \Big| R_t[k] - {\mathbf{a'}^l}^H \cdot \mathbf{v_t^k} \Big|^2 \ , \tag{3.30}$$

where $\mathbf{v_t^k}$ is given by

$$\begin{aligned}
\mathbf{v_t^k} &= \left[\mathbf{v_t^k}^{0H}, \mathbf{v_t^k}^{1H}, \cdots, \mathbf{v_t^k}^{L-1H}\right]^H, \\
\mathbf{v_t^k}^l &= \frac{1}{N}\sum_{i\in\mathcal{P}_f} d_t[i]\cdot\exp\left(j\frac{-2\pi il}{N}\right)\cdot\left(\sum_{n=0}^{N-1}\exp\left(j\frac{2\pi(i-k)n}{N}\right)\cdot\mathbf{q_t^n}\right) \quad (3.31)
\end{aligned}$$

Finally, the modified polynomial channel estimator results in the solution

$$\begin{aligned}
\mathbf{a}' &= \mathbf{V}'^{-1}\cdot\mathbf{b}' \ , \\
\mathbf{V}' &= \sum_{(t,k)\in\mathcal{P}} \mathbf{v_t^k}\cdot\mathbf{v_t^k}^H \ , \\
\mathbf{b}' &= \sum_{(t,k)\in\mathcal{P}} R_t^H[k]\cdot\mathbf{v_t^k} \ . \qquad (3.32)
\end{aligned}$$

3.4 OFDM Data Detection Techniques

In this section, we describe a MMSE-based data detection technique and the conventional OFDM signal detection technique. Both detection techniques rely on the channel estimates that are obtained in Section 3.3.

3.4.1 Conventional OFDM Signal Detection

According to equation (3.14), we observe that the simplest and most commonly used OFDM detection technique performs detection based on the following decision symbol,

$$\widehat{d}_t[k] = \frac{N\big(\sum_{n=0}^{N-1} \widehat{\tilde{h}}_t^k[n]\big)^H}{\Big|\sum_{n=0}^{N-1} \widehat{\tilde{h}}_t^k[n]\Big|^2} \cdot R_t[k] \ , \tag{3.33}$$

where $\widehat{\tilde{h}}_t^k[n]$ is the estimated frequency-domain channel response obtained by the estimation algorithm described in the previous section.

By substituting for $R_t[k]$ from (3.14) into (3.33), we obtain

$$\begin{aligned}
\widehat{d}_t[k] &= \frac{\big(\sum_{n=0}^{N-1} \tilde{h}_t^k[n]\big)\big(\sum_{n=0}^{N-1} \widehat{\tilde{h}}_t^k[n]\big)^H}{\Big|\sum_{n=0}^{N-1} \widehat{\tilde{h}}_t^k[n]\Big|^2} \cdot d_t[k] \\
&+ \sum_{\substack{i=0 \\ i\neq k}}^{N-1} \frac{\Big(\sum_{n=0}^{N-1} \tilde{h}_t^i[n] \cdot \exp\big(j\tfrac{2\pi(i-k)n}{N}\big)\Big)\big(\sum_{n=0}^{N-1} \widehat{\tilde{h}}_t^k[n]\big)^H}{\Big|\sum_{n=0}^{N-1} \widehat{\tilde{h}}_t^k[n]\Big|^2} \cdot d_t[i] \\
&+ \frac{N\big(\sum_{n=0}^{N-1} \widehat{\tilde{h}}_t^k[n]\big)^H}{\Big|\sum_{n=0}^{N-1} \widehat{\tilde{h}}_t^k[n]\Big|^2} \cdot n_t[k] \quad .
\end{aligned} \tag{3.34}$$

As expected, the decision symbol is distorted not only by the additive Gaussian noise, but also the intercarrier interference (ICI) from other subcarriers. Hence the system performance is affected by the time variation of the channel through the introduction of the ICI. As shown in Section 3.5, there exists an error floor resulting from the ICI, even when the signal to additive noise ratio is sufficient high.

3.4.2 MMSE Based Detection

Motivated by the similarities between ICI distortion in OFDM systems and ISI distortion in single carrier systems, we consider an MMSE based detection technique to suppress ICI. By taking both ICI and additive noise into account, the MMSE-based OFDM detection technique is superior to the conventional OFDM detection scheme described above.

Starting from equation (3.12), suppose the best linear receiver structure of the data $d_t[k]$, which minimizes the mean square error, is given by,

$$\widehat{d}_t[k] = \mathbf{c_t^k}^H \cdot \mathbf{R_t} \ , \tag{3.35}$$

where the optimal coefficient vector $\mathbf{c_t^k}$ is a column vector of size $N \times 1$, and minimizes the following mean square error,

$$\min_{\mathbf{c_t^k}} E\Big[\big|d_t[k] - \widehat{d}_t[k]\big|^2\Big] \ . \tag{3.36}$$

By applying the orthogonality principle, we have,

$$E\Big[\mathbf{R_t} \cdot (d_t[k] - \widehat{d}_t[k])^H\Big] = 0 \ . \tag{3.37}$$

which is equivalent to solving the linear equation,

$$E\Big[\mathbf{R_t} \cdot \mathbf{R_t}^H\Big] \cdot \mathbf{c_t^k} = E\Big[\mathbf{R_t} \cdot d_t[k]^H\Big] \ . \tag{3.38}$$

It is straightforward to show that,

$$E\Big[\mathbf{R_t} \cdot \mathbf{R_t}^H\Big] = \mathbf{G_t}\mathbf{G_t}^H + \sigma^2\mathbf{I_N} \ , \tag{3.39}$$

$$E\Big[\mathbf{R_t} \cdot d_t[k]^H\Big] = \mathbf{g_t^k} \ , \tag{3.40}$$

where $\mathbf{g_t^k}$ is the k^{th} row of matrix $\mathbf{G_t}$, and σ^2 is the noise-to-signal ratio N_0/E_s. Hence the optimal linear weighting vector $\mathbf{c_t^k}$ is given by

$$\mathbf{c_t^k} = \big(\mathbf{G_t}\mathbf{G_t}^H + \sigma^2\mathbf{I_N}\big)^{-1} \cdot \mathbf{g_t^k} \ . \tag{3.41}$$

If written in a concise matrix format, the MMSE-based OFDM estimated symbol vector is given by,

$$\widehat{\mathbf{d_t}} = \mathbf{G_t}^H \left(\mathbf{G_t}\mathbf{G_t}^H + \sigma^2 \mathbf{I_N}\right)^{-1} \cdot \mathbf{R_t} \ . \tag{3.42}$$

When we replace $\mathbf{G_t}$ in equation (3.42) by $\widehat{\mathbf{G}}_\mathbf{t}$, we obtain

$$\widehat{\mathbf{d_t}} = \widehat{\mathbf{G}}_\mathbf{t}^H \left(\widehat{\mathbf{G}}_\mathbf{t}\widehat{\mathbf{G}}_\mathbf{t}^{\ H} + \sigma^2 \mathbf{I_N}\right)^{-1} \cdot \mathbf{R_t} \ . \tag{3.43}$$

as the final decision symbol for the new MMSE-based detection technique.

By substituting (3.41) into (3.36), we obtain the minimum mean square error, which is given as

$$E\left[\left|d_t[k] - \widehat{d}_t[k]\right|^2\right] = 1 - \mathbf{g_t^k}^H \left(\mathbf{G_t}\mathbf{G_t}^H + \sigma^2 \mathbf{I_N}\right)^{-1} \mathbf{g_t^k} \ . \tag{3.44}$$

Thus, the average mean square error for the t^{th} OFDM symbol is

$$\frac{1}{N}\sum_{k=0}^{N-1} E\left[\left|d_t[k] - \widehat{d}_t[k]\right|^2\right] = 1 - \frac{1}{N}\left(tr\left[\mathbf{G_t}^H \left(\mathbf{G_t}\mathbf{G_t}^H + \sigma^2 \mathbf{I_N}\right)^{-1} \mathbf{G_t}\right]\right) \ . \tag{3.45}$$

3.5 Numerical Results

In this section, we provide numerical and simulation results for the channel estimation algorithm as well as the performance of the different OFDM detection techniques described in the previous section.

3.5.1 Channel Estimation Results

In general, a multivariate polynomial function of infinite order $p \to \infty$ is required to describe a 2-D continuous frequency selective and time-varying channel $\tilde{h}_t^k[n]$. However, since the channels in which practical OFDM systems operate are slowly time varying and have limited multipath delays, they can be represented by a small order polynomial.

In this chapter, we consider uncoded 16-QAM OFDM systems that have either 16 or 256 subcarriers with carrier frequency of 5 GHz and total bandwidth $W = 1/T = 1MHz$. This system is transmitting over a 4-path frequency selective fading channel having an exponential power delay profile with a Doppler spread $F_d = 312.5Hz$, corresponding to a mobile speed of 67.5 Km/hr. In the system, one entire OFDM channel estimation block is composed of $T = 16$ OFDM symbols, where each symbol has $N = 16$ orthonormal subcarriers. Pilots are inserted every $p_f = 4$ subcarriers, and every $p_t = 4$ OFDM symbols, with pilots overhead ratio $1/(p_t \cdot p_f) = 6.25\%$. The actually channel as well as the estimated channel are shown in Fig. 3.2 and Fig. 3.3 with system signal to noise ratio $E_s/N_0 = 4dB$, where the 2-D polynomial channel model is of order up to $p = 2$. As we can expect, the channel estimation error will become even smaller with higher order p.

As we can see from the above plot when the normalized Doppler spread is small, the channel experiences slow variations over the time index and hence can be represented by a low order polynomial function. However, frequency-selectivity makes the channel changes relatively fast over the fre-

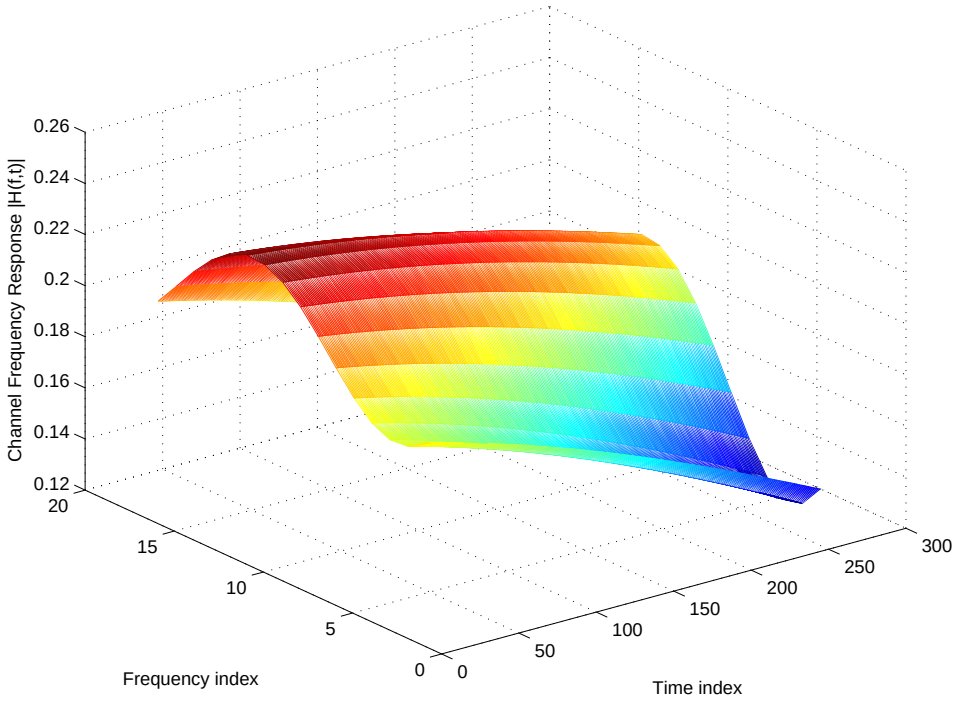


Figure 3.2: Actual Channel

quency domain (index). Therefore, the modified polynomial channel estimator can provide better estimation results with a low order p because it only estimates the time domain polynomial coefficients. The frequency response of the actual channel as well as the estimated channel (generated from the estimated coefficients $\mathbf{a}'$ of the time domain channel impulse response) are shown in Fig. 3.4 and Fig. 3.5, where the polynomial model is of order up to $p = 2$.

3.5.2 Performance Comparison under Perfectly Known Channel

Before applying the channel estimation technique proposed in Section 3.3, a comparison among different detection schemes with perfect channel state information is insightful. Fig. 3.6 demonstrates the system performance curves in terms of the average number of symbol errors versus the signal to noise ratio of conventional OFDM and MMSE-based OFDM receiver structures. The

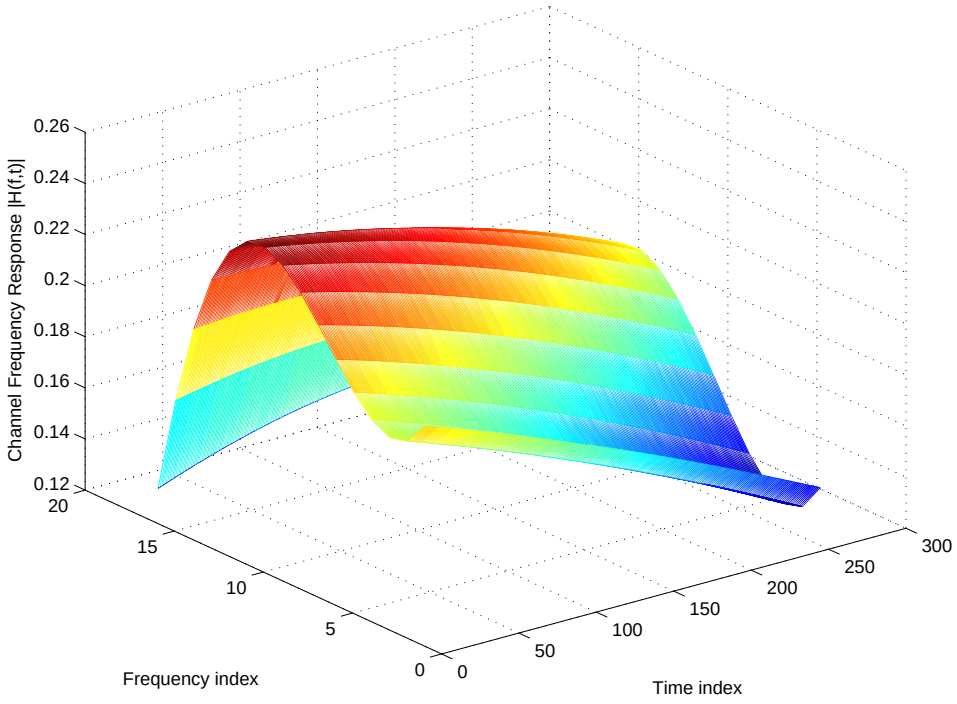


Figure 3.3: Estimated Channel

simulation is performed on the same OFDM system with 16 and 256 subcarriers over the frequency selective time varying fading channel with the same parameters as is described in Section 3.5.1.

As we observe from Fig. 3.6, the conventional OFDM receiver structure has an error floor and its performance is limited by the ICI. The proposed MMSE-based receiver structure performs not only slightly better in low signal to noise ratio range, but is also able to remove the error floor completely in high signal to noise range.

3.5.3 Performance Comparison under Channel Estimation

When the channel state information is not perfectly known at the receiver, the modified polynomial channel estimator is applied to obtain the channel state information. Fig. 3.7 demonstrates the system performance curve of conventional OFDM and MMSE-based OFDM receiver structure using the

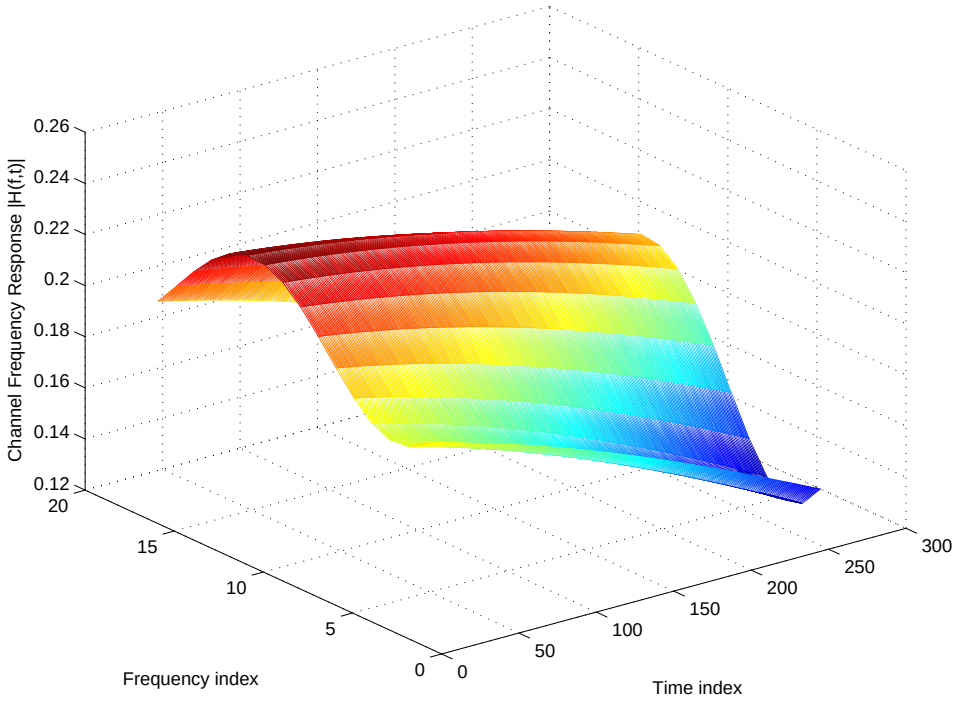


Figure 3.4: Actual Channel

estimated channel state information. The pilots pattern described in Section 3.5.1 is used under the same OFDM system as well as the fading channel parameters.

As expected, we observe from Fig. 3.7 that MMSE-based OFDM receiver structure outperforms the conventional OFDM receiver over the entire signal to noise range using estimated channel state information.

3.5.4 Performance Comparison under Different Channel Estimation Quality

From Section 3.4, we know that there is a mismatch between the actual and the estimated channel state information. Therefore, the quality of the channel estimation directly determines the overall system performance. As a straightforward result, the number of pilot numbers inserted in the OFDM system, or the equivalent pilot overhead ratio $1/(p_f \cdot p_t)$, plays an important

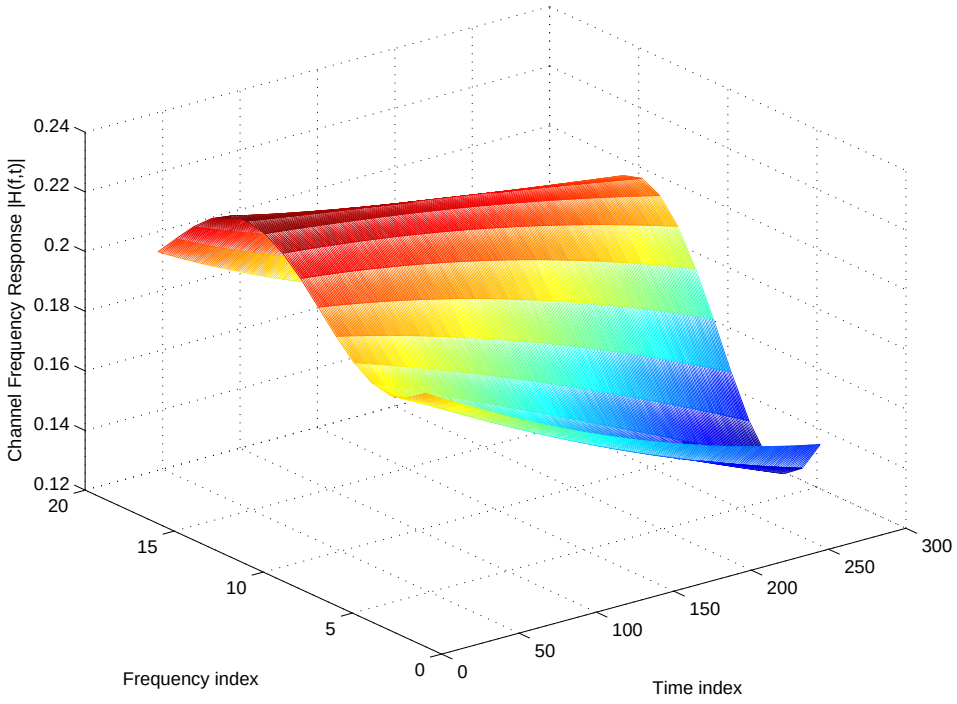


Figure 3.5: Estimated Channel

role in determining the system performance and spectral efficiency trade-offs.

We demonstrate in Fig. 3.8 the average symbol error rate of the same OFDM system with 16 subcarriers over the same channel condition as in Section 3.5.1. The pilots pattern described in Section 3.5.1 is used with different pilots over head, $(p_f, p_t) = (4,4), (4,2), (2,4)$, and $(2,2)$. Similarly, the system performance curves of the same OFDM system with 256 subcarriers over the same fading channels are shown in Fig. 3.9, with all other parameters unchanged. From Fig. 3.8 and Fig. 3.9, we can observe clearly the trade-offs between the system performance and spectral efficiency (pilot overhead ratio).

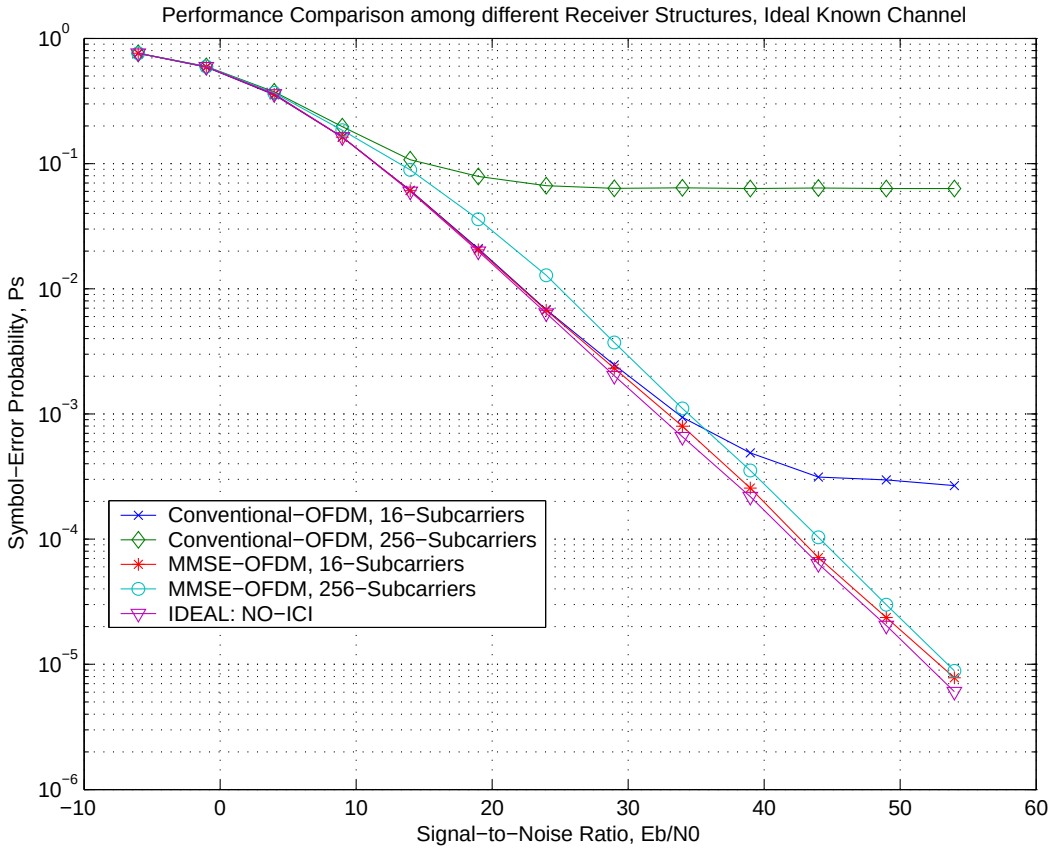


Figure 3.6: Error rate performance for a known channel

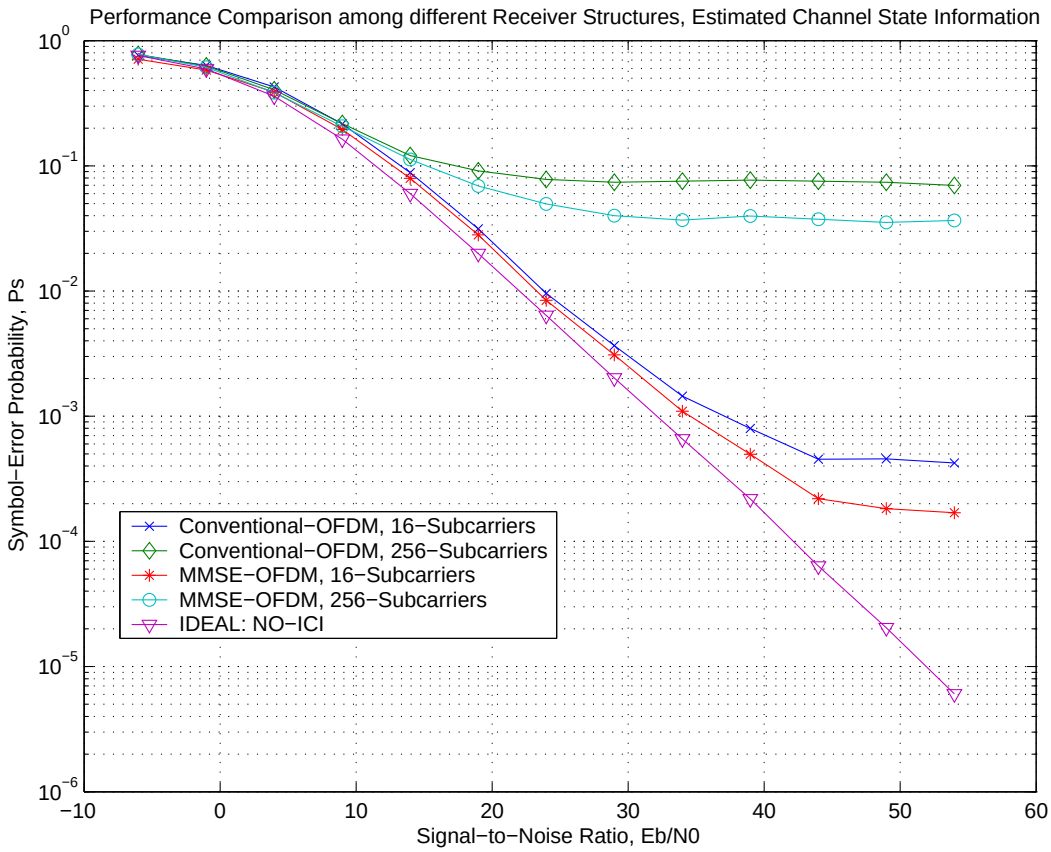


Figure 3.7 Error rate performance using modified polynomial channel estimation

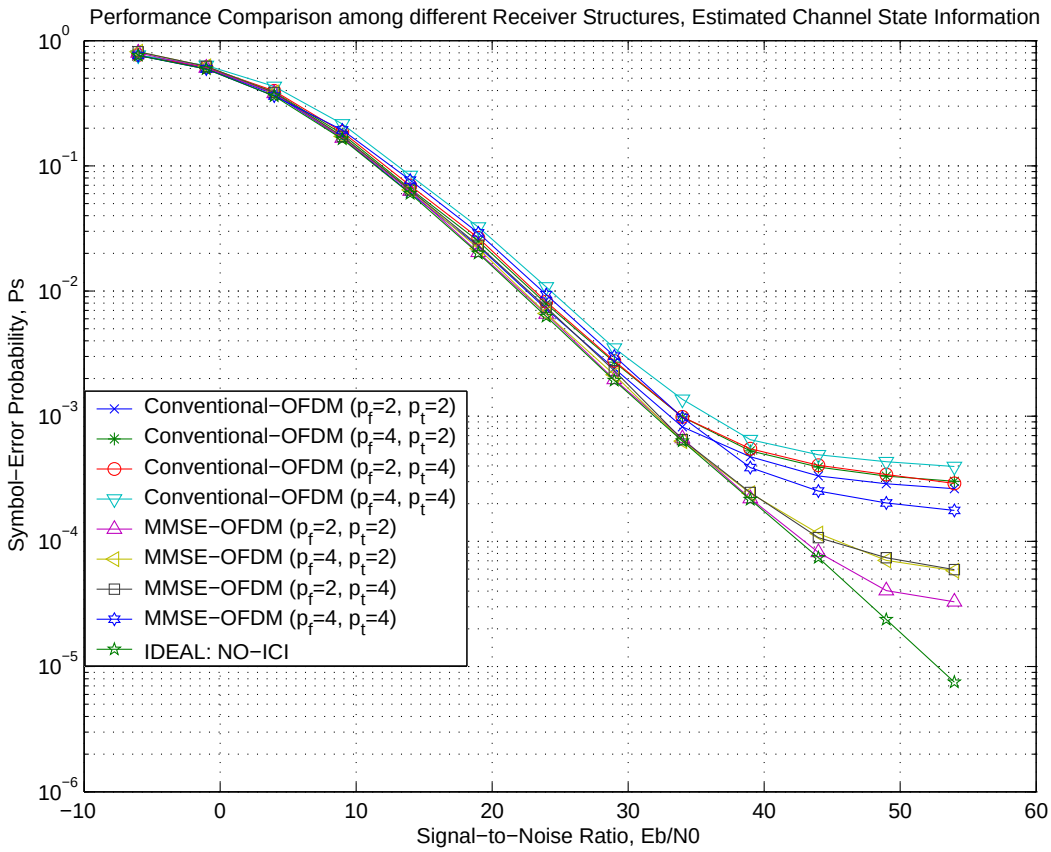


Figure 3.8 Symbol error rate comparison of OFDM system with 16 subcarriers under different channel estimation quality

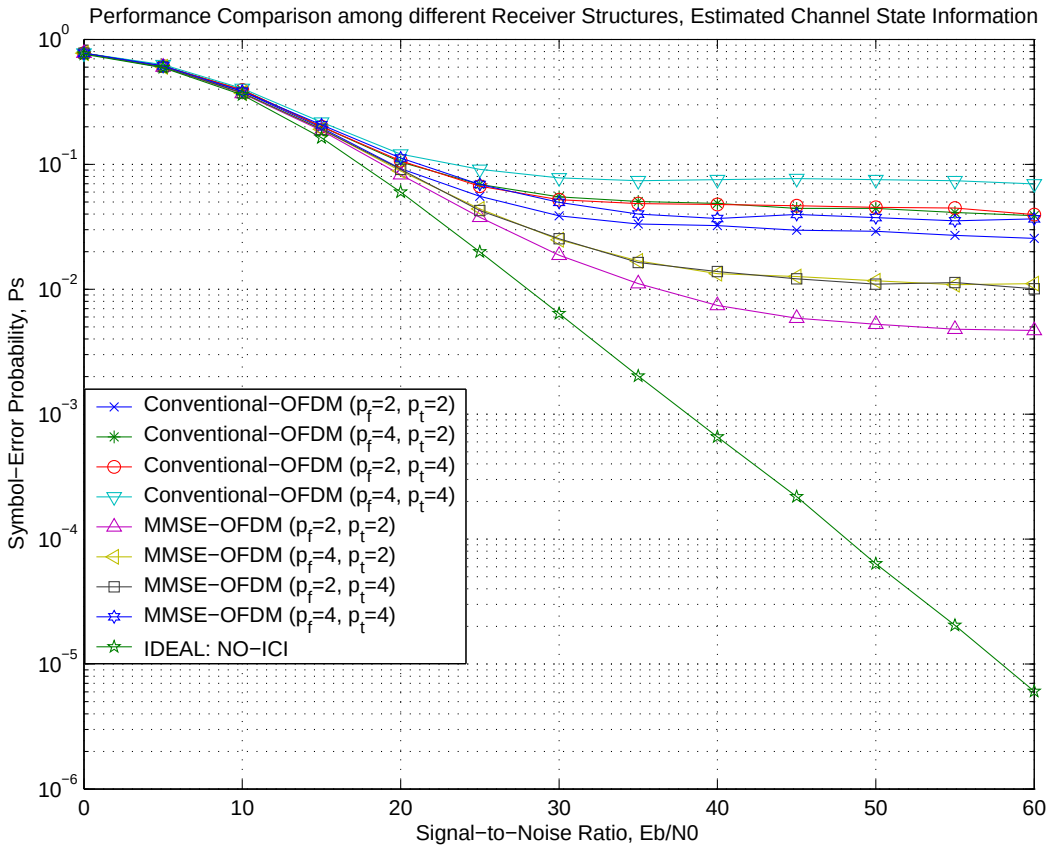


Figure 3.9 Symbol error rate comparison of OFDM system with 256 subcarriers under different channel estimation quality

3.6 Conclusion

In this chapter, in order to combat the ICI distortion caused by Doppler-spread of the time-varying fading channels, the MMSE-based OFDM receiver structure is proposed as the detection technique. System performance is compared with the conventional OFDM receivers under the same channel conditions.

By applying a modified polynomial surface channel estimator, we provide in this chapter the simulation results of the overall system performance, which further confirms that the new MMSE-based OFDM receiver can reduce the symbol error rate more than conventional OFDM receivers under the same Doppler-spread channel environments.

Acknowledgment

The text in this chapter, in part, was originally published in the following papers, of which I was the primary researcher and author: T. Wang, J. Proakis, and J. Zeidler, "Techniques for suppression of Intercarrier Interference in OFDM system," *in Proc. on IEEE Wireless Communications and Network Conference*, IEEE WCNC'05, Vol. 1, pp. 39-44, March 2005.

4

Filtered Multitone Modulation vs. OFDM

4.1 Motivation

Filtered multitone (FMT) modulation is a form of multicarrier modulation that satisfies the perfect reconstruction conditions, in a sense that the sampling signals from the matched filter at the receiver side are free from intersymbol (ISI) as well as interchannel (ICI) interferences. Filtered multitone modulation avoids spectral overlapping between subcarriers by resorting to a noncritical sampling technique [67], where the transmitter upsampling factor K is larger than the number of subcarriers M. FMT has been proposed for data transmission on very high-speed digital subscriber lines (VDSL) [67] [68] and wireless channels [69] to provide high data rate communications with high spectral efficiency, and convenience in spectrum management [67] -[69].

OFDM is another widely used multicarrier modulation in mobile radio applications, such as 802.11a and DVB systems. In contrast, conventional OFDM [70] has overlapping spectra and rectangular impulse responses. Consequently, each OFDM subchannel exhibits a Sinc shape frequency response. Therefore, the time variations of the channel during one OFDM symbol duration destroy the orthogonality of different subcarriers and result in power leakage among subcarriers, known as Intercarrier Interference (ICI), which causes degradation in system performance [71][72][73]. To be specific, the orthogonality of the channel responses in different OFDM subchannels is destroyed at the receiver by the amplitude and phase distortion caused by the fading channel impulse response under certain channel conditions. The fading channel impairments on the orthogonality conditions generally fall into three categories depending on the fading characteristics: quasi-static frequency-flat fading channels do not introduce ISI or ICI to a multi-carrier system; frequency-selective fading channels introduce intersymbol interference, but preserve the orthogonality among different subchannel signals; time-varying frequency-selective channels introduce both intersymbol and interchannel interference.

As compared to an OFDM system using a cyclic prefix (sacrificing

spectral efficiency) to remove ISI, an FMT system uses a noncritical sampling rate technique to mitigate the interference caused by the fading channel. The interference (including ISI and ICI) in an FMT system may be suppressed by choosing a larger non-critical sampling factor (the ratio of the upsampling factor over the number of subcarriers) and hence sacrificing spectral efficiency. The trade-off between possible interchannel (and intersymbol) interference and the corresponding spectral efficiency (or data rate) of the FMT system is therefore an important issue for the system design and comparison with conventional OFDM. Recently, several interesting papers have appeared, addressing this problem from different perspectives in a time-variant and possibly frequency-selective fading environment [74] -[77]. Assalini et al. investigated in [74][75] the effects of frequency offsets and phase noise in FMT and OFDM systems. By evaluating the achievable bit rates of the two systems over different types of channels, they found that FMT has a higher spectral efficiency and is more robust to frequency offset than OFDM. Tonello [76][77] calculated the exact matched filter performance bound for multitone modulated signals in time-varying and frequency-selective fading channels when optimal maximum likelihood detection is employed. In [78] -[81], practical FMT systems including the filter bank design were considered, with the objective of minimizing the intersymbol and interchannel interferences while at the same time maximizing the spectral efficiency.

In this chapter, a system performance analysis is provided for the FMT system over time-frequency dispersive channels. It is known that when the baseband filter at the transmitter and the matched filter at the receiver maintain orthogonality among the subcarriers and also satisfy the Nyquist sampling criterion, there is no interchannel or intersymbol interference in the system as long as the fading channel impulse response is flat and stationary. However, this is not the case for most practical wireless environments when the channel response is not only frequency selective and also time variant.

Basically, both ICI and ISI exist in an FMT system when transmitting over time-varying frequency-selective fading channels. The ICI results from the time-varying channel response which destroys the orthogonality among different sub-channels. In addition, the frequency-selectivity of the fading channel breaks the perfect reconstruction (Nyquist criterion) condition of the base band filters, which leads to the ISI.

First, we focus our attention on investigating the average system carrier to interference (C/I) ratio of the un-equalized FMT system over time-varying frequency-selective fading channels. Through the analysis of the average carrier to interference ratio of the FMT system, an understanding of the trade-off between spectral efficiency and system performance degradation is provided. Furthermore, we provide in this chapter comparisons (both in system C/I ratio and average symbol error rate) between FMT and OFDM systems under the same channel conditions and spectral efficiency.

Secondly, it is shown in Section 4.3 that both ICI and ISI exit in the un-equalized FMT system over over frequency-selective time-varying fading channels, the expected performance gain by using the per-channel equalizer to mitigate the ISI caused by frequency-selective would be significant. By using a per-channel equalizer at the FMT receiver of sufficient length to span the ISI, the ISI is mitigated significantly, but the ICI still exists. On the other hand, OFDM systems usually rely on the presence of the cyclic prefix to combat the ISI. Therefore, it is interesting to investigate the system performance of a per-channel equalized FMT system compared to a un-equalized FMT system as well as a standard OFDM system. A closed-form expression of the upper bound for its C/I ratio is provided for the FMT system with a per-channel equalizer. Numerical and simulation results of the system C/I ratio as well as the average symbol error rate further confirm and support the obtained analytical results.

This chapter is organized as follows: In Section 4.2 we describe the FMT system model, as well as the frequency-selective time-varying fading chan-

nel model considered in this chapter. In Section 4.3, the demodulated signal at the receiver is analyzed in detail under several different channel conditions. The average carrier to interference C/I ratio is also determined to demonstrate the trade-off between performance and spectral efficiency. In Section 4.4, we consider the performance of an FMT system with a per-channel equalizer over frequency-selective time-varying fading channels. In Section 4.5, numerical results of performance for both un-equalized FMT system and per-channel equalized FMT system are presented and compared with an OFDM system under several different channel conditions. Section 4.6 concludes this chapter.

4.2 FMT System Setup

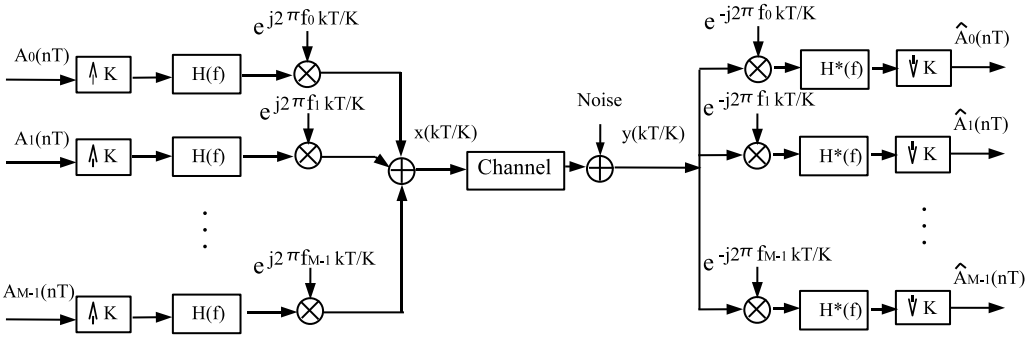


Figure 4.1: System model of the filtered multitone (FMT) modulation system

As illustrated in Fig. 4.1, the complex valued QAM symbols $A_m(nT)$, $m = 0, 1, \cdots, M-1$, are provided at the symbol rate of $1/T$. After upsampling by a factor of K, each symbol stream is filtered by a baseband filter with frequency response $H(f)$ and impulse response $h(k/T)$. The transmitted signal $x(kT/K)$ is obtained by adding the frequency shifted versions of the M filtered outputs from the filters at the transmission rate of K/T, which is given by

$$\begin{aligned} x\big(k\frac{T}{K}\big) &= \sum_{m=0}^{M-1}\sum_{n=-\infty}^{\infty} A_m(nT)\cdot h\Big[(k-nK)\frac{T}{K}\Big]\cdot e^{j2\pi m(\frac{K}{MT})k\frac{T}{K}} \\ &= \sum_{m=0}^{M-1}\sum_{n=-\infty}^{\infty} A_m(nT)\cdot h\Big[(k-nK)\frac{T}{K}\Big]\cdot e^{j2\pi\frac{mk}{M}}\ , \end{aligned} \tag{4.1}$$

where M is the total number of subchannels in the FMT system and K/MT is the frequency spacing between adjacent subchannels. The obtained signal $x(kT/K)$ is transmitted over a time varying, frequency-selective channel. At the receiver end, the received signal after sampling may be expressed as

$$y\big(k\frac{T}{K}\big) = \sum_{l=0}^{L-1} x\Big[(k-l)\frac{T}{K}\Big]\cdot g_l\big(k\frac{T}{K}\big) + w\big(k\frac{T}{K}\big)\ , \tag{4.2}$$

where $g_l(kT/K)$ represents the channel impulse response of the l^{th} path at time kT/K, L represents the total number of paths of the frequency-selective fading

channel, and $w(kT/K)$ represents the additive Gaussian noise with zero mean and variance $E[|w(kT/K)|^2] = \sigma^2 = N_0/E_s$.

The fading channel coefficients $g_l(kT/K)$ are modeled as zero mean complex Gaussian random variables. Based on the wide sense stationary and uncorrelated scattering (WSSUS) assumption, the fading channel coefficients in different delay taps are statistically independent. We also assume that they have an exponential power delay profile, which is given by

$$E\big[\big|g_l(k\frac{T}{K})\big|^2\big] = \alpha \cdot \exp(-\beta \cdot l), \qquad \alpha = \frac{1-\exp(-\beta)}{1-\exp(-L\cdot\beta)} \ . \tag{4.3}$$

The number of fading taps L is given by $\tau_{max}/(T/K)$, where τ_{max} is the maximum multipath delay, and $W = K/T$ is the entire channel bandwidth of the FMT system. The parameter β in equation (4.3) controls the coherence bandwidth of the channel. The $3dB$ channel coherence bandwidth is given by $f_{coh} = \frac{\sqrt{3}\beta K}{2\pi T}$. In the time domain, the fading coefficients $g_l(kT/K)$ are correlated and have a Doppler power spectrum density modeled as in Jakes[84], given by

$$D(f) = \begin{cases} \frac{1}{\pi F_d \cdot \sqrt{1-\left(\frac{f}{F_d}\right)^2}} & |f| \le F_d \\ 0 & otherwise \end{cases} \ , \tag{4.4}$$

where F_d is the maximum Doppler bandwidth. Hence $g_l(kT/K)$ has an autocorrelation function given by

$$E[g_l(n\frac{T}{K}) \cdot g_l(m\frac{T}{K})^{\star}] = \alpha \cdot \exp(-\beta \cdot l) \cdot J_0\Big(2\pi(n-m)\frac{F_d T}{K}\Big) \ . \tag{4.5}$$

where $J_0(\cdot)$ is the first kind Bessel function of zero order.

As demonstrated in Fig. 4.2, the baseband filter $H(f)$ is designed to have the following two important properties. First, it has a limited bandwidth of K/TM, and hence adjacent subchannels have non-overlapping frequency responses, which can be represented as

$$H(f) \cdot H^{\star}(f - i/M) \cdot e^{-j2\pi(p_1-p_2)f} = 0 \, , \qquad 0 \le i \le M-1 \ , \tag{4.6}$$

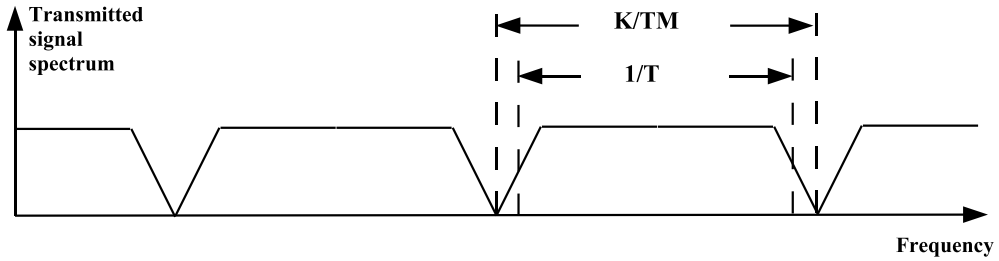


Figure 4.2 Frequency spectrum of an FMT system with M subcarriers under upsampling (or downsampling) factor of K

and which is equivalent to the following condition in the time domain

$$\sum_{k=-\infty}^{\infty} h\Big[(k-p_1)\frac{T}{K}\Big]\cdot h^{\star}\Big[(k-p_2)\frac{T}{K}\Big]\cdot e^{-j2\pi\frac{ik}{M}}=0, \qquad 0<i\leq M-1\ , \quad (4.7)$$

where p_1 and p_2 are different positive integers.

It also satisfies the Nyquist perfect sampling condition, which can be expressed in the following way:

$$\sum_{p=-\infty}^{\infty} h\Big[(pM+i-nK)\frac{T}{K}\Big]\cdot h^{\star}\Big[(pM+i-mK)\frac{T}{K}\Big]=\delta(n-m)\ . \qquad (4.8)$$

Note that both conditions given by equation (4.7) and (4.8) hold only approximately in real systems, where the practical filters have finite length time domain impulse responses. However, it is assumed in this chapter that the filter impulse response $h(t)$ is sufficiently long and hence conditions (4.7) and (4.8) are valid.

The sampled signal $y(kT/K)$ at the receiver is frequency shifted, which generates M substreams. Each stream is then filtered by a matched filter $\tilde{h}(k)$, followed by subsampling with a factor of K. Therefore, the i^{th} output of the substream $\hat{A}_i(n'T)$ at time n' is given by

$$\hat{A}_i(n'T)=\sum_{k=-\infty}^{\infty} y\big(k\frac{T}{K}\big)e^{-j2\pi\frac{ik}{M}}\cdot\tilde{h}\Big[(Kn'-k)\frac{T}{K}\Big]\ . \qquad (4.9)$$

4.3 Interference Analysis

In this section an analysis of the interference generated under different channel conditions is provided, and further used to define the trade-offs between spectrum efficiency and system performance degradation.

4.3.1 FMT Transmitter and Receiver Structures

Similar to the derivations given in [67], we first briefly describe in this subsection the FMT transmitter and receiver structure for the purpose of interference analysis. With the change of variables by $k = pM + i$, we can rewrite equation (4.1) into the following form:

$$\begin{aligned} x\Big((pM+i)\cdot\frac{T}{K}\Big) &= \sum_{m=0}^{M-1}\sum_{n=-\infty}^{\infty} A_m(nT)\cdot h\Big[(pM+i-nK)\frac{T}{K}\Big]\cdot e^{j2\pi\frac{im}{M}} \\ &= \sum_{n=-\infty}^{\infty} a_i[nT]\cdot h\Big[(pM+i-nK)\frac{T}{K}\Big] \ , \end{aligned} \tag{4.10}$$

where $a_i[nT]$ is the inverse Fourier transformation of the input signal $A_m(nT)$, and given by

$$a_i[nT] = \sum_{m=0}^{M-1} A_m(nT)\cdot e^{j2\pi\frac{im}{M}} \ . \tag{4.11}$$

We further decompose k/K into the following sum of integer index and fractional index as,

$$\begin{aligned} \frac{k}{K} &= \frac{pM+i}{K} = \eta_{p,i} + \nu_{p,i} \ , \\ \eta_{p,i} &= \lfloor\frac{pM+i}{K}\rfloor \ , \\ \nu_{p,i} &= \frac{pM+i}{K} - \eta_{p,i} \ , \\ q &= \eta_{p,i} - n \ , \end{aligned} \tag{4.12}$$

Then, the transmitted signal (4.10) can be simplified as

$$\begin{aligned} x\Big((pM+i)\cdot\frac{T}{K}\Big) &= x^{\{i\}}\Big(p\frac{MT}{K}\Big) \\ &= \sum_{q=-\infty}^{\infty} a_i\Big[(\eta_{p,i}-q)T\Big]\cdot h^{\{K\nu_{p,i}\}}(qT) \ , \end{aligned} \tag{4.13}$$

where $h^{\{K\nu_{p,i}\}}(qT) = h[(q+\nu_{p,i})T]$ belongs to a filter set $\left\{h^{\{j\}}(qT)\,\middle|\, j = 0,1,\cdots,K-1\right\}$, whose elements are the polyphase components (with respect to K) of the prototype filter with impulse response $h(k)$. The filter index $(K\nu_{p,i})$ of $h^{\{K\nu_{p,i}\}}(qT)$ provides the address of the polyphase component that needs to be applied to the i^{th} $(i = k_{mod-M})$ output of the IDFT to generate the transmitted signal $x(kT/K)$. Therefore, the transmitted signal $x\big((pM+i)T/K\big)$ can actually be viewed as an OFDM signal with M subcarriers passing through K baseband filters with periodically shifting filter index of period K.

For similar reasonings, the polyphase components (with respect to M) of the matched filter at the receiver can be denoted as

$$\tilde{h}^{\{M\mu_{n',m}\}}\Big(q'\frac{MT}{K}\Big) = \tilde{h}^{\{M\mu_{n',m}\}}\Big((q'+\mu_{n',m})\frac{MT}{K}\Big), \qquad 0 \le m \le M-1\ , \tag{4.14}$$

where $\tilde{h}(t)$ is the matched prototype filter, and the transformation of the indexes is illustrated as follows:

$$\begin{aligned} \frac{n'K-m}{M} &= \xi_{n',m} + \mu_{n',m}, \\ \xi_{n',m} &= \lfloor \frac{n'K-m}{M} \rfloor, \\ \mu_{n',m} &= \frac{n'K-m}{M} - \xi_{n',m}, \\ q' &= \xi_{n',m} - p'\ . \end{aligned} \tag{4.15}$$

Correspondingly, the received signal $y(kT/K)$ can also be represented in the polyphase form given by

$$y^{\{M\mu_{n',m}\}}\Big(q'\frac{MT}{K}\Big) = y\Big((q'+\mu_{n',m})\frac{MT}{K}\Big)\ . \tag{4.16}$$

Following similar derivations given by (4.13) and by employing the change of variable $k = p'M + m$, the i^{th} output signal of the demodulator at time $n'T$ at

the receiver can be represented in the following form

$$\begin{aligned}\hat{A}_i(n'T) &= \sum_{m=0}^{M-1}\sum_{p'=-\infty}^{\infty} y\Big[(p'M+m)\frac{T}{K}\Big]e^{-j2\pi\frac{ik}{M}}\cdot\tilde{h}\Big[(n'-\frac{p'M+m}{K})T\Big] \\ &= \sum_{m=0}^{M-1} u_m(n'T)\cdot e^{-j2\pi\frac{im}{M}}\ , \end{aligned} \tag{4.17}$$

where $u_m(n'T)$ is given by

$$\begin{aligned}u_m(n'T) &= \sum_{p'=-\infty}^{\infty} y\Big[(p'M+m)\frac{T}{K}\Big]\cdot\tilde{h}\Big[(n'-\frac{p'M+m}{K})T\Big] \\ &= \sum_{p'=-\infty}^{\infty} y^{\{m\}}\Big(p'\frac{MT}{K}\Big)\cdot\tilde{h}\Big[(\frac{Kn'-m}{M}-p')\frac{MT}{K}\Big] \\ &= \sum_{q'=-\infty}^{\infty} y^{\{m\}}\Big[(\xi_{n',m}-q')\frac{MT}{K}\Big]\cdot\tilde{h}^{\{M\mu_{n',m}\}}(q'\frac{MT}{K})\ . \end{aligned} \tag{4.18}$$

4.3.2 FMT Over Quasi-static Frequency-Flat Fading Channel

In order to see how time variations and frequency selectivity affect the interchannel (or intersymbol) interference, it is insightful to first investigate an FMT system over frequency-flat and quasi-static fading channels, where the channel response remains static within the data burst. The performance of FMT system over such channel conditions has been analyzed and characterized in [67]. In this subsection, we briefly describe the main results.

First, by substituting equation (4.2) (for the case of quasi-static flat fading channel) into equation (4.18), the signal $u_m(n'T)$ can be represented as

$$\begin{aligned}&u_m(n'T) \\ &= g_0\cdot\sum_{p'=-\infty}^{\infty}\sum_{n=-\infty}^{\infty} a_m(nT)\cdot h\Big[(p'M+m-nK)\frac{T}{K}\Big]\cdot\tilde{h}\Big[(Kn'-m-p'M)\frac{T}{K}\Big] \\ &+ \sum_{p'=-\infty}^{\infty} w\Big[(p'M+m)\frac{T}{K}\Big]\cdot\tilde{h}\Big[(Kn'-m-p'M)\frac{T}{K}\Big]\ , \end{aligned} \tag{4.19}$$

where g_0 is the channel gain or impulse response of the frequency flat fading

channel. According to the property (4.8), the following results can be obtained:

$$\begin{aligned}
&\sum_{p'=-\infty}^{\infty} h\Big[(p'M+m-nK)\frac{T}{K}\Big]\cdot\tilde{h}\Big[(Kn'-m-p'M)\frac{T}{K}\Big] \\
&= \sum_{p'=-\infty}^{\infty} h\Big[(p'M+m-nK)\frac{T}{K}\Big]\cdot h^{\star}\Big[(p'M+m-n'K)\frac{T}{K}\Big] \\
&= \delta(n-n') \ . \qquad (4.20)
\end{aligned}$$

Therefore, equation (4.19) can be simplified to

$$u_m(n'T) = g_0 \cdot a_m(n'T) + w'_m(n'T) \ , \qquad (4.21)$$

where $w'_m(n'T)$ is the equivalent additive Gaussian noise with variance

$$E[w'_m(n'T)^2] = N_0/E_s \ . \qquad (4.22)$$

Hence, the output signal from the demodulator is given by

$$\begin{aligned}
\hat{A}_i(n'T) &= \sum_{m=0}^{M-1} u_m(n'T)\cdot e^{-j2\pi\frac{im}{M}} \\
&= g_0 \cdot A_i(n'T) + w''_i(n'T) \ , \qquad (4.23)
\end{aligned}$$

where $w''_i(n'T)$ is the equivalent (frequency domain) additive Gaussian noise of the i^{th} subcarrier at time instant n' and has the same variance as $w'_m(n'T)$.

4.3.3 FMT Over Frequency-Selective Channel

When the FMT system is transmitting over a frequency-selective fading environment, the spectrum of the received signal is shaped by the channel frequency response. Hence the Nyquist perfect sampling condition of the baseband filters of the FMT system is no longer satisfied, and consequently, we have intersymbol interference. In this case, by substituting (4.2) and (4.1) into

(4.9), the output signals from the demodulator are given by

$$\begin{aligned}\hat{A}_i(n'T) &= \sum_{l=0}^{L-1} g_l \cdot \sum_{k=-\infty}^{\infty} x\Big[(k-l)\frac{T}{K}\Big] \cdot e^{-j2\pi\frac{ik}{M}} \cdot h^{\star}\Big[(k-Kn')\frac{T}{K}\Big] + w'' \\ &= \sum_{i'=0}^{M-1}\sum_{l=0}^{L-1} g_l e^{-j2\pi\frac{i'l}{M}} \cdot \sum_{n=-\infty}^{\infty}\sum_{k=-\infty}^{\infty} A_{i'}(nT) h\Big[(k-l-nK)\frac{T}{K}\Big] \\ &\quad \cdot e^{-j2\pi\frac{(i-i')k}{M}} \cdot h^{\star}\Big[(k-Kn')\frac{T}{K}\Big] + w''(n'T) \ . \end{aligned} \tag{4.24}$$

It is evident that the first term of equation (4.24) can be re-organized as the following form

$$\begin{aligned}&\sum_{i'=0}^{M-1}\sum_{l=0}^{L-1} g_l e^{-j2\pi\frac{i'l}{M}} \sum_{n=-\infty}^{\infty}\sum_{k=-\infty}^{\infty} A_{i'}(nT) h\Big[(k-l-nK)\frac{T}{K}\Big] \\ &\cdot e^{-j2\pi\frac{(i-i')k}{M}} \cdot h^{\star}\Big[(k-Kn')\frac{T}{K}\Big] \\ &= \sum_{i'=0}^{M-1}\sum_{l=0}^{L-1} g_l e^{-j2\pi\frac{il}{M}} \sum_{n=-\infty}^{\infty} A_{i'}(nT) \\ &\quad \cdot \left(\sum_{k=-\infty}^{\infty} h\Big[(k-l-nK)\frac{T}{K}\Big] h^{\star}\Big[(k-Kn')\frac{T}{K}\Big] e^{-j2\pi\frac{(i-i')(k-l)}{M}}\right). \end{aligned} \tag{4.25}$$

Due to the property of the filter impulse response given by equation (4.7), we can obtain the following equality

$$\begin{aligned}&\sum_{k=-\infty}^{\infty} h\Big[(k-l-nK)\frac{T}{K}\Big] h^{\star}\Big[(k-Kn')\frac{T}{K}\Big] \cdot e^{-j2\pi\frac{(i-i')(k-l)}{M}} \\ &= \sum_{(k-l)=-\infty}^{\infty} h\Big[(k-l-nK)\frac{T}{K}\Big] h^{\star}\Big[\big((k-l)+(l+Kn')\big)\frac{T}{K}\Big] \cdot e^{-j2\pi\frac{(i-i')(k-l)}{M}} \\ &= 0, \quad i \neq i'. \end{aligned} \tag{4.26}$$

By substituting equations (4.25) and (4.26) into (4.24), the output signals from the demodulator can be simplified into the following form

$$\begin{aligned}
&\hat{A}_i(n'T) \\
&= \sum_{l=0}^{L-1} g_l e^{-j2\pi\frac{il}{M}} \sum_{n=-\infty}^{\infty}\sum_{k=-\infty}^{\infty} A_i(nT) h\Big[(k-l-nK)\frac{T}{K}\Big] \cdot h^{\star}\Big[(k-Kn')\frac{T}{K}\Big] \\
&\quad + w''(n'T) \\
&= A_i(n'T)\sum_{l=0}^{L-1} g_l \cdot e^{-j2\pi\frac{il}{M}}\, R_h(l) \\
&\quad + \sum_{\substack{n=-\infty \\ n\neq n'}}^{\infty} A_i(nT) \sum_{l=0}^{L-1} g_l \cdot e^{-j2\pi\frac{il}{M}} \cdot R_h\Big[l+(n-n')K\Big] + w''(n'T),
\end{aligned} \tag{4.27}$$

where the second term is the intersymbol interference caused by frequency selectivity, and $R_h(n)$ is the time domain autocorrelation function of the prototype filter impulse response $h(k)$ defined as

$$R_h(n) = \sum_{k=-\infty}^{\infty} h\Big[(k-n)\frac{T}{K}\Big] \cdot h^{\star}\Big[k\frac{T}{K}\Big] \ . \tag{4.28}$$

If we further define $\tilde{G}_i(n)$ as the Fourier transformation of the weighted autocorrelation function, in the following form

$$\tilde{G}_i(n) = \sum_{l=0}^{L-1} g_l \cdot e^{-j2\pi\frac{il}{M}} \cdot R_h(l+nK) \ , \tag{4.29}$$

then equation (4.24) can be simplified to be

$$\hat{A}_i(n'T) = \tilde{G}_i(0)\cdot A_i(n'T) + \sum_{\substack{n=-\infty \\ n\neq n'}}^{\infty} \tilde{G}_i(n-n')\cdot A_i(nT) + w''(n'T) \ . \tag{4.30}$$

It is evident that the output signal from the demodulator is corrupted by both additive noise and intersymbol interference, which is represented by the second term of equation (4.30). After some manipulations, the variance of the ISI disturbance conditioned on the instantaneous channel realizations can

be expressed by the following form

$$E[|z_i|^2] = \sum_{\substack{n=-\infty \\ n\neq n'}}^{\infty} \left|\tilde{G}_i(n-n')\right|^2, \tag{4.31}$$

where z_i is given by

$$z_i = \sum_{\substack{n=-\infty \\ n\neq n'}}^{\infty} A_i(nT) \cdot \tilde{G}_i(n-n') \ . \tag{4.32}$$

Therefore, given a certain channel realization, the signal-to-interference plus noise ratio (SINR) is given by

$$\rho_{SINR}(i) = \frac{|\tilde{G}_i(0)|^2}{N_0/E_s + \sum_{\substack{n=-\infty \\ n\neq n'}}^{\infty} \left|\tilde{G}_i(n-n')\right|^2} \ , \tag{4.33}$$

Notice that the interference z_i given by equation (4.32) comes only from the same subchannel and there is no interchannel interference. This is due to the fact that the baseband filter $H(f)$ is bandlimited to be within a frequency band of width K/TM, and hence maintains orthogonality among different subcarriers. When the channel is frequency selective, the frequency response of the received signal after the matched filter no longer satisfies the Nyquist perfect sampling condition, but still maintains non-overlapping frequency bands. Therefore, different subcarriers remain orthogonal to each other and the received signal only contains intersymbol interference, but no interchannel interference.

If we use BPSK modulation and further approximate the interference as a Gaussian random variable [72] [73], then the average bit error probability of the FMT system over the frequency selective channel is given by

$$\overline{P}_b = \frac{1}{M} \sum_{i=0}^{M-1} E_{\{g_l\}_{l=0}^{L-1}} \ Q(\sqrt{2\rho_{SINR}(i)}) \ . \tag{4.34}$$

It is evident from equation (4.34) that the average bit error probability does not have an analytical close form expression, and hence it is very difficult to

provide useful insight into the trade-off between performance degradation and spectral efficiency. Therefore, we evaluate the carrier to interference (C/I) ratio of the FMT system, which is given by

$$\frac{C}{I} = \frac{\frac{1}{M}\sum_{i=0}^{M-1} E\Big[\big|\tilde{G}_i(0)\big|^2\Big]}{\frac{1}{M}\sum_{i=0}^{M-1}\sum_{\substack{n=-\infty \\ n\neq n'}}^{\infty} E\Big[\big|\tilde{G}_i(n-n')\big|^2\Big]} \quad . \tag{4.35}$$

In order to simplify the above equation, let us denote $S_h(f)$ as the Fourier transformation of $R_h(l+nK)$, which is given by

$$\begin{aligned} S_h(f) &= \sum_{n=-\infty}^{\infty} R_h(l+nK)\cdot e^{-j2\pi fn} \\ &= \sum_{n=-\infty}^{\infty} R_h(l+n)\cdot\Big(\frac{1}{K}\sum_{k=0}^{K-1} e^{j2\pi kn/K}\Big)\cdot e^{-j2\pi fn/K} \\ &= \frac{1}{K}\sum_{k=0}^{K-1}\Big|H(\frac{f-k}{K})\Big|^2\cdot e^{j2\pi l(f-k)/K} \quad , \end{aligned} \tag{4.36}$$

where $H(f)$ is the frequency response of the baseband filter, given by

$$H(f) = \sum_{n=-\infty}^{\infty} h\Big[n\frac{T}{K}\Big]\cdot e^{-j2\pi nf} \quad . \tag{4.37}$$

By substituting the power delay profile given by equation (4.3) into the Fourier transformation of the weighted autocorrelation function given by (4.29), we obtain the following result

$$\begin{aligned} \sum_{n=-\infty}^{\infty} E\Big[\big|\tilde{G}_i(n)\big|^2\Big] &= \sum_{l=0}^{L-1}\alpha\cdot\exp(-\beta\cdot l)\cdot\sum_{n=-\infty}^{\infty}\Big|R_h(l+nK)\Big|^2 \\ &= \sum_{l=0}^{L-1}\alpha\cdot\exp(-\beta\cdot l)\cdot\int_0^1\Big|S_h(f)\Big|^2\,df \quad . \end{aligned} \tag{4.38}$$

Moreover, by substituting the expression of $S_h(f)$ given by (4.36) into equation (4.38), it can be further simplified to the form

$$\sum_{n=-\infty}^{\infty} E\Big[\big|\tilde{G}_i(n)\big|^2\Big] = \frac{1}{K^2}\sum_{l=0}^{L-1}\alpha\cdot\exp(-\beta\cdot l)\int_0^1\Big|\sum_{k=0}^{K-1}\Big|H(\frac{f-k}{K})\Big|^2\cdot e^{-j2\pi\frac{lk}{K}}\Big|^2 df \quad . \tag{4.39}$$

Following similar derivations, we also obtain the following expectation:

$$E\Big[\big|\tilde{G}_i(0)\big|^2\Big] = \sum_{l=0}^{L-1} \alpha \cdot \exp(-\beta \cdot l) \cdot |R_h(l)|^2$$
$$= \sum_{l=0}^{L-1} \alpha \cdot \exp(-\beta \cdot l) \cdot \Big| \int_0^1 |H(f)|^2 \cdot e^{j2\pi l f}\ df \Big|^2 \ , \quad (4.40)$$

Substituting (4.39) and (4.40) into (4.35), we obtain the C/I ratio in terms of the number of subcarriers M, upsampling factor K, and the baseband filter $H(f)$. Hence, we have provided a close form expression of the trade-off between performance degradation and spectral efficiency K/M.

4.3.4 FMT Over Frequency-Selective Time-Varying Channel

In this section, we consider the time-varying fading channel, where the orthogonality among different subchannels is no longer valid. Therefore, both interchannel interference as well as intersymbol interference are going to disturb the transmitted signal. In this case, the output signal from the FMT demodulator is given by

$$\hat{A}_i(n'T) = \sum_{l=0}^{L-1} \sum_{k=-\infty}^{\infty} g_l(k\frac{T}{K}) \cdot x\Big[(k-l)\frac{T}{K}\Big] \cdot e^{-j2\pi \frac{ik}{M}} \cdot h^{\star}\Big[(k-Kn')\frac{T}{K}\Big] + w''$$
$$= \sum_{i'=0}^{M-1} \sum_{l=0}^{L-1} e^{-j2\pi \frac{i'l}{M}} \sum_{n=-\infty}^{\infty} A_{i'}(nT) \sum_{k=-\infty}^{\infty} g_l(k\frac{T}{K}) \cdot h\Big[(k-l-nK)\frac{T}{K}\Big]$$
$$\times e^{-j2\pi \frac{(i-i')k}{M}} \cdot h^{\star}\Big[(k-Kn')\frac{T}{K}\Big] + w''$$
$$= \sum_{i'=0}^{M-1} \sum_{l=0}^{L-1} \sum_{n=-\infty}^{\infty} e^{-j2\pi \frac{i'l}{M}} \cdot A_{i'}(nT) \cdot \tilde{g}_{i,i'}(l,n,n') + w''(n'T) \ , \quad (4.41)$$

where $\tilde{g}_{i,i'}(l,n,n')$ is defined as

$$\tilde{g}_{i,i'}(l,n,n') = \sum_{k=-\infty}^{\infty} g_l(k\frac{T}{K}) \cdot h\Big[(k-l-nK)\frac{T}{K}\Big] \cdot e^{-j2\pi \frac{(i-i')k}{M}} \cdot h^{\star}\Big[(k-Kn')\frac{T}{K}\Big] \ . \quad (4.42)$$

If we further denote $\tilde{G}_{i,i'}(n,n')$ as the following form

$$\tilde{G}_{i,i'}(n,n') = \sum_{l=0}^{L-1} \tilde{g}_{i,i'}(l,n,n') \cdot e^{-j2\pi \frac{i'l}{M}} \ , \quad (4.43)$$

then equation (4.41) can be easily represented as

$$\begin{aligned}\hat{A}_i(n'T) &= \sum_{i'=0}^{M-1}\sum_{n=-\infty}^{\infty} A_{i'}(nT)\cdot\tilde{G}_{i,i'}(n,n') + w'' \\ &= \tilde{G}_{i,i}(n',n')\cdot A_i(n'T) + \sum_{\substack{n=-\infty \\ n\neq n'}}^{\infty}\tilde{G}_{i,i}(n,n')\cdot A_i(nT) \\ &+ \sum_{\substack{i'=0 \\ i'\neq i}}^{M-1}\sum_{n=-\infty}^{\infty} A_{i'}(nT)\cdot\tilde{G}_{i,i'}(n,n') + w''(n'T)\ . \end{aligned} \tag{4.44}$$

It is evident from the above equation that the second term represents the intersymbol interference, the third term represents the interchannel interference, and the last term represents the additive Gaussian noise. Similarly, the SINR of the i^{th} subcarrier at time instant n' can be expressed as the following form

$$\rho_{SINR}(i,n') = \frac{|\tilde{G}_{i,i}(n',n')|^2}{N_0/E_s + \sum_{i'=0}^{M-1}\sum_{n=-\infty}^{\infty}\left|\tilde{G}_{i,i'}(n,n')\right|^2 - |\tilde{G}_{i,i}(n',n')|^2}\ . \tag{4.45}$$

The average bit error probability of the FMT system over the fading channel can also be expressed by equation (4.34) when BPSK modulation is used.

Due to the fact that (4.34) is intractably complicated, we use the carrier to interference ratio (CIR) to analyze the trade-offs between the spectral efficiency and performance degradation of the FMT system over time-varying fading channels. First, according to the uncorrelated assumption between different fading paths responses, we have the following result

$$E\Big[|\tilde{G}_{i,i'}(n,n')|^2\Big] = \sum_{l=0}^{L-1} E\Big[\Big|\tilde{g}_{i,i'}(l,n,n')\Big|^2\Big]\ , \tag{4.46}$$

where the R.H.S. of the above equation can further be simplified to be

$$\begin{aligned} & E\Big[\Big|\tilde{g}_{i,i'}(l,n,n')\Big|^2\Big] \\ &= \alpha\int_0^1\int_0^1\int_0^1 H\Big(f' - \frac{(i-i')}{M}\Big)\cdot H^{\star}\Big(f - \frac{(i-i')}{M}\Big)\cdot H(f-s) \\ &\cdot H^{\star}(f'-s)\cdot D_g(s)\cdot e^{-j2\pi(f-f')(n-n')K}\cdot e^{-l(j2\pi(f-f')+\beta)}\ \cdot df\cdot df'\cdot ds\,, \end{aligned} \tag{4.47}$$

where $D_g(f)$ is the discrete Doppler spectrum, given by

$$D_g(f) = \frac{K}{T} \cdot D(\frac{fK}{T}) = \begin{cases} \frac{K}{\pi F_d T \cdot \sqrt{1-\left(\frac{fK}{F_d T}\right)^2}} & |f| \leq \frac{F_d T}{K} \\ 0 & otherwise \end{cases} . \quad (4.48)$$

Given the fact that

$$\sum_{n=-\infty}^{\infty} e^{-j2\pi nfK} = \frac{1}{K} \sum_{k=0}^{K-1} \delta(f - \frac{k}{K}) \ , \quad (4.49)$$

we can simplify the following expectation:

$$\begin{aligned} &\sum_{n=-\infty}^{\infty} E\Big[\Big|\tilde{g}_{i,i'}(l,n,n')\Big|^2\Big] \\ &= \alpha \cdot e^{-l\beta} \cdot \int_0^1 \int_0^1 \Big(\frac{1}{K} \sum_{k=0}^{K-1} H(f - \frac{k}{K} - \frac{i-i'}{M}) \cdot H^\star(f - \frac{k}{K} - s) \\ &\cdot H^\star(f - \frac{i-i'}{M}) \cdot H(f-s) \cdot e^{-j2\pi lk/K}\Big) \cdot D_g(s) \cdot df \cdot ds \ , \end{aligned} \quad (4.50)$$

Therefore, the summation of the average signal power C and the average interference power I is given by

$$C + I = \alpha \int_0^1 \int_0^1 S_{all}(f,s) \cdot D_g(s) \cdot df \cdot ds \ , \quad (4.51)$$

where $S_{all}(f,s)$ is the power spectrum density of the interferences plus signals, which is given by

$$\begin{aligned} S_{all}(f,s) &= \frac{1}{K} \sum_{i=0}^{M-1} \sum_{k=0}^{K-1} H(f - \frac{k}{K} - \frac{i}{M}) \cdot H^\star(f - \frac{k}{K} - s) \\ &\times H^\star(f - \frac{i}{M}) \cdot H(f-s) \cdot \frac{1 - e^{-L(\beta + j2\pi k/K)}}{1 - e^{-(\beta + j2\pi k/K)}} \ . \end{aligned} \quad (4.52)$$

Following similar derivations, the average signal power C can also be obtained as the following form after some manipulations,

$$\begin{aligned} C &= E\Big[|\tilde{G}_{i,i}(n',n')|^2\Big] \\ &= \alpha \int_0^1 \int_0^1 \int_0^1 H(f') \cdot H^\star(f) \cdot H(f-s) \cdot H^\star(f'-s) \\ &\cdot D_g(s) \cdot \frac{1 - e^{-L(\beta + j2\pi(f-f'))}}{1 - e^{-(\beta + j2\pi(f-f'))}} \cdot df \cdot df' \cdot ds \ , \end{aligned} \quad (4.53)$$

Finally, by substituting signal power C given by equation (4.53) and the interference power I by subtracting C from equation (4.52) into the C/I ratio definition, the CIR of the FMT system over frequency-selective time-varying channel can be readily obtained.

4.3.5 Performance Comparison with OFDM System

We know that both FMT and OFDM are different forms of multicarrier modulation. Therefore, it is insightful to compare the performance of these two modulations under the same channel conditions and with the same spectral efficiency.

In OFDM systems, a cyclic prefix is used to combat the multipath spread and to mitigate the ISI. In practical situations, we select the length of the cyclic prefix to be longer than the channel maximum multipath delay spread, and thus, the system is ISI free. According to the ICI analysis of an OFDM system in a time-varying fading channel as provided in [72] [73], the carrier over interference (ICI only) ratio of the i^{th} subcarrier in an OFDM system can be represented as

$$\left(\frac{C}{I}\right)_i = \frac{2}{(MTF_d/K)^2 \sum\limits_{\substack{k=1 \\ k\neq i}}^{M} \frac{1}{(k-i)^2}} \quad , \tag{4.54}$$

where MT/K is the OFDM symbol interval.

In contrast to the OFDM system, both ICI and ISI exist in the FMT system in a frequency-selective time-varying fading channel. As demonstrated in equation (4.44), the second term of the right hand side represents the ISI and the third term represents the ICI. In order to understand the effects of these two interferences on FMT system performance, the average power of the carrier signal (first term), ISI (second term), and ICI (third term) of equation (4.44) are analyzed separately. After similar manipulations as given in Section

4.3.4, the average ICI and ISI powers are given by the following form

$$I_{ici} = \alpha \int_0^1 \int_0^1 S_{ici}(f,s) \cdot D_g(s) \cdot df \cdot ds \ , \tag{4.55}$$

$$I_{isi} = \alpha \int_0^1 \int_0^1 S_{isi+c}(f,s) \cdot D_g(s) \cdot df \cdot ds - C \ , \tag{4.56}$$

where C is given by equation (4.53), and S_{ici}, S_{isi} are given by the following form:

$$\begin{aligned} S_{ici}(f,s) = & \frac{1}{K} \sum_{i=1}^{M-1} \sum_{k=0}^{K-1} H(f - \frac{k}{K} - \frac{i}{M}) \cdot H^{\star}(f - \frac{k}{K} - s) \\ & \times H^{\star}(f - \frac{i}{M}) \cdot H(f-s) \cdot \frac{1 - e^{-L(\beta + j2\pi k/K)}}{1 - e^{-(\beta + j2\pi k/K)}} \ , \end{aligned} \tag{4.57}$$

$$\begin{aligned} S_{isi+c}(f,s) = & \frac{1}{K} \sum_{k=0}^{K-1} H(f - \frac{k}{K}) \cdot H^{\star}(f - \frac{k}{K} - s) \\ & \times H^{\star}(f) \cdot H(f-s) \cdot \frac{1 - e^{-L(\beta + j2\pi k/K)}}{1 - e^{-(\beta + j2\pi k/K)}} \ . \end{aligned} \tag{4.58}$$

We know that the total interference power I, which is equal to the sum of both interference I_{isi} and I_{ici}, is sometimes a coarse performance measure and can not represent the individual effects of each interference especially when compared to the OFDM system which has only ICI. Therefore, it would be reasonable to compare both the carrier over interference ratio $C/(I_{ici} + I_{isi})$ and the carrier over ICI ratio C/I_{ici} with the C/I ratio of an OFDM system, in order to understand the overall interference as well as the ICI on FMT system performance.

As can be expected, the performance degradation of both systems depends heavily on the channel conditions (frequency selectivity and time variance) as well as the system spectral efficiencies. First, in the case when the channel is slowly fading (low Doppler frequency), an OFDM system with cyclic guard intervals is slightly distorted only by the ICI and has a performance close to the interference-free situation in the limit when $F_d \to 0$. However for FMT systems, the ISI always exists due to the loss of the Nyquist sampling condition caused by the channel frequency selectivity, even for channels with small

Doppler spreading and systems with low spectral efficiency $\eta = M/K$. Therefore, OFDM outperforms FMT in a slowly fading environment. Secondly, it is reasonable to expect the FMT system to have a smaller ICI than an OFDM system, since the baseband signal in FMT modulation is pulse-shaped by a filter as contrast to the simple rectangular baseband filter in OFDM modulation. Hence, the C/I_{ici} ratio of an FMT system is expected to be larger than that of an OFDM system. Furthermore, it is apparent from (4.74) that the ICI (power) does not depend on channel frequency selectivity and grows inversely quadratically w.r. the maximum Doppler frequency F_d. In this sense, the FMT system is expected to outperform OFDM in a fast fading (with large Doppler spread) environment as ICI dominates the overall interference. Finally, we observe that the spectral efficiency of the OFDM system depends on the channel frequency selectivity in the sense that the length of the cyclic prefix should be larger than the maximum multipath delay. Thus, an ISI-free OFDM system has a maximum spectral efficiency given by

$$\eta = \frac{M}{M + \tau_{max}/(T/K)} \ , \tag{4.59}$$

where τ_{max} is the maximum multipath delay. Therefore, under the same spectral efficiency, an FMT system is likely to outperform an OFDM system over highly frequency selective fading channels with long channel delay spread.

4.4 Per-Channel Equalized FMT Modulation

Compared with an OFDM system with sufficient long cyclic prefix, where the transmitted signal is free of ISI, it is clear from equation (4.44) that both ICI and ISI exist in an FMT system. Therefore, it is interesting to study the effects of per-channel equalizers in an FMT system over time-varying frequency-selective fading channels.

4.4.1 FMT Modulation with Per-Channel Equalizer

In this subsection, we consider an ideal per-channel equalizer with a infinite number of equalization taps. The m^{th} tap coefficient of the i^{th} sub-channel at time instant n' is denoted as $c_{i,n'}(m)$ for $0 \leq i \leq M-1$. In this case, the output signal from the per-channel equalizer is given by

$$\hat{A}_i^{Eq}(n'T) = \sum_{m=-\infty}^{\infty} c_{i,n'}(m) \cdot \hat{A}_i\big((n'-m)T\big) \ , \tag{4.60}$$

where $\hat{A}_i^{Eq}$ with superscript $(\cdot)^{\text{Eq}}$ represents the received signal after equalization. It is evident that the Z-transform of the channel equalizer, which is defined by the following form

$$C_{i,n'}(z) = \sum_{m=-\infty}^{\infty} c_{i,n'}(m) \cdot z^{-m} \ , \tag{4.61}$$

is the inverse of the Z-transform of the equivalent channel response $\tilde{G}_{i,i}(n,n')$, given by

$$C_{i,n'}(z) = \big[F_{i,i,n'}(z)\big]^{-1} \ , \tag{4.62}$$

with the Z-transform $F_{i,i',n'}(z)$ given by the following form

$$F_{i,i',n'}(z) = \sum_{m=-\infty}^{\infty} \tilde{G}_{i,i'}(n'+m,n') \cdot z^{-m} \ . \tag{4.63}$$

By substituting equation (4.44) into (4.60), we obtain the following

result after some manipulations

$$\hat{A}_i^{Eq}(n'T) = A_i(n'T) + \sum_{\substack{i'=0 \\ i' \neq i}}^{M-1} \sum_{n=-\infty}^{\infty} \sum_{m=-\infty}^{\infty} c_{i,n'}(m) \cdot \times \tilde{G}_{i,i'}(n, n'-m) \cdot A_{i'}(nT) + v \ , \tag{4.64}$$

where v is an additive Gaussian noise with zero mean and variance given by $\sigma_v^2 = \frac{N_0}{E_s} \int_0^1 |C_{i,n'}(j2\pi f)|^2 \, d\, f$. Note that in equation (4.64), the first term is the desired signal, and the second term is the interferences from the other sub-channels in an FMT system. Therefore, the ideal per-channel equalizer eliminates the ISI completely by using a filter with sufficiently large number of equalizer taps. However, the residual interference from adjacent sub-channels due to the loss of orthogonality still exists. In order to investigate the effects of per-channel equalization on the system performance, we provide the C/I ratio analysis of the FMT system over different fading channel conditions in the next section.

4.4.2 Interference Analysis of Per-Channel Equalized FMT System

From equation (4.64), it can be established that the ICI of the per-channel equalized system, which is denoted as u_i, can be expressed as follows:

$$u_i = \sum_{\substack{i'=0 \\ i' \neq i}}^{M-1} \sum_{n=-\infty}^{\infty} \sum_{m=-\infty}^{\infty} c_{i,n'}(m) \tilde{G}_{i,i'}(n, n'-m) A_{i'}(nT). \tag{4.65}$$

Therefore, by assuming the input signal $A_{i'}(nT)$ is i.i.d. with unit variance, the instantaneous variance of the interference signal can be represented in the following format:

$$E[|u_i|^2] = \sum_{\substack{i'=0 \\ i' \neq i}}^{M-1} \sum_{n=-\infty}^{\infty} \sum_{m=-\infty}^{\infty} \left| c_{i,n'}(m) \tilde{G}_{i,i'}(n, n'-m) \right|^2 . \tag{4.66}$$

Using the property of the Z-transform, it can be shown that

$$\sum_{n=-\infty}^{\infty}\sum_{m=-\infty}^{\infty}\left|c_{i,n'}(m)\cdot\tilde{G}_{i,i'}(n,n'-m)\right|^2 = \int_0^1 \left|C_{i,n'}(j2\pi f)\cdot F_{i,i',n'}(j2\pi f)\right|^2 \, df \ . \tag{4.67}$$

By substituting equation (4.62) into equation (4.67), the following lower bound on the instantaneous ICI variance is obtained

$$\begin{aligned} E[|u_i|^2] &= \sum_{\substack{i'=0\\ i'\neq i}}^{M-1}\int_0^1 \left|\frac{F_{i,i',n'}(j2\pi f)}{F_{i,i,n'}(j2\pi f)}\right|^2 \, df \\ &\geq \sum_{\substack{i'=0\\ i'\neq i}}^{M-1}\frac{\left|\int_0^1 F_{i,i',n'}(j2\pi f)\, df\right|^2}{\int_0^1 |F_{i,i,n'}(j2\pi f)|^2 \, df} = \frac{\sum_{\substack{i'=0\\ i'\neq i}}^{M-1}|\tilde{G}_{i,i'}(n',n')|^2}{\sum_{n=-\infty}^{\infty}|\tilde{G}_{i,i}(n,n')|^2}\,. \end{aligned} \tag{4.68}$$

By substituting equation (4.68) into the C/I definition, the average CIR ratio of the per-channel equalized FMT system can be bounded in the following form:

$$\frac{C}{I} \leq \left(\frac{C}{I}\right)\Big|_{up} = \frac{E\left[\sum_{i=0}^{M-1}\sum_{n=-\infty}^{\infty}|\tilde{G}_{i,i}(n,n')|^2\right]}{E\left[\sum_{i=0}^{M-1}\sum_{\substack{i'=0\\ i'\neq i}}^{M-1}|\tilde{G}_{i,i'}(n',n')|^2\right]}. \tag{4.69}$$

For the sake of simplicity, we can denote the numerator and the denominator of the R.H.S. of equation (4.69) as the C_{up} and I_{up} respectively. By substituting the definition of $\tilde{G}_{i,i'}(n,n')$ given by equations (4.42) and (4.43) into (4.69), we obtain the following result after some manipulations

$$C_{up} = \alpha\int_0^1\int_0^1 S_{c,up}(f,s)\cdot D_g(s)\cdot df\cdot ds \ , \tag{4.70}$$

where $S_{c,up}(f,s)$ is the general power spectrum density of the upper bound of the average signal power, which is given by

$$\begin{aligned} S_{c,up}(f,s) = \frac{1}{K}\sum_{k=0}^{K-1} & H(f-\frac{k}{K})\cdot H^{\star}(f-\frac{k}{K}-s) \\ & \times H^{\star}(f)\cdot H(f-s)\cdot\frac{1-e^{-L(\beta+j2\pi k/K)}}{1-e^{-(\beta+j2\pi k/K)}} \ . \end{aligned} \tag{4.71}$$

Similarly, I_{up} is given by

$$I_{up} = \alpha \int_0^1 \int_0^1 \int_0^1 S_{I,up}(f', f, s) \cdot D_g(s) \cdot df' \cdot df \cdot ds \ , \tag{4.72}$$

where

$$S_{I,up}(f', f, s) = \sum_{\substack{i'=0 \\ i' \neq i}}^{M-1} H(f' - \frac{i - i'}{M}) \cdot H^{\star}(f - \frac{i - i'}{M})$$
$$\times H(f - s) \cdot H^{\star}(f' - s) \cdot \frac{1 - e^{-L(\beta + j2\pi(f - f'))}}{1 - e^{-(\beta + j2\pi(f - f'))}} \, . \tag{4.73}$$

By substituting the signal power C_{up} given by equation (4.70) and the interference power I_{up} given by equation (4.72) into the C/I ratio definition, the upper bound of the CIR ratio of the per-channel equalized FMT system over frequency-selective time-varying channel is obtained.

4.4.3 Performance Comparisons with Un-equalized FMT System and OFDM System

It is insightful to compare the performance of both un-equalized FMT and OFDM systems with the same spectral efficiency under the same channel conditions. In practical OFDM systems, we select the length of the cyclic prefix to be longer than the channel maximum multipath delay spread, and thus, the system is ISI free. According to the ICI analysis of an OFDM system in a time-varying fading channel as provided in [72][73], the carrier to interference (ICI only) ratio of the OFDM system can be represented as

$$\frac{C}{I} = \frac{2}{(MTF_d/K)^2 \sum\limits_{\substack{k=1 \\ k \neq i}}^{M} \frac{1}{(k-i)^2}} \ , \tag{4.74}$$

where MT/K is the OFDM symbol interval.

As demonstrated in equation (4.44), the second term of the right hand side represents the ISI and the third term represents the ICI in FMT system. In order to understand the effects of these two interferences on un-equalized FMT

system performance, the average power of the carrier signal (first term), ISI (second term), and ICI (third term) of equation (4.44) were analyzed separately in Section 4.3, where closed-form expressions of both carrier over interference ratio $C/(I_{ici} + I_{isi})$ and the carrier over ICI ratio C/I_{ici} were provided.

In this subsection, we extend the interference analysis to FMT modulations with a per-channel equalizer. Instead of designing specific channel equalizers for the FMT system, we investigate the ideal system performance of the per-channel equalized system with a sufficiently large number of equalizer taps. From equation (4.64), it is evident that the per-channel equalized FMT system is free of ISI, and is only distorted by the ICI from other sub-channels (represented by the second term). Therefore, with the help of per-channel equalization, both OFDM and FMT have the same type of interference, i.e., ICI. The performance comparison between these two modulation forms in terms of CIR ratios, which are given by equations (4.69) and (4.74), provides a better understanding of the trade-offs between spectrum efficiency and system performance of different multi-carrier modulations.

4.5 Numerical and Simulation Results

In this section, we assume that the baseband filter $h[nT/K]$ has a root raised cosine frequency response, which is given by

$$H(f) = \begin{cases} \sqrt{K} & |f| \leq \frac{(1-a)}{2K} \\ 0 & |f| > \frac{(1+a)}{2K} \\ \sqrt{K \cdot \frac{1+\cos(\pi \cdot \frac{2K|f|-(1-a)}{2a})}{2}} & \frac{(1-a)}{2K} \leq |f| \leq \frac{(1+a)}{2K} \end{cases} . \tag{4.75}$$

where the roll-off factor a is given by $a = \frac{K-M}{M}$.

We first demonstrate in Fig. 4.3 the CIR graphs of an FMT system having 64 subcarriers and several different upsampling factors $K = 71, 80, 91, 107$ and 128. Simulation results are shown on the graphs as discrete points. The spectral efficiency $\eta = M/K$, defined as the ratio of the subcarrier number over the upsampling factor, varies from $\eta = 0.5$ to $\eta = 0.9$, which parameterizes the CIR curves. The FMT system has a total bandwidth $W = 0.5M$Hz, where adjacent subcarriers have frequency spacing $7.81K$Hz. By setting the system under the above conditions, we fix the total bandwidth and vary the spectral efficiency by changing the data rate. The FMT system is transmitting over a frequency selective $L = 4$ taps fading channel with $3dB$ coherence bandwidth $W_{3dB} = 0.125M$Hz. For comparison purposes, the CIR graph of an OFDM system having 64 subcarriers with the same subcarrier frequency spacing is also shown in the plot. For sake of fair comparisons, we only consider ISI-free OFDM systems, where the length of the cyclic prefix is longer than the maximum multipath number (tap number) $L = 4$. Therefore, the OFDM system considered has maximum spectral efficiency $\eta_{OFDM} = M/(M + L) = 0.94$.

From Fig. 4.3, we observe that when the FMT system has moderate to low spectral efficiencies ($\eta < 0.9$ in this case), it outperforms the OFDM systems at the cost of losing spectral efficiency ($\eta_{OFDM} > \eta$). However, at high spectral efficiency regimes ($\eta > 0.9$ in this case), OFDM has a better CIR than the regular FMT system. Therefore, we conclude from these results that

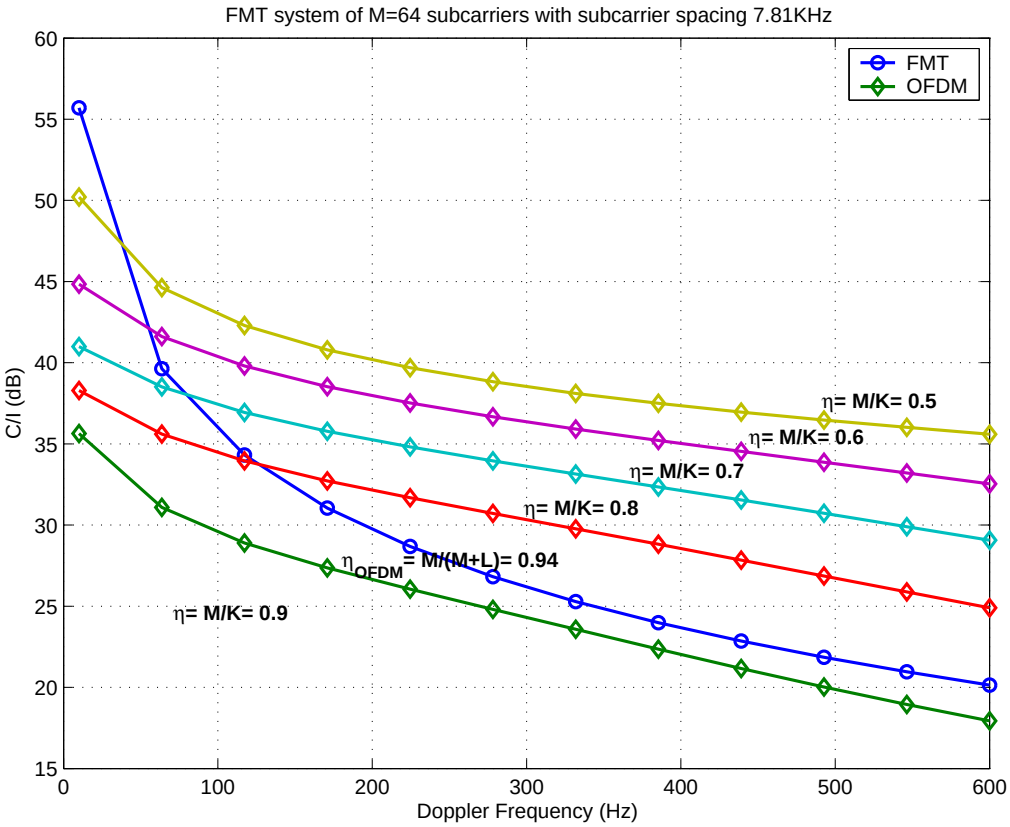


Figure 4.3 CIR graphs of an FMT system with $M = 64$ subcarriers under different upsampling factors $K = 71, 80, 91, 107$, and 128

OFDM is superior to an FMT system under the same spectral efficiency. We also observe from the left part of the plot that an OFDM system outperforms FMT (even with smaller spectral efficiency) over slowly time-varying fading channels with low Doppler frequencies ($F_d < 100Hz$).

It might seem counterintuitive that the simple OFDM system without any baseband pulse-shaping filters outperforms an FMT system with a baseband filter design. However, it can be explained by the different interference types of both systems. As stated in Section 4.3.5, an OFDM system with a cyclic prefix does not have any ISI while an FMT system is distorted by both ISI and ICI. Therefore, due to the additional ISI impairment, it is reasonable to see that OFDM outperforms FMT with the same spectral efficiency. In order

to compare purely the ICI effects on the system performance, we demonstrate in Fig. 4.4 the carrier over ICI ratios of the same FMT system over the same fading channel conditions as in Fig. 4.3. We observe from the plot that an FMT system has less ICI distortion (hence larger C/I_{ici} ratio) compared with an OFDM system having the same spectral efficiency. Furthermore, the group of C/I and C/I_{ici} curves provided in Fig. 4.3 and Fig. 4.4 demonstrate the trade-off between spectral efficiency and system performance (or performance degradation).

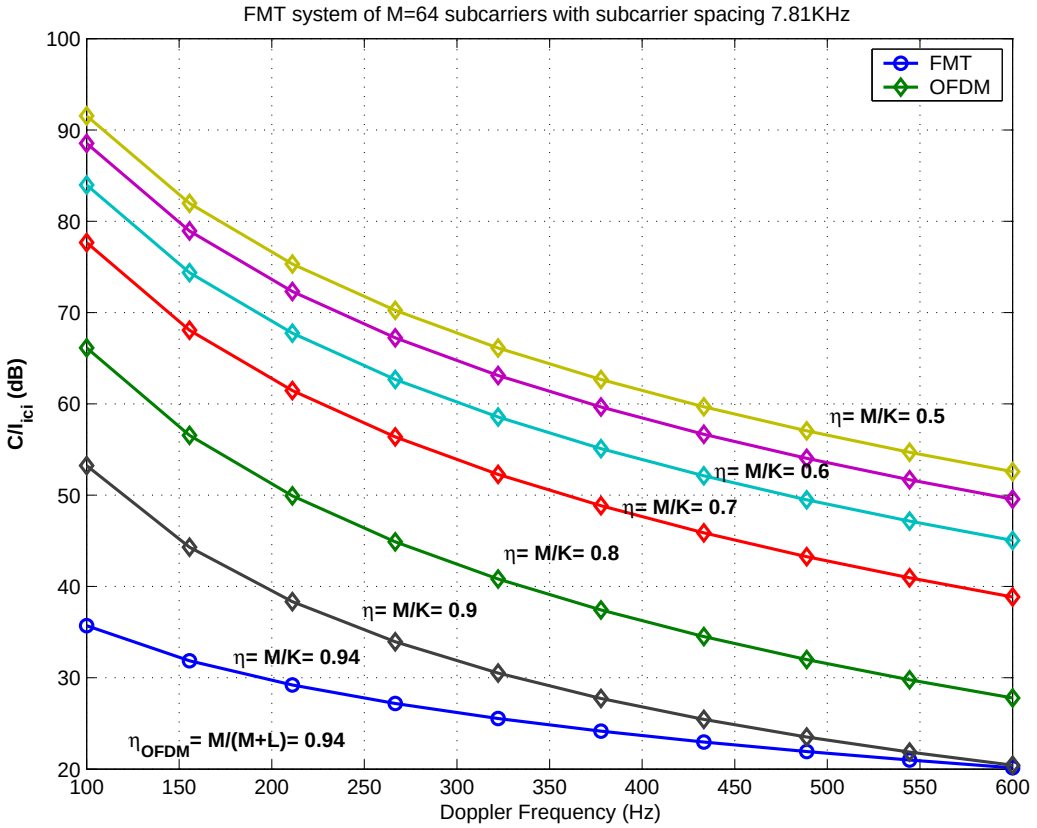


Figure 4.4 Carrier over ICI interference ratio (C/I_{ici}) graphs of an FMT system with $M = 64$ subcarriers under different upsampling factors $K = 68, 71, 80, 91, 107$, and 128

In order to compare the system performance over channels with high frequency selectivity, we demonstrate in Fig. 4.5 the CIR curves of the same

FMT system with 64 subcarriers and different upsampling factors $K = 80$, 84, 91, 107 and 128, with $\eta = M/K$ ranging from $\eta = 0.5$ to $\eta = 0.8$. The system is transmitting over a highly frequency selective fading channel with $3dB$ coherence bandwidth $W_{3dB} = 25$KHz and the number of independent taps $L = 20$. We observe from the above plot that the FMT modulation outperforms an OFDM system with the same spectral efficiency over highly frequency selective fading channels with high Doppler frequency (moderate to fast fading channels).

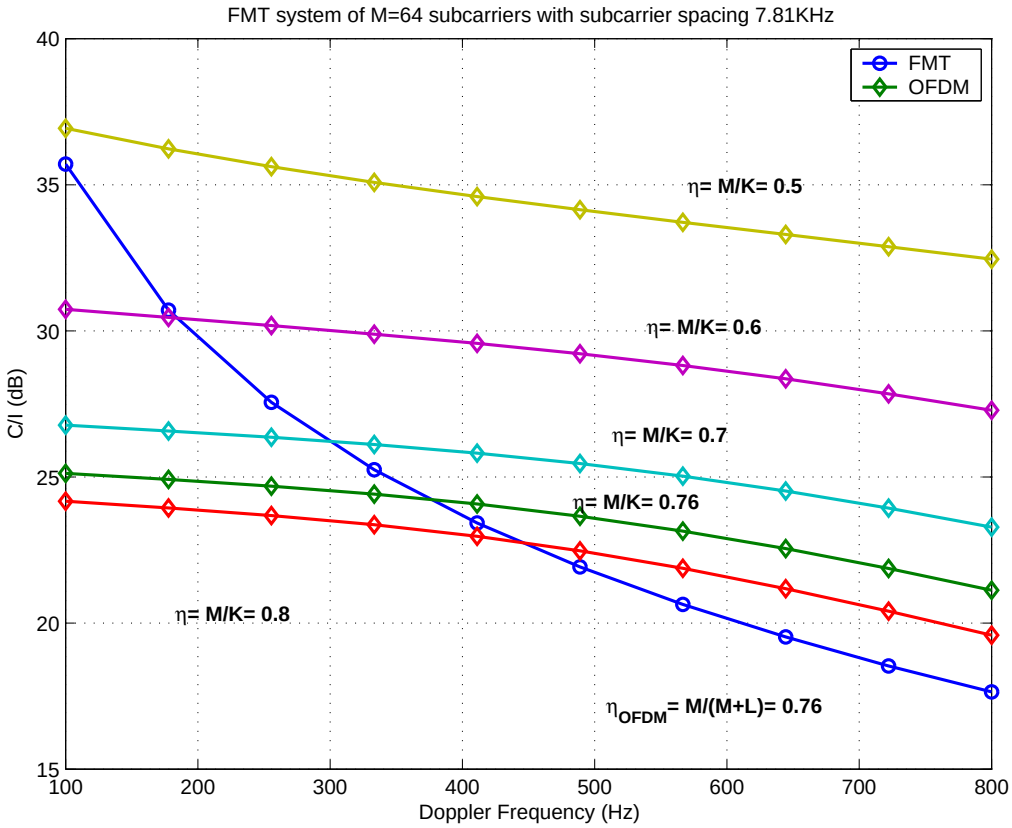


Figure 4.5 CIR curves of an FMT system with ideal per-channel equalizer with $M = 64$ subcarriers under different upsampling factors $K = 80, 84, 91, 107$, and 128

We also demonstrate in Fig. 4.6 and Fig. 4.7 the average symbol error probability of the same FMT system with 16-QAM modulation under several

different spectral efficiencies. The fading channels for these two plots are different in a sense that the former is a slowly fading channel with low frequency selectivity and the latter is highly frequency selective and rapidly time-varying. Specificially, the channel in Fig. 4.6 has $L = 4$ taps of exponential power delay profile with the $3dB$ coherence bandwidth $W_{3dB} = 0.125M$Hz, and the maximum Doppler spread is fixed to be $F_d = 100$Hz; while the channel in Fig. 4.7 has a coherence bandwidth $W_{3dB} = 25$KHz with $L = 20$ and Doppler spread $F_d = 600$Hz. For comparison purposes, the average symbol error probability of an OFDM system with 64 subcarries over the same fading channels is also included in both plots. From the above two plots, we observe the trade-off between spectral efficiency and performance degradation. Furthermore, consistent with the results of the CIR curves provided in this section, an OFDM system outperforms (in average symbol error rate sense) an FMT system with the same spectral efficiency in slowly fading and low frequency selective fading channels, but is outperformed by FMT modulation in fast fading channels with high frequency selectivity. Therefore, FMT modulation is a promising alternative to OFDM in the multicarrier communications family in certain wireless environments, and provides better performance in combating frequency-selective and time-varying fading channels.

Based on the previous results of un-equalized FMT systems, we extend to show the performance results of FMT system with per-channel equalizer. We first demonstrate in Fig. 4.8 the CIR graphs of an FMT system having 64 subcarriers and several different upsampling factors $K = 91, 80$ and 71. The spectral efficiency $\eta = M/K$, defined as the ratio of the subcarrier number over the upsampling factor, varies from $\eta = 0.7$ to $\eta = 0.9$, which parameterizes the CIR curves. The FMT system has a total bandwidth $W = 0.5M$Hz, where adjacent subcarriers have frequency spacing $7.81K$Hz. The FMT system is transmitting over a frequency selective $L = 4$ taps fading channel with $3dB$ coherence bandwidth $W_{3dB} = 0.125M$Hz. For purposes of comparison, the

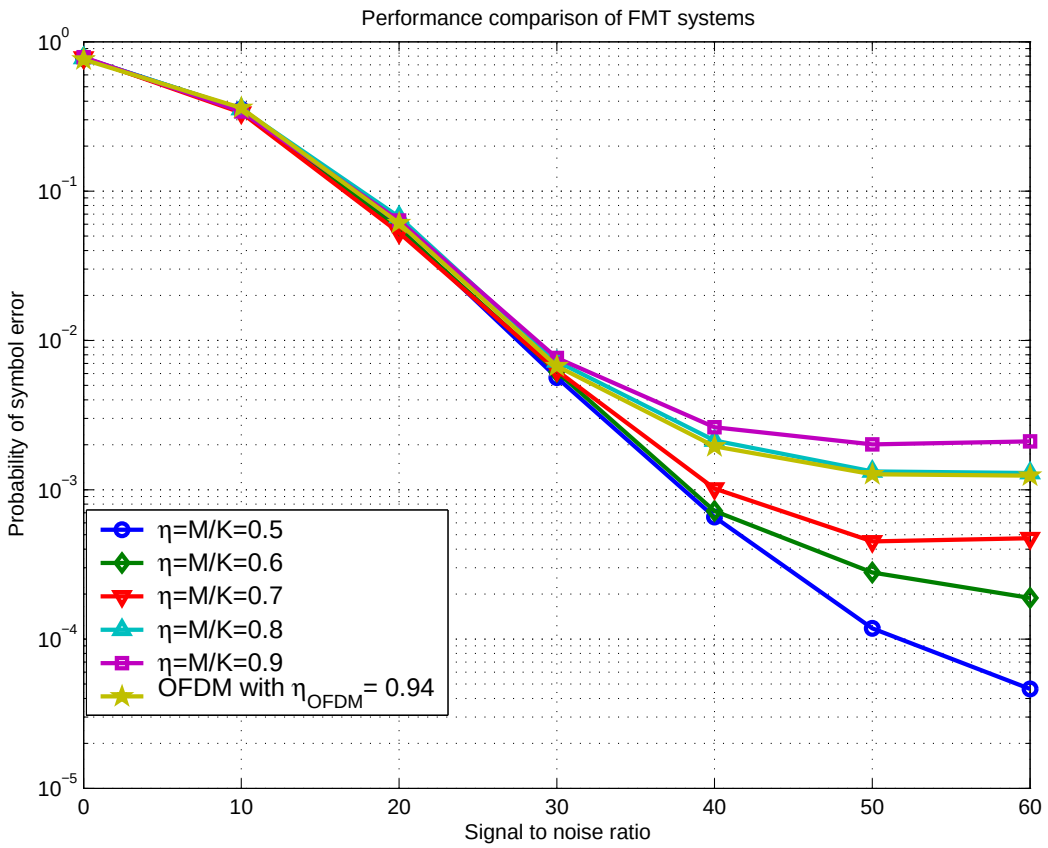


Figure 4.6 Comparison of symbol error probability of an FMT system with $M = 64$ subcarriers under different spectral efficiency over low frequency selective and slowly time-varying fading channel

upper bound of the CIR graph of the same FMT system with per-channel equalizer is illustrated in the plot. In order to compare the performance of the per-channel equalized FMT system with an OFDM system, we demonstrate in Fig. 4.9 the CIR graph of the same per-channel equalized FMT system with that of a standard OFDM system having 64 subcarriers and the same subcarrier frequency spacing over the same fading channel conditions as in Fig. 4.8.

The CIR for the three mulitcarrier systems, illustrated in Fig. 4.8 and Fig. 4.9, clearly show that the per-channel equalized FMT system has the best performance of the three systems. The conclusion reached from the results on output CIR is that the per-channel equalizer significantly improves

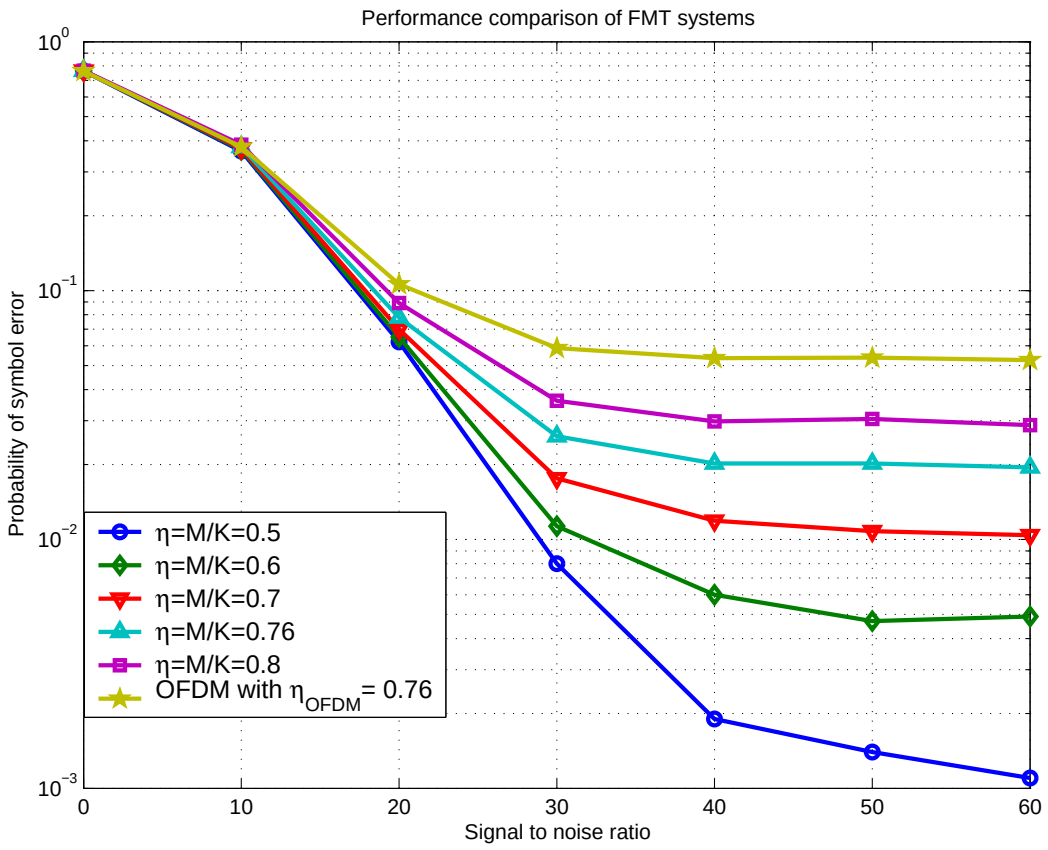


Figure 4.7 Comparison of symbol error probability of an FMT system with $M = 64$ subcarriers under different spectral efficiency over highly frequency selective and fast fading channel

the performance of an FMT system.

The intuitive explanations for the above results are the followings. The simple rectangular pulse shape in OFDM modulations causes more severe ICI effects comparing with FMT systems. In contrast, FMT systems resort to noncritically sampled filter-bank design that achieves tight subchannel spectral containment. Therefore, the sidelobes of spectral characteristics (Sinc function) for each OFDM subchannel attenuate much slower than the FMT systems. Without per-channel equalizer, the previous results in Section 4.3 [82] had shown that OFDM performance exceeded that of FMT at low Doppler range but FMT was better at high Doppler, but this subsection shows that with the

elimination of the ISI with per-channel equalizer, FMT is better than OFDM at all Doppler rates with a convergence to equal performance as M/K approaches unity at high Doppler rates.

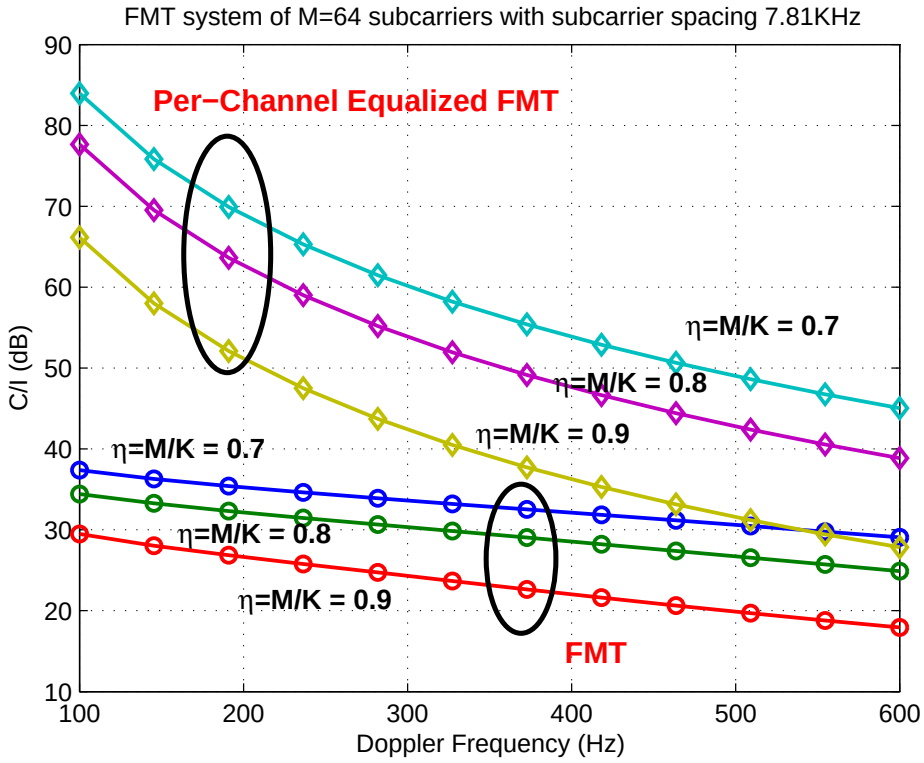


Figure 4.8 CIR graphs of an FMT system with $M = 64$ subcarriers under different upsampling factors

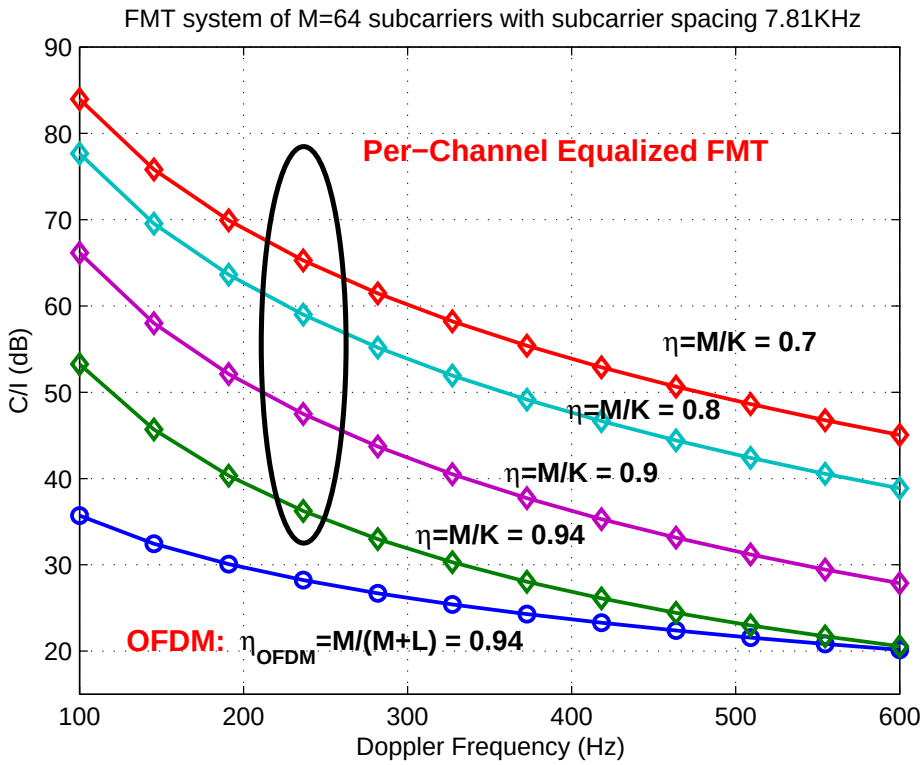


Figure 4.9 CIR graphs comparison between OFDM and FMT system with $M = 64$ subcarriers under different upsampling factors

4.6 Conclusion

In this chapter, we first considered an FMT modulation system in frequency-selective time-varying fading channels. The interchannel as well as intersymbol interference of the FMT system, which is caused by the time variations and frequency selectivity of the fading channel, has been analyzed in detail. By analyzing the demodulated signals at the receiver under different fading channels, we showed analytically that quasi-static frequency-flat fading channels do not introduce ISI or ICI to a multi-carrier system; frequency-selective fading channels introduce ISI, but preserve the orthogonality between different subchannel signals; whereas time-varying frequency-selective channels introduce both ISI and ICI in an FMT system. We provided the analysis of the effects of ISI and ICI in an FMT system separately under different channel conditions. The obtained carrier to interference ratio (C/I) analysis provided insight into the trade-off between spectral efficiency and system performance degradation. Finally, a comparison between OFDM and FMT leads us to the conclusion that OFDM outperforms FMT in a slowly (or near static) fading and low frequency selective fading channel but is inferior to FMT modulation in highly frequency-selective and time-varying fading environments.

We also considered the performance of an FMT system with per-channel equalization over frequency-selective time-varying fading channels. Due to the distortion caused by the time-frequency dispersive channel response, both ICI and ISI exist in an FMT system and cause performance degradation. By using a per-channel equalizer at the FMT receiver with a sufficiently large number of equalizer taps, the ISI is mitigated significantly, but the ICI still exists. In later part of this chapter, the effects of the ICI and ISI on the FMT system performance was quantified by analyzing the average system carrier to interference (C/I) ratio under different fading conditions. A closed-form expression of the C/I ratio and its upper bound were provided, which led to a better understanding of the trade-off between spectral efficiency and perfor-

mance degradation. Moveover, comparisons between FMT and OFDM systems under the same channel conditions and spectral efficiency were also provided.

Acknowledgment

The text in this chapter, in part, was originally published in the following papers, of which I was the primary researcher and author: T. Wang, J. Proakis, and J. Zeidler, "Interference analysis of filtered multitone modulation over time-varying fading channels," *in Proc. on IEEE Globecom*, Vol. 6, pp. 3586-3591, November 2005; T. Wang, J. Proakis, and J. Zeidler, "Interference analysis of filtered multitone modulation over time-varying fading channels," to appear in *IEEE Transactions on Communications*, 2006; T. Wang, J. Proakis, and J. Zeidler, "Analysis of per-channel equalized filtered multitone modulation over time-varying fading channels," accepted by *IEEE PIMRC*, 2006.

Bibliography

[1] R. van Nee and R. Prasad, OFDM for wireless multimedia communications, Artech House Publishers, 2000.

[2] A. R. S. Bahai and B. R. Saltzberg, Multi-Carrier Digital Communications: Theory and Applications of OFDM, Kluwer Academic Publishers, 1999.

[3] R. W. Chang, "Synthesis of band limited orthogonal signals for multichannel data transmission," *Bell Systems Technical Journal, vol.45, Dec. 1966.*

[4] B. R. Salzberg, "Performance of an efficient parallel data transmission system," IEEE Transactions on Communications, vol.COM-15, Dec. 1967.

[5] S. Weinstein and P. Ebert, "Data transmission by frequency-division multiplexing using the discrete Fourier transform," *IEEE Trans. Commun. Technol.*, vol. COM-19, pp. 628-634, Oct. 1971.

[6] B. Hirosaki, "An orthogonal multiplexed QAM system using the discrete Fourier transform," *IEEE Transactions on Communications, vol.COM-29, Jul. 1981.*

[7] B. Hirosaki, "A 19.2 kbits voice band data modem based on orthogonaly multiplexed QAM techniques," in Proceedings of IEEE ICC85, pp.21.1.1-5, 1985.

[8] P. S. Chow, J. C. Tu and J. M. Cioffi, "Performance evaluation of a multichannel transceiver system for ADSL and VHDSL services," *IEEE Journal on Selected Areas in Communications, vol. 9, Issue 6, pp. 909-919, Aug. 1991.*

[9] P. S. Chow, J. C. Tu and J. M. Cioffi, "A discrete multitone transceiver system for HDSL applications," IEEE Journal on Selected Areas in Communications, vol. 9, Issue 6, pp. 895-908, Aug. 1991. 62

[10] A. Vahlin and N. Holte, "Optimal finite duration pulses for OFDM," *IEEE Transactions on Communications, vol. 44, Issue 1, pp. 10-14, Jan. 1996.*

[11] M. J. Medley, G. J. Saulnier and P. K. Das, "Narrow-band interference excision in spread spectrum systems using lapped transforms," IEEE Transactions on Communications, vol. 45, Issue 11, pp. 1444-1455, Nov. 1997.

[12] G. L. Stuber, Principles of Mobile Communications, Kluwer Academic publishers, Boston, 1996.

[13] M. Russell and G. L. Stuber, "Interchannel interference analysis of OFDM in a mobile environment," *Vehicular Technology Conference,* vol. 2, pp. 820-824, July 1995.

[14] L. Wan and V. K. Dubey, "Bit error probability of OFDM system over frequency nonselective fast Rayleigh fading channels," *Electronics Letters*, vol. 36, pp. 1306-1307, July 2000.

[15] E. Chiavaccini and G.M. Vitetta, "Error performance of OFDM signaling over doubly-selective Rayleigh fading channels," *IEEE Communications Letters*, vol. 4, pp. 328-330, Nov 2000.

[16] P. Robertson and S. Kaiser, "Analysis of the loss of orthogonality through Doppler spread in OFDM system," *in Proc. Globecom'99*, pp. 701-706, Dec 1999.

[17] P. Robertson and S. Kaiser, "The effects of Doppler spreads in OFDM (A) mobile radio systems," *in Proc.50th IEEE Vehicular Technology Conference*, vol. 1, pp. 329-333, 1999.

[18] J. Li and M. Kavehrad, "Effects of time selective multipath fading on OFDM systems for broadband mobile applications," *IEEE Communications Letters*, vol. 3, pp. 332-334, 1999.

[19] Y. Li and L. J. Jr. Cimini, "Bounds on the interchannel interference of OFDM in time-varying impairments," *IEEE Transactions on Communications*, vol. 49, pp. 401-404, March 2001.

[20] Y.-S. Choi, P. J. Voltz, F. Cassara, "On channel estimation and detection for multicarrier signals in fast and frequency selective Rayleigh fading channel," *IEEE Transations on Communications*, vol. 49, pp. 1375-1387, Aug 2001.

[21] P. Bello, "Characterization of Randomly Time-Variant Linear Channels," *IEEE Transactions on Communications*, vol. 11, pp. 360-393, Dec 1963.

[22] W. G. Jeon, K. H. Chang, and Y. S. Cho, "An equalization technique for orthogonal frequency-division multiplexing systems in time-variant multipath channels," *IEEE Transactions on Communications*, vol. 47, pp. 27-32, Jan 1999.

[23] A. Gorokhov and J. P. Linnarts, "Robust OFDM receiver for dispersive time varying channels: equalization and channel acquisition," *IEEE Transactions on Communications*, vol. 52, pp. 572-583, Apr 2004.

[24] H. Zou, B. McNair, and B. Daneshrad, "An integrated OFDM receiver for high-speed mobile data communications," *in Global Telecommunications Conference 2001*, vol. 5, pp. 25-29, Nov 2001.

[25] W. C. Jakes, Microwave Mobile Communications, IEEE Press, Reprinted, 1994.

[26] P. Hoeher, "A statistical discrete-time model for the WSSUS multipath channel," *IEEE Transactions on Vehicular Technology*, vol. 41, pp. 461-468, Nov 1992.

[27] R. H. Clarke, "A statistical theory of mobile radio reception," *Bell Syst. Tech. J.*, vol. 47, pp. 957-1000, July 1968.

[28] T. S. Rappaport, Wireless Communication: Principles & Practice, Prentice-Hall, 1996.

[29] J. G. Proakis, Digital Communications, 4^{th} Ed., McGraw Hill, 2000

[30] D. Brillinger, Time Series Data Analysis and Theory, Holt, Rinehart, and Winston, 1974.

[31] H. Cramer, Mathematical Methods of Statistics, Princeton University Press, Princeton, 1946.

[32] W. E. Milne, "On the Degree of Convergence of the Gram-Charlier Series," *Transactions of the American Mathematical Society*, vol. 31, pp. 422-443, July 1929.

[33] P.W. Sauer and G.T. Heydt, "A convenient multivariate Gram-Charlier," *IEEE Transactions on Communications*, vol. 27, pp. 247-248, January 1979.

[34] A. Papoulis, Probability, Random Variables and Stochastic Processes, McGraw-Hill, 1984.

[35] T. Wang, J. Proakis, and J. Zeidler, "Performance Analysis of High QAM OFDM System Over Frequency Selective Time-Varying Fading Channel," *in Proc. 14th IEEE PIMRC*, vol. 1, pp. 793-798, Sep 2003.

[36] J. A. C. Bingham, "Multicarrier modulation for data transmission: An idea whose time has come," *IEEE Commun. Mag.*, pp. 5-14, May 1991.

[37] H. Sari, G. Karam, and I. Jeanclaude,"Transmission techniques for digital terrestrial TV broadcasting," *IEEE Commun. Mag.*, vol. 33, pp. 100-109, Feb 1995.

[38] Y. Li and L. J. Jr. Cimini, "Bounds on the interchannel interference of OFDM in time-varying impairments," *IEEE Transactions on Communications*, vol. 49, pp. 401-404, March 2001.

[39] P. Robertson, and S. Kaiser,"The effects of Doppler spreads in OFDM(A) mobile radio systems", *Vehicular Technology Conference 1999*, vol. 1, pp. 329-333, Sept. 1999.

[40] P. Robertson, and S. Kaiser,"Analysis of the loss of orthogonality through Doppler spread in OFDM system", in *Proc. Globecom'99*, pp. 701-706, Dec. 1999.

[41] T. Wang, J. Proakis, J. Zeidler, "Performance Analysis of High QAM OFDM System Over Frequency Selective Time-Varying Fading Channel," in *Proc. 14th IEEE PIMRC*, vol. 1, pp. 793-798, Sept. 2003.

[42] T. Wang, J. Proakis, E. Masry, and J. Zeidler, "Performance degradation of OFDM system due to Doppler spreading," *IEEE Trans. on Wireless Communications*, Vol. 6, June 2006.

[43] J. van de Beek, O. Edfors, M. Sandell, S.K. Wilson, P.O. Borjesson, "On channel estimation in OFDM systems," in *Proc. IEEE Vehicular Technology Conference*, vol. 2, pp. 815-819, July 1995.

[44] O. Edfors, M. Sandell, J. van de Beek, S.K. Wilson, P.O. Borjesson, "OFDM channel estimation by singular value decomposition," *IEEE Transactions on Communications*, vol. 46, pp. 931-939, July 1998.

[45] Y. Li, L.J. Cimini, N.R. Sollenberger, "Robust channel estimation for OFDM systems with rapid dispersive fading channels," *IEEE Transactions on Communications*, vol. 46, pp. 902-915, July 1998.

[46] C. Li and S. Roy, "Subspace-based blind channel estimation for OFDM by exploiting virtual carriers," *IEEE Transactions on Wireless Communications*, vol. 2, pp. 141-150, Jan 2003.

[47] Y. Gong and K.B. Letaief, "Low complexity channel estimation for space-time coded wideband OFDM systems," *IEEE Transactions on Wireless Communications*, vol. 2, pp. 876-882, Sept. 2003.

[48] X. Wang and K. J. R. Liu, "OFDM channel estimation based on time-frequency polynomial model of fading multipath channel," *Vehicular Technology Conference 2001*, vol. 1, pp. 460-464, 2001.

[49] Ming-Xian Chang and Yu.T. Su, "Model-based channel estimation for OFDM signals in Rayleigh fading," *IEEE Transactions on Communications*, vol. 50, pp. 540-544, April 2002.

[50] Y. Zhao and S. G. Haggman, "Intercarrier interference self-cancellation scheme for OFDM mobile communication systems," *IEEE Transaction on Communications*, vol. 49, pp. 1185-1191, July 2001.

[51] K. Sathananathan, C. Tellambura, "Forward error correction codes to reduce intercarrier interference in OFDM," in *proc. IEEE International Symposium on Circuits and Systems*, vol. 4, pp. 566-569, May 2001.

[52] L. Wang and C. Tellambura, "A novel ICI cancellation technique for OFDM systems using adaptive mapping signal constellation," in *IEEE Pacific Rim Conference on Communications, Computers and signal Processing*, vol. 1, pp. 442-445, Aug, 2003.

[53] Y. Mostofi, D.C. Cox, A. Bahai, "ICI mitigation for mobile OFDM receivers," in *proc. IEEE International Conference on Communications*, vol. 5, pp. 3351-3355, May 2003.

[54] J.-P.M.G. Linnartz, A. Gorokhov, "New equalization approach for OFDM over dispersive and rapidly time varying channel," in *proc. IEEE International Symposium on Personal, Indoor and Mobile Radio Communications*, vol. 2, pp. 1375-1379, Sept. 2000.

[55] J. Ahn, H.S. Lee, "Frequency domain equalisation of OFDM signals over frequency nonselective Rayleigh fading channels," *Electronics Letters*, vol. 29, pp. 1476-1477, Aug. 1993.

[56] N. Dhahir, J.M. Cioffi, "Optimum finite-length equalization for multicarrier transceivers," *IEEE Transactions on Communications*, vol. 44, pp. 56-64, Jan. 1996.

[57] Renyuan Li, G. Stette, "Time-limited orthogonal multicarrier modulation schemes," *IEEE Transactions on Communications*, vol. 43, pp. 1269-1272, April 1995.

[58] C. Muschallik, "Improving an OFDM reception using an adaptive Nyquist windowing," *IEEE Transactions on Consumer Electronics*, vol. 42, pp. 259-269, Aug.1996.

[59] A. Stamoulis, S.N. Diggavi, N Al-Dhahir, "Intercarrier interference in MIMO OFDM," *IEEE Transactions on Signal Processing*, vol. 50, pp. 2451 - 2464, Oct. 2002.

[60] S.Diggavi, S.N. Diggavi, A. Stamoulis, "Intercarrier interference in MIMO OFDM," in *Proc.IEEE International Conference on Communications*, vol. 1, pp. 485 - 489, May 2002.

[61] A. Stamoulis, S.N. Diggavi, N Al-Dhahir, "Estimation of fast fading channels in OFDM," in *Proc.Wireless Communications and Networking Conference*, vol. 1, pp. 465 - 470, March 2002.

[62] J. Li, "Pilot-symbol-aided channel estimation for OFDM in wireless systems," *IEEE Transactions on Vehicular Technology*, vol. 1, pp. 1207 - 1215, July 2000.

[63] Y. Li, L.J. Cimini, and N.R. Sollenberger, "Robust channel estimation for OFDM systems with rapid dispersive fading channels," *IEEE Transactions on Communications*, pp. 902 -1015, July 1998.

[64] R. Negi and J. Cioffi, "Pilot tone selection for channel estimation in a mobile OFDM system," *IEEE Transactions on Consumer Electronics*, pp. 1122 - 1128, August 1998.

[65] S. Ohno and G. B. Giannakis, "Capacity maximizing pilots and precoders for wireless OFDM over rapidly fading channels," *IEEE Transactions on Information Theory*, May 2001.

[66] U. Tureli, D. Kivanc, and H. Liu, "Experimental and analytical studies on a high-resolution OFDM carrier frequency offset estimator," *IEEE Transactions on Vehicular Technology*, pp. 629 - 643, March 2001.

[67] G. Cherubini, E. Eleftheriou, and S. Ölçer,"Filtered multitone modulation for very high-speed digital subscriber lines," *IEEE Journal on Selected Areas in Communications,* vol.20, pp. 1016-1028, June 2002.

[68] G. Cherubini, E. Eleftheriou, S. Ölçer, and J. M Cioffi, "Filter bank modulation techniques for very high speed digital subscriber lines," *IEEE Communications Magazine,* vol. 38, pp. 98-104, May 2000.

[69] N. Benvenuto, G. Cherubini, and L. Tomba, "Achievable bit rates of DMT and FMT systems in the presence of phase noise and multipath," *Vehicular Technology Conference Proceedings*, vol. 3, pp. 2108-2112, May 2000.

[70] S. B. Weinstein and P. M. Ebert, "Data transmission by frequencydivision multiplexing using the discrete Fourier transform," *IEEE Trans. Commun. Technol.*, vol. COM-19, pp. 628-634, Oct. 1971.

[71] P. Robertson and S. Kaiser, "Analysis of the loss of orthogonality through Doppler spread in OFDM system," *in Proc. Globecom'99*, pp. 701-706, Dec 1999.

[72] T. Wang, J. Proakis, E. Masry, and J. Zeidler, "Performance degradation of OFDM system due to Doppler spreading," *IEEE Transactions on Wireless Communicaitons*, Vol. 6, June 2006.

[73] T. Wang, J. Proakis, and J. Zeidler, "Performance analysis of high QAM OFDM System over frequency selective time-varying fading channel," *in Proc. 14th IEEE PIMRC*, vol. 1, pp. 793-798, Sep., 2003.

[74] A. Assalini, S. Pupolin, and L. Tomba, "DMT and FMT Systems for Wireless Applications: Performance Comparison in the Presence of Frequency Offset and Phase Noise," *In Proc. WPMC03, Yokosuka, Kanagawa, Japan*, pp. 19-22, Oct., 2003.

[75] A. Assalini, S. Pupolin, and A. M. Tonello, "Analysis of the Effects of Phase Noise in Filtered Multitone (FMT) Modulated Systems," *In IEEE Global Telecommunications Conference, Globecom'04*, vol. 6, pp. 3541-3545, Dec., 2004.

[76] A. Tonello, "Exact matched filter performance bound for multitone modulation in fading channels," *In Proc. WPMC03, Yokosuka, Kanagawa, Japan*, Oct., 2003. submitted to IEEE Trans. Wireless. Comm., April 2003.

[77] A. Tonello, "Performance limits of multicarrier based systems in fading channels with optimal detection," *The 5th International Symposium on Wireless Personal Multimedia Communications*, vol. 3, pp.1005-1009, Oct., 2002.

[78] Y. Gao, Z. Gao, W. Zhu, and X. Yang "The research on the design of filter banks in filtered multitone modulation," *2005 IEEE Wireless Communications and Networking Conference*, vol. 1, pp.584-588, Mar., 2005.

[79] Van Acker et al., "Per tone equalization for DMT-based systems ," *IEEE Trans. on Comm.*, vol. 49, pp. 109-119, Jan. 2001.

[80] B. Borna and T. N. Davidson, "Efficient filter bank design for filtered multitone modulation," *2004 IEEE International Conference on Communications*, vol. 1, pp.38-42, June, 2004.

[81] A. Tonello, "An efficient implementation of a wavelet based filtered multitone modulation scheme," *The 4th IEEE International Symposium on Signal Processing and Information Technology*, pp.225-228, Dec., 2004.

[82] T. Wang, J. Proakis, and J. Zeidler, "Interference analysis of filtered multitone modulation over time-varying fading channels," *in Proc. IEEE Global Telecommunications Conference, Globecom'05*, vol. 6, pp. 3586-3591, Nov., 2005.

[83] J. G. Proakis, *Digital Communications, 2nd ed.*, New York: McGraw-Hill, 1989.

[84] W. C. Jakes, *Microwave Mobile Communications*, IEEE press, Reprinted, 1994.

[85] G. J. Foschini, "Layered Space-Time Architecture for Wireless Communication in a Fading Environment When Using Multi-Element Antennas," *Bell Labs Technical Journal*, vol. 1, no. 2, pp. 41-59, 1996

[86] R. Blum, Y. Li, J. Winters, and Q. Yan, "Improved space-time coding for MIMO-OFDM wireless communications," *IEEE Transactions on Communications,* vol. 49, pp. 1873-1878, Nov, 2001.

[87] W. Su, Z. Safar, and K. J. R. Liu, "Full-rate full-diversity space-frequency codes with optimum coding advantage," *IEEE Transactions on Information Theory,* vol. 51, pp. 229-249, Jan, 2005.

[88] M. Guillaud and D. T. M. Slock, "Multi-stream coding for MIMO OFDM systems with space-time-frequency spreading," *The 5th International Symposium on Wireless Personal Multimedia Communications,* vol. 1, pp. 120-124, Oct, 2002.

[89] S. Suthaharan, A. Nallanathan, and B. Kannan, "Space-time coded MIMO-OFDM for high capacity and high data-rate wireless communication over frequency selective fading channels," *4th International Workshop on Mobile and Wireless Communications Network,* pp. 424-428, Sept, 2002.

[90] T. M. Cover and J. A. Thomas, *Elements of Information Theory.*, Wiley, New York, 1991.

[91] R. G. Gallager, *Information Theory and Reliable communication.* New York: Wiley, 1968.

[92] A. J. Viterbi and J. K. Omura, *Principles of Digital Communication and Coding.* Tokyo, Japan: McGraw-Hill, 1979.

[93] S. Arimoto, " On the converse to the coding theorem for discrete memoryless channels," *IEEE Personal Commun.*, vol. IT-19, pp. 357-359, May 1973.